MULTIDIMENSIONAL EARLY POSTNATAL STRESS PERMANENTLY PROGRAMS METABOLISM, DEVELOPMENT, AND BEHAVIOUR: LINKING TRAUMA TO ADVERSE HEALTH OUTCOMES

JANET POPLAWSKI
Bachelor of Science, University of Lethbridge, 2017

A thesis submitted
in partial fulfilment of the requirements for the degree of

MASTER OF SCIENCE

in

NEUROSCIENCE

Department of Neuroscience
University of Lethbridge
LETHBRIDGE, ALBERTA, CANADA

MULTIDIMENSIONAL EARLY POSTNATAL STRESS PERMANENTLY PROGRAMS METABOLISM, DEVELOPMENT, AND BEHAVIOUR: LINKING TRAUMA TO ADVERSE HEALTH OUTCOMES

JANET POPLAWSKI

Date of Defence: August 12th, 2019

Dr. Gerlinde Metz	Professor	Ph.D.
Tony Montina	Instructor	M.Sc.
Thesis Co-Supervisors		

Dr. Igor Kovalchuk	Professor	Ph.D.
Thesis Examination Committee Member		

Dr. Artur Luczak	Professor	Ph.D.
Thesis Examination Committee Member		

Dr. Majid Mohajerani	Associate Professor	Ph.D.
Chair, Thesis Examination Committee		

To Marek, Helena, and Angelika.

ABSTRACT

Stress is one of the most critical determinants of lifetime health. To gain insight into the underlying gene-environment interactions governing the effects of stress on development and behaviour, we (i) utilized proton nuclear magnetic spectroscopy to analyze cardiorenal and cerebral metabolomes of animals exposed to a multidimensional early-life stressor, and (ii) used immunohistochemical, transcriptomic, and behavioural analyses to examine the impacts of multidimensional early-life stress on offspring anxiety-like behaviours and visual development. Metabolomic profiles revealed significant changes as a result of early postnatal stress. Dysregulation of energy and protein metabolism suggests an increased risk of metabolic diseases like insulin resistance, cardiorenal syndrome, diabetes, obesity, and mental health disorders. Additionally, multidimensional early-life stress accelerated the functional and cellular development of the visual system. These findings provide novel insights into the effects of early-life stress on metabolism, development, and behaviour by combining behavioural, histological, metabolomic, and transcriptomic approaches in a rodent model.

ACKNOWLEDGEMENTS

First and foremost, I would first like to thank my family for their unwavering support and encouragement throughout my education. I would also like to thank Dr. Keiko McCreary, Dr. Jamshid Faraji, Dr. Mirela Ambeskovic, Dennis Bettenson, Ana Radmilovic, Erin Falkenberg, Nasrin Soltanpour, Hannah Scott, and Candace Chan for their great ideas, conversations, and contributions to these experiments, as well as the rest of the Metz lab for all their help and support over the past several years; Tanzi Hoover, Elani Bykowski, Jamie Peterson, Marrissa Buchan, Jaira Ranger, and Rebecca McHugh for the laughs and friendship, and Josh Heynen for putting up with my cheek. I would also like to thank Mike Opyr for his support of the NMR lab and technological troubleshooting. Finally, I would like to thank my exceptional supervisors, Dr. Gerlinde Metz and Tony Montina, for their infinite patience, guidance, support, and reference letters.

TABLE OF CONTENTS

LIST OF TABLES

LIST OF FIGURES

LIST OF ABBREVIATIONS

ANOVA	Analysis of Variance
BCAA	Branched-Chain Amino Acids
BDNF	Brain-Derived Neurotrophic Factor
BSA	Bovine Serum Albumin
CKD	Chronic Kidney Disease
CVD	Cardiovascular Disease
DAPI	4′,6-diamidino-2-phenylindole
ELS	Early-Life Stress
FDA	False Discovery Rate Adjusted
FDR	False Discovery Rate
GABA	Gamma-Aminobutyric Acid
GAD65/67	Glutamic Acid Decarboxylase 65/67
^{1}H NMR	Proton Nuclear Magnetic Resonance
HPA	Hypothalamic-Pituitary-Adrenal
KEGG	Kyoto Encyclopedia of Genes and Genomes
LOX-1	Lectin-like, oxidized low-density lipoprotein receptor-1
mRNA	Messenger Ribonucleic Acid
MSEA	Metabolite Set Enrichment Analysis
mTORC1	mammalian target of rapamycin complex 1
MW	Mann-Whitney U test
NCD	Non-communicable Disease
NMDA	N-methyl-D-aspartate
NMR	Nuclear Magnetic Resonance
OPLS-DA	Orthogonal Projection of Latent Structures Discriminant Analysis
P	Postnatal day
PBS	Phosphate-Buffered Saline
PBST	Phosphate-Buffered Saline/Triton
PCA	Principal Component Analysis
PFA	Paraformaldehyde
PLS-DA	Partial Least Squares Discriminant Analysis
PNNs	Perineuronal Nets
PV	Parvalbumin
tRNA	Transfer Ribonucleic Acid
TSP	Trimethylsilyl Propanoic Acid
VIP	Variable Importance in Projection
WFA	Wisteria floribunda agglutinin

CHAPTER 1: INTRODUCTION TO THE EFFECTS OF EARLY LIFE STRESS ON METABOLISM, DEVELOPMENT, AND BEHAVIOUR

"If we hit that bullseye, the rest of the dominoes will fall like a house of cards."

- *Captain Brannigan*

INTRODUCTION

OVERVIEW

Effects of Early-Life Stress on Lifelong Health & Behavioural Outcomes

Early-life stress has been associated with lifelong adverse health and physiological outcomes in offspring (Cottrell & Seckl, 2009; Evans & Kim, 2007; Singer & Ryff, 1999). In both animal and human studies, early-life stress has been found to program accelerated telomere shortening (Epel et al., 2004), adult inflammation (Danese, Pariante, Caspi, Taylor, & Poulton, 2007; Pace et al., 2006), neurodevelopmental disorders (Bale et al., 2010), and an increased prevalence of non-communicable diseases (NCDs) (Barouki, Gluckman, Grandjean, Hanson, & Heindel, 2012; G. Wang, Walker, Hong, Bartell, & Wang, 2013). For instance, in a human cohort exposed to the Dutch famine *in utero*, prenatal undernutrition was linked to the early onset of coronary artery disease in adulthood (Painter et al., 2006; Roseboom et al., 2000) as well as other non-communicable diseases; however, the effects of perinatal undernutrition depend upon which physiological systems are developing at that critical time window (Roseboom et al., 2001).

Several studies have found a strong correlation between stressful early-life experiences and impaired cognitive performance in adulthood (McEwen & Gianaros, 2011; Naninck et al., 2015). In humans, early-life stress has been associated with enhanced responsiveness to psychosocial stress and has been causally implicated in the development of major depressive disorder as well as increased stress-induced inflammatory responses in adolescence and adulthood (Pace et al., 2006). In animal models, chronic stress early in life has been found to alter neurogenesis across development and impair cognitive function in late adulthood. For example, mice exposed to early-life stress exhibited impaired performance in learning and memory tasks (Hoeijmakers, Lucassen, & Korosi, 2015). These environmentally-induced deficits

are associated with lasting changes in hippocampal plasticity, as well as plasticity in other brain areas. Of interest, regions in the prefrontal cortex and amygdala are known to exhibit experience-dependent changes in neuronal circuitry and have been implicated in stress-related vulnerability to mental health disorders, including anxiety and depression (McEwen & Gianaros, 2011).

Animal models focused on early environmental influences, including perinatal stress, have been critical in revealing the effects of an animal's environment on neural physiology, function, and lifelong health outcomes (Bock, Wainstock, Braun, & Segal, 2015; Hubel & Wiesel, 1968; Nowicki, Searcy, & Peters, 2002; Rice & Barone Jr, 2000; Wiesel & Hubel, 1963). Although the effects of the perinatal environment on brain development, plasticity, and lifelong non-communicable disease risk have garnered much interest, little is known about the mechanisms underlying these stress-induced adverse health and behavioural outcomes.

Critical periods of development are periods of time during which physiological systems display drastically heightened plasticity in response to environmental stimuli (Rice & Barone Jr, 2000). First studied in the context of visual development in kittens (Wiesel & Hubel, 1963), these transiently heightened critical periods of plasticity allow for an experience-dependent, long-term adaptive commitment to a pattern of neuronal connectivity (Hensch, 2004). In the murine visual cortex, the opening of the critical period for experience-dependent plasticity is characterized by the transfer of orthodenticle homeobox 2 (Otx2) homeoprotein into parvalbumin (PV)-expressing GABAergic interneurons (Beurdeley et al., 2012). Similarly, the closure of this critical period is characterized by the rapid appearance of perineuronal nets in the primary visual cortex. In normal, healthy mice, the critical period for visual cortical plasticity typically occurs from postnatal days (P)20 to P35, after which the visual system is no longer hypersensitive to environmental stimuli (Espinosa & Stryker, 2012). These physiological

milestones correlate with behavioural and functional changes in the animal. In mice, visual acuity and contrast sensitivity improve rapidly with the onset of the critical period for visual system plasticity, correlating with improved performance in behavioural tasks such as the elevated plus maze and visual cliff (Pinto & Enroth-Cugell, 2000). For example, once the critical period for the visual system begins, animals typically begin to show a side preference and exhibit cliff avoidance on the visual cliff apparatus, indicating the presence of depth perception. However, despite the visual system being the premier model for experience-dependent brain plasticity, virtually nothing is known about the effects of early-life stress on the timing of visual development.

STRESS & CARDIORENAL FUNCTION

Comorbidity of Cardiorenal Diseases & Mental Health Disorders

Chronic non-communicable diseases are a major public health problem with a high economic cost to health systems (Beaglehole & Yach, 2003; Cravedi & Remuzzi, 2008; Habib & Saha, 2010; Hill et al., 2016). At least a third of all individuals with one NCD are subsequently diagnosed with additional chronic non-communicable conditions (Licher et al., 2019). Cardiovascular diseases (CVDs) are the most prevalent category of NCDs, accounting for nearly half of all NCD-related mortalities (Organization, 2018). CVDs often co-occur with mental health disorders (Chaddha, Robinson, Kline-Rogers, Alexandris-Souphis, & Rubenfire, 2016; Chauvet-Gelinier & Bonin, 2017) and decreased renal function, with CVDs being twice as common in patients with chronic kidney disease (CKD) and advancing at twice the rate (Collins et al., 2003; Hill et al., 2016). Moreover, individuals suffering from emotional disorders are twice as likely to experience myocardial infarction relative to the general population, and this

cardiovascular comorbidity significantly increases mortality in patients with depression (Chauvet-Gelinier & Bonin, 2017; Kozela et al., 2016). An estimated 40% of individuals with chronic CVDs also suffer from anxiety, and overall anxiety levels are 60% higher in CVD patients relative to healthy adults (Konstam, Moser, & De Jong, 2005; Moser et al., 2010).

The comorbidity of adverse cardiovascular events, renal dysfunction, and affective disorders suggests shared pathways in the pathogenesis of these conditions (Baigent, Burbury, & Wheeler, 2000; Chauvet-Gelinier & Bonin, 2017; Go, Chertow, Fan, McCulloch, & Hsu, 2004; Muntner, He, Hamm, Loria, & Whelton, 2002; Napoli, Casamassimi, Crudele, Infante, & Abbondanza, 2011). An individual's susceptibility to NCDs is predominantly, although not exclusively, environmentally determined (Gluckman, Hanson, & Mitchell, 2010; Maher, 2008; Taylor, 1983). However, traditional risk factors for chronic diseases such as poor nutrition, inactivity, and adiposity do not fully account for the excess burden of NCDs in the population (Greenland et al., 2003). Thus, other factors such as stress may be precipitating events in the development and progression of chronic non-communicable conditions (Everson-Rose & Lewis, 2005).

Stress & Non-Communicable Disease Risk

Growing evidence implicates stress and its effector system, the hypothalamic-pituitary-adrenal (HPA) axis, in the pathophysiology of cardiorenal and affective disorders (Boubred et al., 2013; Everson-Rose & Lewis, 2005; McEwen & Magarinos, 2001; Post, 1992; Steptoe & Kivimäki, 2012). During infancy, distinct organ systems exhibit transient critical periods of heightened plasticity (Hamilton, 1952) and increased vulnerability to environmental insults (Thornburg & Louey, 2005). Accordingly, early life stress (ELS) has lasting deleterious effects on physiology and behaviour (Langley-Evans, 2013; Vieau, 2011; X.-M. Wang, 2013), risk of

affective disorders (Chaby et al., 2015), metabolic disease (G. Chrousos, 2000) and cardiovascular (Barker, 1995) and renal diseases (Hershkovitz, Burbea, Skorecki, & Brenner, 2007; Langley-Evans, 2013). The mechanisms underlying its association with cardiorenal and emotional disorders, however, are poorly understood (Everson-Rose & Lewis, 2005; Tain & Hsu, 2017).

Stress & Cardiorenal Metabolism

Comprehensive metabolic profiling of biological samples has emerged as a promising approach to characterizing the pathophysiological consequences of maladaptive gene-environment interactions (Beckonert et al., 2007; Emwas, Salek, Griffin, & Merzaban, 2013; Fiehn, 2002; Nicholson, Lindon, & Holmes, 1999; Wishart, 2008). Metabolic phenotypes represent an organism's downstream physiological responses to epigenetically regulated cellular processes; therefore, metabolic profiling is a powerful tool for identifying stress-induced adverse health outcomes (Kiss, Ambeskovic, Montina, & Metz, 2016).

STRESS & DEVELOPMENTAL TIMING

Critical Periods & Experience-Dependent Brain Plasticity

Heightened physiological plasticity in the perinatal period has been recognized by biologists for decades. Nearly a century ago, it was demonstrated that a developing embryo exposed to chemicals at specific times would acquire predictable malformations, with the most rapidly-growing systems being most susceptible to environmental toxicant exposures (Stockard, 1921). Similarly, the developing nervous system is molded by environmental factors (Dobbing, 1972; Gale, O'Callaghan, Godfrey, Law, & Martyn, 2004; Ismail, Fatemi, & Johnston, 2017). Neuronal circuits across the developing brain demonstrate remarkable plasticity in responseto

early-life sensory inputs, with discrete periods of heightened sensitivity in specific brain regions where structural modification becomes essentially irreversible beyond a certain age (Hensch, 2005). These transiently heightened "critical periods" of plasticity allow for an experience-dependent, long-term adaptive commitment to a pattern of neuronal connectivity (Hensch, 2004). Although the experience-dependent reorganization of neural circuits is possible throughout life, the magnitude and permanence of anatomical changes distinguish critical periods of development from adult plasticity (Hensch, 2004).

Stress & Developmental Timing

The perinatal environment is one of the most critical determinants of lifetime health (Boubred et al., 2013; Chaby, Cavigelli, Hirrlinger, Caruso, & Braithwaite, 2015; Gluckman et al., 2010; Idris et al., 2013; Langley-Evans, 2013; Maher, 2008; Portrait, Teeuwiszen, & Deeg, 2011; Tain & Hsu, 2017; Thornburg & Louey, 2005; Vieau, 2011; Wang, 2013). Recently, it has been found that early adversity results in the accelerated maturation of emotion-relevant brain circuits and associated behaviours (Callaghan & Tottenham, 2016), and that this acceleration results from the stress-induced "reprioritization" of developmental trajectories that may accelerate some brain regions or functions at the expense of others. This "reprioritization" of developmental trajectories may result in a topographical desynchronization of brain development, thus contributing to the well-documented lifelong adverse health and behavioural outcomes in stressed populations. Stress-induced developmental acceleration has also been observed in other biological contexts. For example, accelerated pubertal development has been linked to adverse early-life experiences as well as subsequent mental and physical health impairments (Saxbe, Negriff, Susman, & Trickett, 2015). In this case, pubertal timing was found to be mediated by HPA axis activity, with accelerated pubertal development occurring alongside

attenuated HPA axis functioning. In the brain, early-life stress has been found to accelerate the behavioural and neural maturation of certain areas, including the hippocampus (Bath, Manzano-Nieves, Goodwill, & behavior, 2016; Kerr, Campbell, Applegate, Brodish, & Landfield, 1991). Specifically, stressed animals exhibited an accelerated decline in the expression of cell proliferation (Ki-67) and differentiation (doublecortin) markers, as well as an earlier switch in NMDA receptor subunit expression (a marker of synaptic maturity) and displayed precocious timed developmental suppression of contextual fear in a contextual fear-conditioning task (Bath et al., 2016). Similarly, elevated plasma corticosteroids due to stress have been found to accelerate electrophysiological and morphometric biomarkers of hippocampal aging in rats (Kerr et al., 1991). However, while several studies have detailed the effects of early-like stress on the developmental trajectory of hippocampal and emotion-relevant brain circuits, little has been done to explore the impact of stress on other brain areas.

The Visual System

A significant proportion of our current understanding of the mechanisms underlying experience-dependent brain plasticity during cortical development has been derived from studies of the mammalian visual cortex. For over 50 years, the visual cortex has been a proving ground for the study of experience-dependent plasticity because visual input can easily be manipulated and the consequences of these manipulations easily observed at the behavioural, anatomical, and physiological levels (Tropea, Van Wart, & Sur, 2008). Although the development of visual system circuitry begins prior to the onset of vision (Crowley & Katz, 1999; Sur & Leamey, 2001; Sur & Rubenstein, 2005), sensory experience is necessary for the proper development of visual function. While visual input exerts the most drastic effect on the developing visual cortex, other environmental stimuli have also been found to affect the development of the visual system. For

instance, complex sensory-motor stimulation provided by an enriched environment was previously found to accelerate eye-opening, the development of visual acuity, and the decline of white-matter induced long-term potentiation (Cancedda et al., 2004). These effects were accompanied by a significant increase in BDNF protein and GAD65/67 expression in enriched pups (Cancedda et al., 2004). Nevertheless, while the physiological, molecular, and behavioural milestones of visual system development have been well-characterized, there are currently no studies detailing the impact of non-visual adverse stimuli, such as early-life stress, on visual system development.

THEORY

Developmental Programming Theory

The developmental programming theory emphasizes that, during rapid early-life growth, biological systems are in a state of transiently heightened plasticity during which they are highly susceptible to both beneficial and adverse environmental stimuli (Heim & Binder, 2012; Weiss & Wagner, 1998). During this state of heightened developmental plasticity, organisms respond to environmental stimuli with epigenetic and physiological changes that, whether transient or long-lasting, aim to increase the individual's chances of survival and reproduction (i.e., evolutionary success). While some of these environmentally-induced changes are reversible, the magnitude of experience-dependent plasticity in the perinatal period is unmatched by any other development phase (Fagiolini, Jensen, & Champagne, 2009). Thus, maladaptive developmental events can result in permanent lifelong pathological consequences for an animal (Heim & Binder, 2012; Hertzman, 1999; Johnson, Riley, Granger, & Riis, 2013; Shonkoff et al., 2012).

HYPOTHESES

The work underlying this thesis was designed to investigate two main hypotheses.

Hypothesis 1: The Cardiorenal Programming Hypothesis

If stress early in life results in long-lasting adaptive changes to organ systems, then adult animals exposed to perinatal stress should exhibit drastically altered heart and kidney metabolomic profiles relative to controls. Furthermore, if early-life stress is causally implicated in the pathogenesis of adverse cardiorenal health outcomes and mental health disorders, stressed animals should exhibit (i) increased anxiety-like behaviours on the open-field test as well as (ii) changes in individual metabolites and metabolic pathways that have previously been implicated in psychopathologies (Experiment 1).

Hypothesis 2: The Stress Acceleration Hypothesis

According to the stress acceleration hypothesis, adverse early-life experiences should result in the "reprioritization" of developmental trajectories that may accelerate some brain regions or functions at the expense of others. If the primary visual cortex is one of these regions, stressed animals should exhibit precocious visual development relative to controls. Furthermore, because the stress acceleration hypothesis posits that not all areas will develop at the same rate, global cerebral metabolomic profiling should reveal altered metabolites and metabolic pathways indicative of a topographical desynchronization of brain development – that is, metabolites and metabolic pathways indicative of accelerated development as well as metabolites and metabolic pathways indicative of delayed development (Experiment 2).

THESIS OBJECTIVES & RATIONALE

Stress & Cardiorenal Metabolism

Here, ^{1}H NMR spectroscopy was used to determine whether ELS in a mouse model permanently alters cardiorenal metabolism. Comprehensive cardiorenal metabolomic profiles were acquired in conjunction with behavioural data quantifying anxiety-like behaviour in an animal model exposed to an early-life stressor (i.e., multidimensional transportation stress). Univariate and multivariate statistical approaches, along with metabolite set enrichment analysis and metabolomic pathway analysis, were utilized to correlate metabolic profiles to (i) altered pathways involved in cardiorenal metabolism and health outcomes, and (ii) anxiety-like behaviours in the open field apparatus. By investigating the direct impact of early-life stress on cardiorenal tissues, this approach provides novel insights into the direct effects of multidimensional early-life stress on heart and kidney metabolism while allowing for the identification of clearly distinguishable cardiorenal metabolic signatures and mechanistic pathways linking impaired cardiorenal function to mental health disorders.

Stress & Developmental Timing of the Visual System

Here, ^{1}H NMR spectroscopy was used along with transcriptomic, morphological, and behavioural approaches to determine how early-life stress in a mouse model alters cerebral metabolism as well as the developmental trajectory of the visual system, the premier model of experience-dependent brain plasticity. Comprehensive left and right cerebral metabolomic profiles were acquired in conjunction with behavioural, morphological, and visual cortical mRNA (messenger ribonucleic acid) expression data from an animal cohort exposed to an early-life stressor (i.e., multidimensional transportation stress). Univariate and multivariate statistical approaches, along with metabolite set enrichment analysis and metabolomic pathway analysis, were utilized to determine (i) the impacts of multidimensional early-life stress on cerebral

metabolism, while also investigating (ii) the impacts of early-life transportation stress on lateralization of brain metabolite changes, and (iii) the effects of early-life stress on the developmental trajectory of the visual system. Global mRNA expression profiles of visual cortical tissues were utilized to investigate potential upstream transcriptomic changes leading to downstream stress-induced metabolomic changes. Eye-opening observations were collected as a measure of visual system development, and behavioural assessments were performed throughout the duration of the critical period for visual cortical plasticity (P20 to P35 in mice) to assess the functional developmental trajectory of the visual system in response to early postnatal stress. Immunofluorescent staining of perineuronal nets (P35) was used to pinpoint the timing of visual critical period closure in perinatally-stressed and control animals. By investigating the direct impact of early-life stress on brain metabolism and the impact of multidimensional early-life stress on visual system development, this approach provides novel insights into the underlying mechanisms linking early-life stress to the topographical desynchronization of brain development and impaired cognitive function in adulthood.

CHAPTER 2: METABOLIC BIOMARKERS LINK EARLY-LIFE STRESS TO RISK OF NON-COMMUNICABLE CHRONIC DISEASES

INTRODUCTION TO EXPERIMENT 1

In order to characterize the lifelong effects of multidimensional early-life stress on cardiorenal metabolism, hearts and kidneys from shipped animals and controls were collected and subjected to global metabolomic profiling by ^{1}H NMR spectroscopy.

MATERIALS AND METHODS

Experimental Design

Twenty-three male C57BL/6 mice (*Mus musculus*) were used. Control animals (n=9) came from an animal cohort bred and raised under consistent laboratory conditions at the local vivarium for at least four generations. Stressed animals (n=14) had been shipped from Charles River Laboratories (Charles River Laboratories, QC, Canada). Pups remained with their mother until weaning at 9.6 grams, after which animals were housed in groups of at least two. Anxiety-like behaviour was assessed at 10:00 am on P25 using a standard open-field task for video recordings of number of central squares entered in a 1-min session (Erickson, Falkenberg, & Metz, 2014). To assess the impact of multidimensional early-life transportation stress on cardiorenal metabolism, kidney and heart tissues from adult (P50) mice were extracted, weighed, and processed for metabolomic profiling by ^{1}H NMR spectroscopy.

Stress Procedure

Pups and their mothers were shipped from 7:30 am to 7:30 pm on P12. The shipment included 3.25-h of ground transportation and a 5-h flight as airfreight.

Metabolomic Analyses

Sample Collection and Preparation

Mice received an intraperitoneal overdose of sodium pentobarbital (150 mg/kg; Euthansol; Merck, QC, Canada). Kidney and heart tissues were extracted, weighed, and stored at

–80 ºC. To isolate water-soluble metabolites for NMR analysis, tissues were thawed at room temperature and subjected to methanol-based protein precipitation as well as chloroform-based lipid extraction (Bligh & Dyer, 1959). Finally, samples were centrifuged at 12,000 g for 5 minutes at 4 ºC to precipitate any particulate matter, and 550 µL of the supernatant was transferred to a 5-mm NMR tube for NMR analysis.

NMR Data Acquisition and Processing

Data were acquired using a 700 MHz Bruker Avance III HD spectrometer (Bruker, ON, Canada). Spectra were obtained using a Bruker triple resonance TBO-Z probe with the outer coil tuned to the nuclei of ^{1}H, ^{31}P and ^{2}H and the inner coil tuned to the ^{13}C nucleus. The standard Bruker 1-D NOESY gradient water suppression pulse sequence 'noesygppr1d' was used with a mixing time of 10 ms. Each sample was acquired with 128 K data points, a sweep width of 20.5136 ppm, and a recycle delay of 4 s. Tissue samples were run for 512 scans to a total acquisition size of 128 k. The resulting spectra were then zero filled to 256 k, line-broadened by 0.3 Hz, transformed to the frequency domain, phased, and baseline-corrected. Spectral processing was performed using the Bruker Topspin software (version 3.2, patch level 6), after which spectra were exported to MATLAB (MathWorks, MA, USA) for spectral binning, data normalization, and scaling. Spectra were binned using Dynamic Adaptive Binning (Anderson et al., 2011). Datasets were normalized using the Constant Sum method (Paxman et al., 2018) to remove effects of imperfect water signal suppression. The dataset was then Pareto-scaled (mean-centered and divided by the square root of each variable's standard deviation). All peaks were referenced to TSP (0.00δ).

Metabolite Identification

The Chenomx 8.2 NMR Suite (Chenomx Inc., AB, Canada) was used to identify metabolites present in tissue spectra. Metabolite identities were validated using the Human Metabolome Database (Wishart et al., 2012; Wishart, Knox, et al., 2008; Wishart et al., 2007).

Statistical Analyses

Spectral bins were first analyzed for all comparison groups and classified as either significant or non-significant using a decision tree algorithm (Goodpaster, Romick-Rosendale, & Kennedy, 2010) and a Mann-Whitney U test (Emwas et al., 2013). One hundred and seventy bins were initially included in the kidney analyses and 347 spectral bins were included in the heart analyses. All *p*-values obtained from these analyses were Bonferroni-Holm corrected for multiple comparisons. Variation in spectral data was visualized using Principal Component Analysis (PCA), Partial Least Squares Discriminant Analysis (PLS-DA), and Orthogonal Projection of Latent Structures Discriminant Analysis (OPLS-DA) using Metaboanalyst (Xia, Psychogios, Young, & Wishart, 2009; Xia, Sinelnikov, Han, & Wishart, 2015; Xia & Wishart, 2011, 2016). Double cross-validation and permutation testing (2,000 iterations) were performed to validate statistically significant PLS-DA and OPLS-DA results (Szymańska, Saccenti, Smilde, & Westerhuis, 2012; Westerhuis et al., 2008). Variable Importance in the Projection (VIP) analysis was performed and VIP plots were made using the weighted sum of squares of the PLS loadings.

Metabolite Set Enrichment Analysis (MSEA) and Pathway Topology Analysis were performed using Metaboanalyst. Metabolic pathway analysis identified the most relevant pathways (Xia & Wishart, 2010a) based on the Kyoto Encyclopedia of Genes and Genomes (KEGG) pathway database (*Mus musculus*) and the Over Representation Analysis (Paxman et

al., 2018) selected, using a hypergeometric test. The number of central squares entered by each animal in the open-field apparatus was related to metabolic changes using Pearson *R* correlations.

RESULTS

Tissue Phenotype

Multidimensional ELS led to abnormal kidney and heart weights. Specifically, absolute kidney weights were significantly increased [$t(21)=–3.194$, $p<0.01$] and relative heart weights were significantly decreased [$t(9.172)=3.175$, $p<0.01$] in stressed animals compared to non-stressed controls (Figures 1A and 1B).

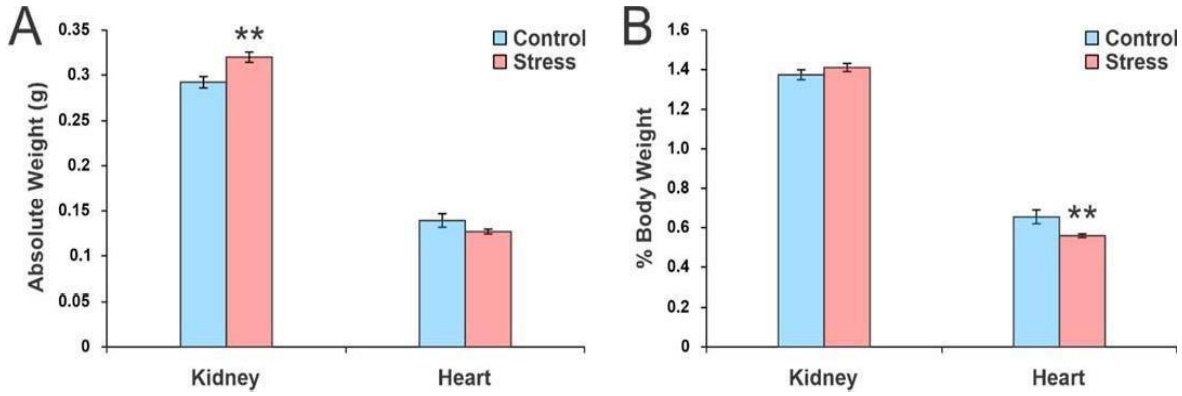

Figure 1. *Early life stress alters heart and kidney weights in adulthood. (**A**) Absolute organ weights. (**B**) Organ weights as a percentage of total body weight. Animals exposed to stress showed significantly increased absolute kidney weights and significantly decreased relative heart weights at P50 compared to non-stressed controls. Asterisks indicate significances: **p<0.01. Error bars represent ± SEM.*

Exploratory Statistical Analyses

The kidney and heart analyses included 170 and 347 spectral bins, respectively. A MW test was applied to each comparison group to identify which features (Chaddha et al.) led to univariate statistical differences between the groups. These analyses revealed 81 (47.6% of all spectral bins) and 241 (69.5% of all spectral bins) significantly altered features in kidney and heart tissues, respectively. Unsupervised multivariate PCA tests were initially performed using all features. In kidney tissues, separation of the groups was observed in the PCA scores plot, with principal components 1 and 2 accounting for 45.1% and 16.1% of the total variance, respectively (Figure 2). In heart tissues, no separation of groups was observed when considering all bins.

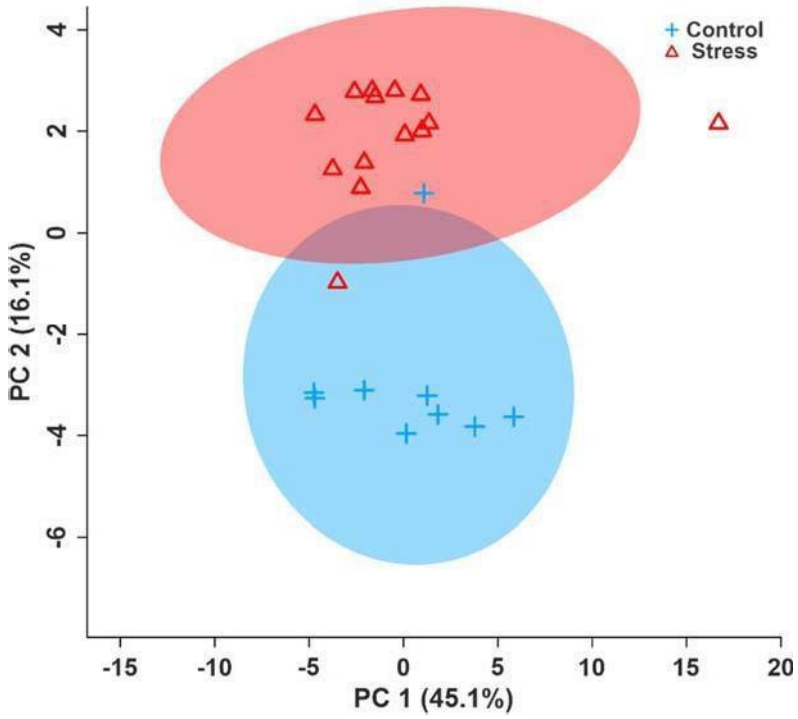

Figure 2. *PCA scores plot showing statistically significant unsupervised separation between adult mice exposed to early life stress and controls for kidney tissues. Each triangle or cross represents one individual under study, plotted using all kidney metabolites. The x- and y-axes show principal components 1 and 2, respectively. The percentages shown in brackets along each axis indicate the amount of data variance explained by that component.*

Supervised and unsupervised multivariate statistical tests were then performed using the bins identified as significant from the MW test. In both kidney and heart tissues, the unsupervised PCA scores plots show clear group separation, with principle component 1 being equal to 41.4% and 50.3% of the total variance and principle component 2 being equal to 18.3% and 31.4% of the total variance, respectively (Figures 3A and 3B). The scores plots from supervised PLS-DA (Figures 3C and 3D) and OPLS-DA (Figures 3E and 3F) tests also both display distinct group separation, supporting the PCA findings. Cross-validation and permutation tests validated the observed supervised separation results as a function of multidimensional ELS in both kidney (PLS-DA: $p<0.01$, R2=90.2%, Q2=83.9%; OPLS-DA: $p<0.001$, R2=94.9%, Q2=85.9%) and heart (PLS-DA: $p<0.01$, R2=74.4%, Q2=56.1%; OPLS-DA: $p<0.001$, R2=98.7%, Q2=95.5%).

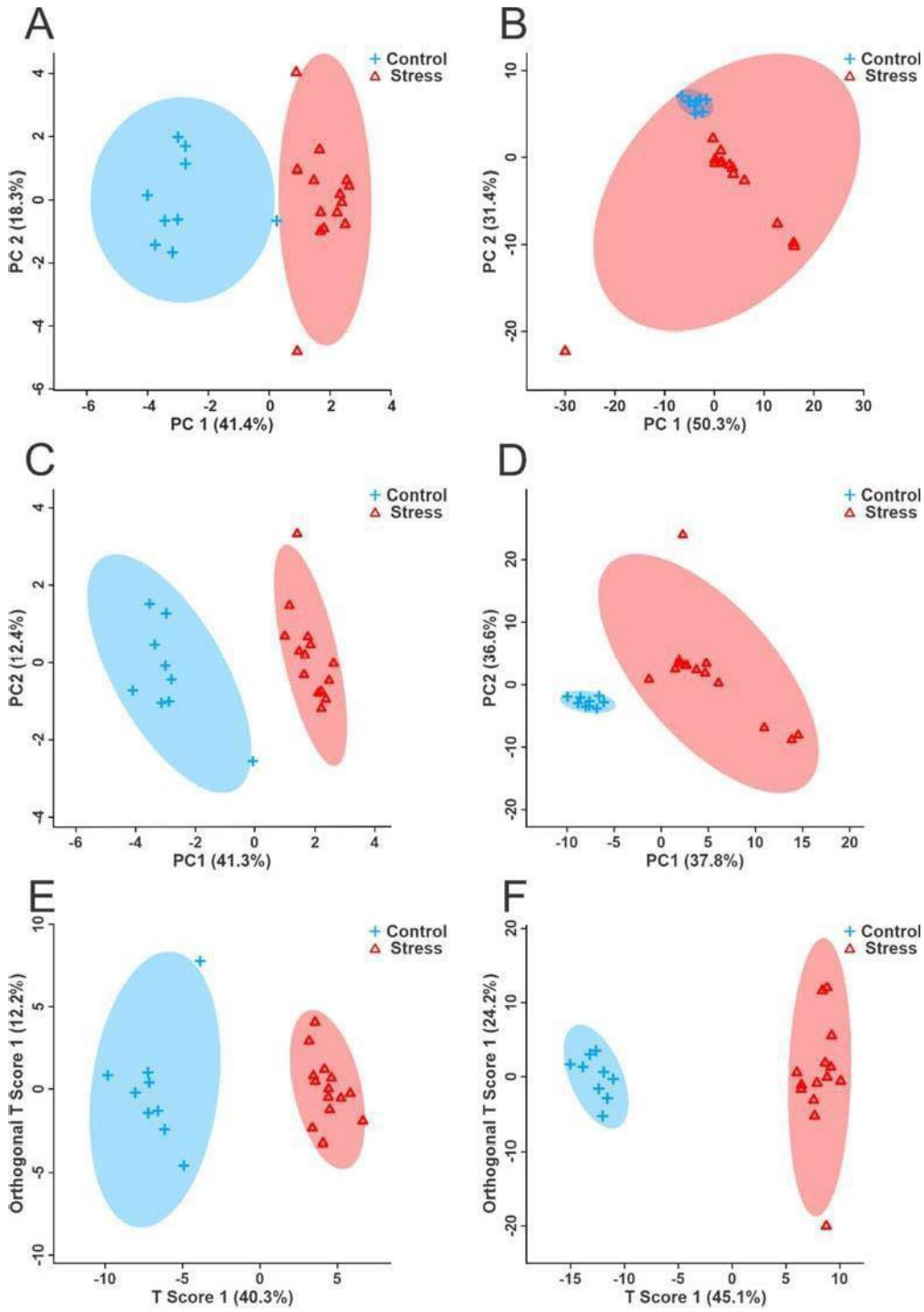

Figure 3. *PCA (**A, B**) PLS-DA (**C, D**) and OPLS-DA (**E, F**) scores plots showing statistically significant supervised separation between adult mice exposed to early life stress versus controls for both kidney (**A, C, E**) and heart (**B, D, F**) tissues. Each triangle or cross represents one individual under study, plotted using a list of kidney or heart metabolites found to be statistically significant by a MW test. For the PCA (**A, B**) and PLS-DA (**C, D**) plots, the x- and y-axes show principal components 1 and 2, respectively. For the OPLS-DA plots (**E, F**), the x- and y-axes show the variance explained across and within the groups, respectively. The percentages shown in brackets along each axis indicate the amount of data variance explained by that component.*

VIP plots (Figure 4) indicate which variables contributed most to the group separation observed in the PLS-DA scores plot. In kidney tissues, dimethylamine, uridine, and malate contributed most to the separation (Figure 4A), with VIP scores of 3.00, 1.61, and 1.58, respectively (Table 1). In heart tissues, glucuronate, adenosine, and uridine contributed most to the separation (Figure 4B), with VIP scores of 3.41, 2.80, and 2.66, respectively (Table 1). In kidneys, 22/44 (50.0%) unique, significantly altered metabolites (as determined by the MW test) were up-regulated in stressed animals compared to controls, with the remaining metabolites being down-regulated (Supplementary Table 1). In hearts, 54/82 (65.9%) unique, significantly altered metabolites were down-regulated in stressed animals compared to controls, with the remainder being up-regulated (Supplementary Table 1).

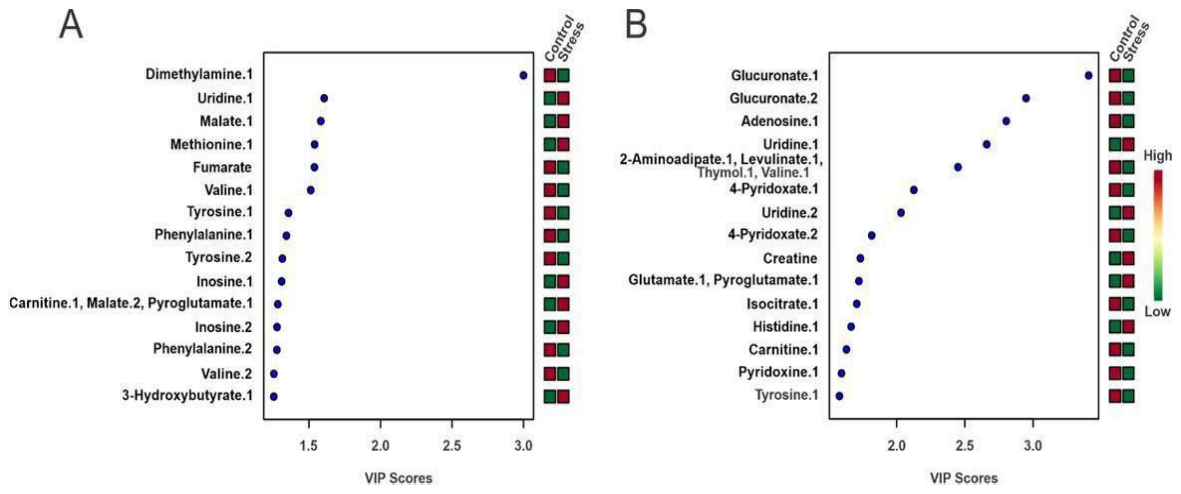

Figure 4. *VIP plots of adult mice exposed to early postnatal stress and controls, showing the relative contribution of metabolites. (**A**) Kidney tissues. (**B**) Heart tissues. High VIP values indicate greater contribution of these metabolites to group separation, shown in the PLS-DA plots. Green and red boxes indicate relative metabolite concentration. A VIP score of 1.0 is considered able to discriminate between two phenotypes.*

Functional Analyses

A genome-wide network model of mouse metabolism was used to investigate metabolite sets altered as a result of multidimensional ELS (Figures 5 and 6). In kidney tissues, early postnatal stress exposure most significantly affected arginine and proline metabolism ($p<0.001$), methylhistidine metabolism ($p<0.001$), as well as glycine and serine metabolism ($p<0.01$) (Figure 5A). Additionally, numerous energy metabolism systems were altered, including pathways in aminoacyl-tRNA biosynthesis ($p<0.00000001$), arginine and proline metabolism ($p<0.001$), alanine, aspartate, and glutamate metabolism ($p<0.001$), and valine, leucine, and isoleucine degradation ($p<0.05$) (Figure 5B). In heart tissues, multidimensional ELS most significantly altered methylhistidine metabolism ($p<0.01$), phosphatidylcholine biosynthesis ($p<0.01$), as well as glycine and serine metabolism ($p<0.01$) (Figure 6A). Pathway topology analyses (Figure 6B) revealed significant effects on aminoacyl-tRNA biosynthesis ($p<0.001$), glycine, serine, and threonine metabolism ($p<0.001$), histidine metabolism ($p<0.01$), and valine, leucine, and isoleucine biosynthesis ($p<0.05$).

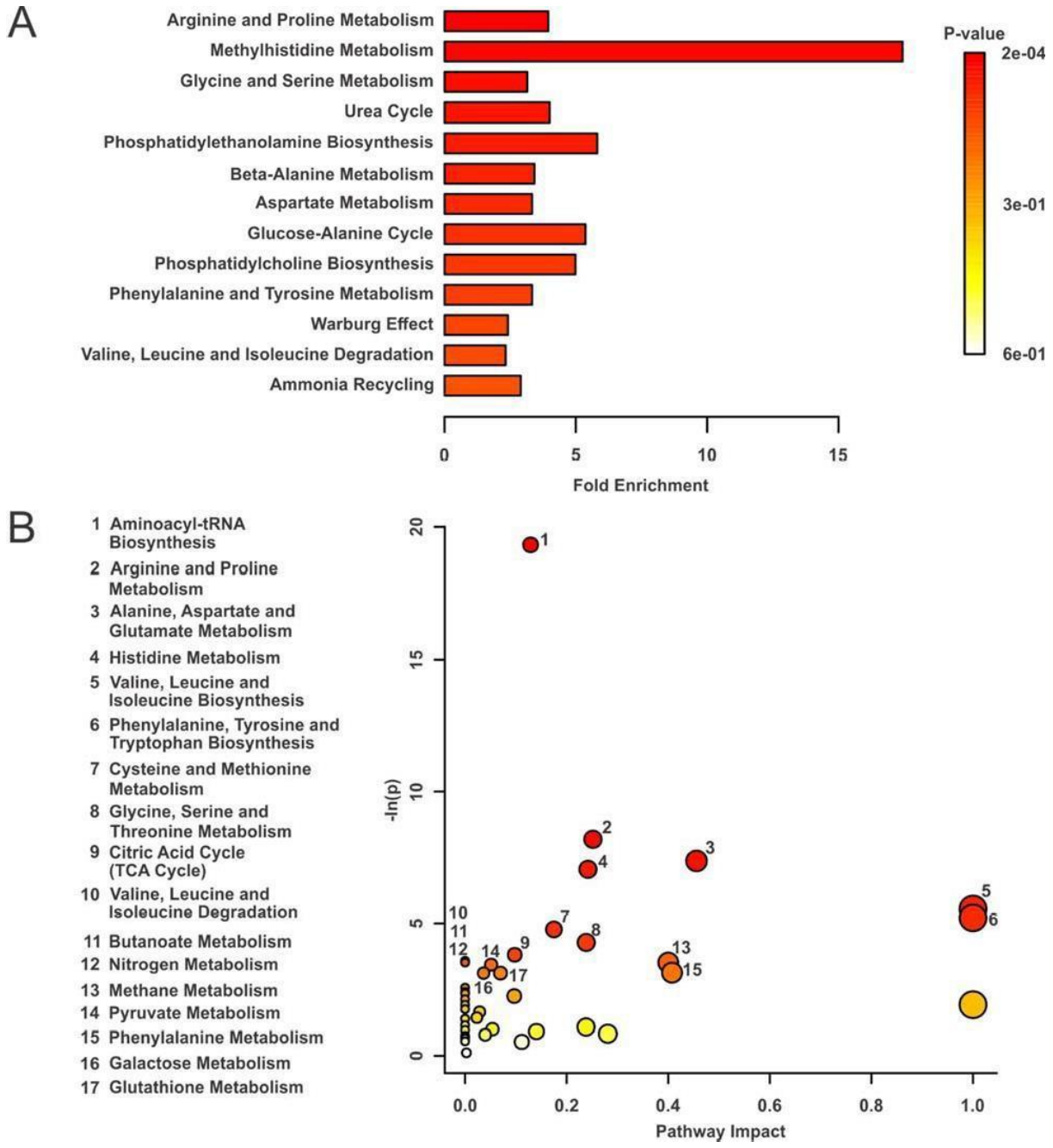

Figure 5. *(**A**) Metabolite Set Enrichment Analysis plot in adult mice exposed to early life stress. (**B**) Metabolomic Pathway Analysis showing all matched pathways according to p-values from pathway enrichment analysis and pathway impact values in kidney tissues. A higher value on the y-axis indicates a lower p-value. The x-axis gives the Pathway Impact. Only metabolic pathways with $p<0.05$ are labeled. This figure was created using the lists of metabolites identified as significant in a MW test.*

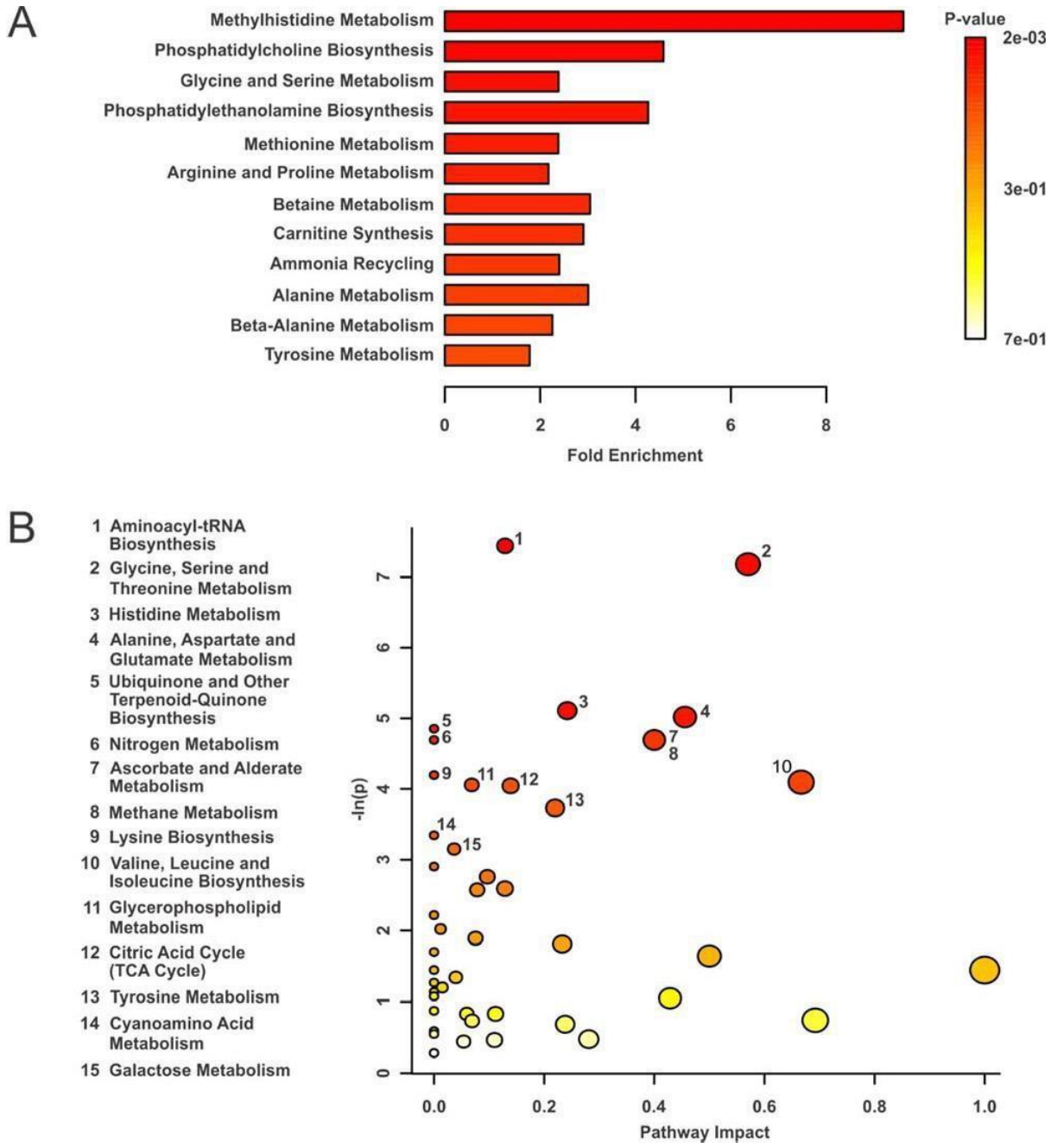

Figure 6. *(**A**) Metabolite Set Enrichment Analysis plot in adult mice exposed to early life stress. (**B**) Metabolomic Pathway Analysis showing all matched pathways according to p-values from pathway enrichment analysis and pathway impact values in heart tissues. A higher value on the y-axis indicates a lower p-value. The x-axis gives the Pathway Impact. Only metabolic pathways with $p<0.05$ are labeled. This figure was created using the lists of metabolites identified as significant in a MW test.*

Behavioural Phenotype

Open-field locomotor profiles revealed increased anxiety-like behaviour in stressed animals compared to non-stressed controls, as reflected by the number of squares traversed in the centre of the open-field arena. [$t(21)=3.069$, $p=0.0060$]. Sixteen and 117 features correlated significantly with increased anxiety-like behaviours in kidney and heart tissues, respectively (Supplemental Table 2). Of interest, the relationship between the number of central squares traversed and the relative concentrations of methionine, malate, and serine indicated a positive correlation for serine [$r=0.45$, $p=0.029$] and negative correlations for methionine [$r=–0.66$, $p=0.00066$] and malate [$r=–0.64$, $p=0.0011$] in kidney tissues (Figure 7A and Table 1). The relationship between the number of central squares traversed and the relative concentrations of malonate, lysine, and creatine indicated a negative correlation for creatine [$r=–0.52$, $p=0.011$] and positive correlations for malonate [$r=0.57$, $p=0.0050$] and lysine [$r=0.49$, $p=0.017$] in heart tissues (Figure 7B and Table 1).

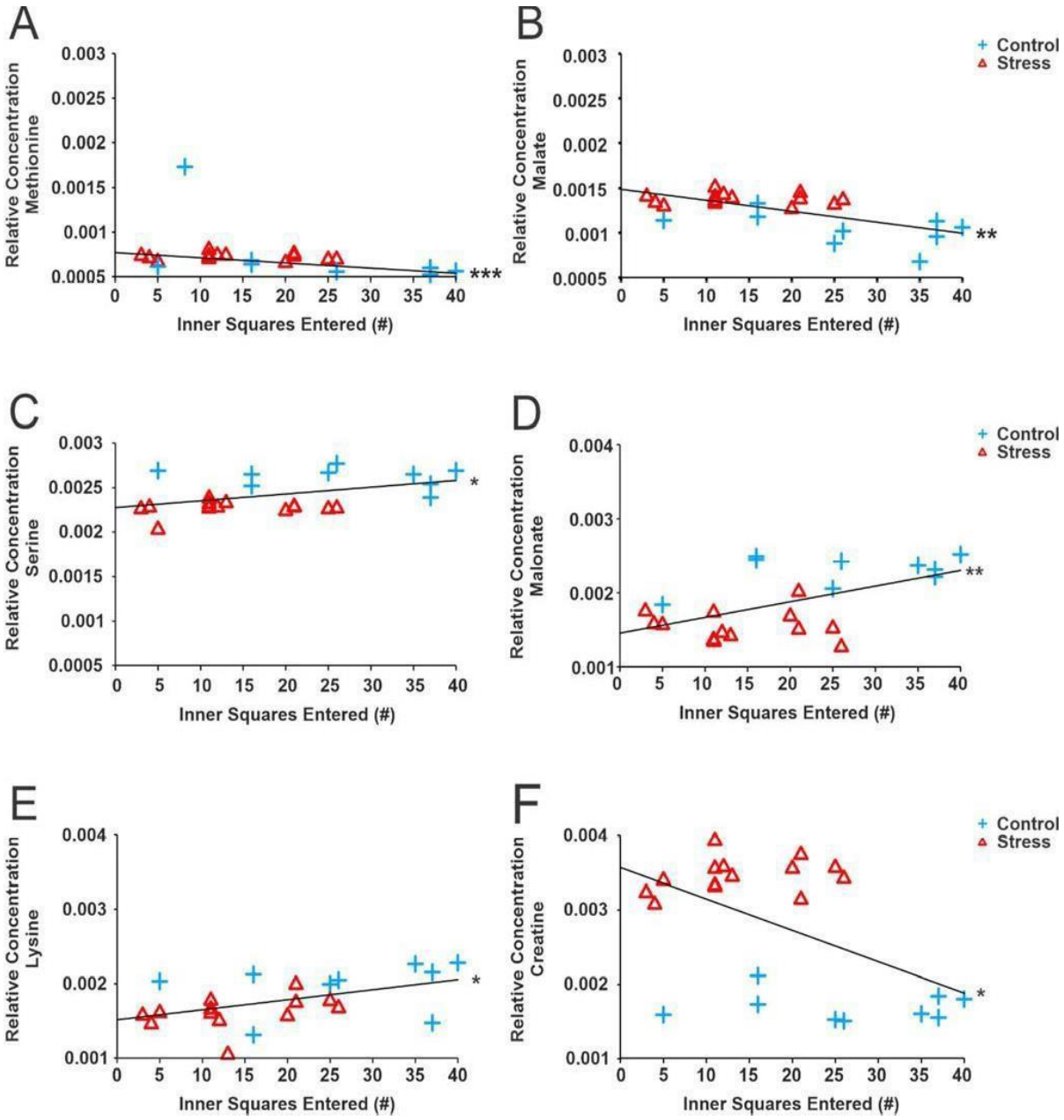

Figure 7. *Pearson correlations to assess the relationship between anxiety-like behaviour and the relative concentrations of (**A**) methionine, (**B**) malate, (**C**) serine, (**D**) malonate, (**E**) lysine, and (**F**) creatine in either kidney (**A, B, C**) or heart (**D, E, F**) tissues. There were negative correlations between the number of center squares entered and methionine (r=–0.66, p=0.0007), malate (r=–0.64, p=0.0011), and creatine (r=–0.52, p=0.0114), indicating that a higher anxiety-like state was linked to higher methionine, malate, and creatine concentrations. There were positive correlations between the number of center squares entered and serine (r=0.45, p=0.0293), malonate (r=0.57, p=0.0050), and lysine (r=0.49, p=0.0173), indicating that a higher anxiety-like state was linked to lower serine, malonate, and lysine concentrations.*

Organ	Metabolite	*r*	*p*	Correlation
Kidney	Methionine.1	–0.66	0.0007	Negative
	Malate.1	–0.64	0.0011	Negative
	Malate.3	–0.61	0.0019	Negative
	Glucose.1	0.60	0.0024	Positive
	2-Aminoadipate‡	0.57	0.0042	Positive
	Cystine	0.56	0.0057	Positive
	Dimethylamine.1	0.54	0.0076	Positive
	Glutamate.1‡, Methionine.2	–0.53	0.0097	Negative
	3-Hydroxybutyrate.1	–0.50	0.0150	Negative
	Glucose.3	0.49	0.0187	Positive
	Serine.1	0.45	0.0293	Positive
	Choline.5‡	–0.45	0.0307	Negative
	Choline.1‡	–0.44	0.0373	Negative
	Alanine‡	0.43	0.0425	Positive
	Glucose.4	0.43	0.0397	Positive
Heart	2-Hydroxybutyrate.1	0.65	0.0009	Positive
	Alanine.3‡, N-Phenylacetylglycine.2, O-Acetylcholine.1	–0.63	0.0012	Negative
	3-Hydroxyisovalerate.2	0.63	0.0014	Positive
	Cholate.1	0.61	0.0019	Positive
	Formate	0.61	0.0018	Positive
	Galactitol.1	0.61	0.0020	Positive
	Methylmalonate.2	0.61	0.0022	Positive
	Thymol.7	0.61	0.0018	Positive
	4-Pyridoxate.1	0.60	0.0025	Positive
	Cholate.3	0.60	0.0025	Positive
	3-Methylglutarate.1	0.60	0.0022	Positive
	Methylmalonate.1	0.59	0.0033	Positive
	Alanine.4‡, N-Phenylacetylglycine.4, O-Acetylcholine.2	–0.59	0.0033	Negative
	Glutamate.8‡	–0.59	0.0033	Negative
	2-Aminoadipate.1‡, Levulinate.1, Thymol.1, Valine.1	0.58	0.0038	Positive

Heart	Malonate.1	0.57	0.0050	Positive
	Creatine	–0.52	0.0114	Negative
	Lysine.1	0.49	0.0173	Positive

Table 1. *Kidney and heart metabolites found to be most significantly altered by stress in a Mann-Whitney U test. Top 20 VIP scores, shown in descending order, correspond to Fig. 3A, B. Metabolite regulation is shown as a function of relative concentration in high early postnatal stress individuals. Metabolites for which more than one NMR resonance peak was identified as significant are represented as metabolite.1, metabolite.2, … metabolite.n.*

[†]Indicates metabolites that were differentially regulated in both kidney and heart tissues.

Organ	Metabolite	NMR Chemical Shift Range of Bin (ppm)	Mann-Whitney U Test	Percent Difference	VIP Score	Regulation by Stress
Kidney	Dimethylamine.1†	2.771–2.756	8.25E-05	–86.21	3.00	Down
	Uridine.1†	4.344–4.320	1.82E-02	40.14	1.61	Up
	Malate.1†	2.653–2.639	1.38E-04	28.94	1.58	Up
	Methionine.1	2.639–2.630	1.07E-04	27.16	1.54	Up
	Fumarate†	6.533–6.519	1.82E-03	–34.74	1.54	Down
	Valine.1†	2.326–2.248	8.25E-05	–24.00	1.51	Down
	Tyrosine.1†	3.051–2.980	1.38E-04	–20.13	1.36	Down
	Phenylalanine.1	7.813–7.801	1.18E-03	–24.54	1.34	Down
	Tyrosine.2†	2.870–2.854	1.82E-03	–24.50	1.31	Down
	Inosine.1†	4.466–4.441	1.82E-02	–34.38	1.31	Up
	Carnitine.1†, Malate.2†, Pyroglutamate.1†	2.476–2.429	8.25E-05	18.03	1.28	Up
	Inosine.2†	6.817–6.806	2.53E-02	29.34	1.28	Up
	Phenylalanine.2	7.453–7.415	1.18E-03	–19.81	1.28	Down
	Valine.2†	1.058–1.029	1.82E-03	–19.24	1.26	Down
	3-Hydroxybutyrate.1	0.901–0.886	1.47E-03	22.37	1.25	Up
	Aspartate.1†	2.722–2.709	1.38E-04	–17.36	1.25	Down
	Phenylalanine.3	7.354–7.321	1.18E-03	–18.58	1.23	Down
	Acetate.1	1.967–1.873	5.97E-04	–17.93	1.23	Down
	Dimethylamine.2†	2.738–2.722	8.25E-05	–15.33	1.18	Down
	Aspartate.2†	2.697–2.686	8.25E-05	–15.24	1.17	Down
Heart	Glucuronate.1	4.675–4.663	7.51E-04	–149.75	3.41	Down
	Glucuronate.2	4.663–4.652	7.51E-04	–143.00	2.95	Down
	Adenosine.1	4.437–4.321	7.51E-04	–83.06	2.80	Down
	Uridine.1†	7.930–7.921	8.25E-05	137.40	2.66	Up
	2-Aminoadipate.1†, Levulinate.1, Thymol.1, Valine.1†	2.242–2.234	8.25E-05	–122.46	2.45	Down
	4-Pyridoxate.1†	7.938–7.930	8.25E-05	–131.59	2.13	Down

Heart	Uridine.2†	8.079–8.069	8.25E-05	94.58	2.03	Up
	4-Pyridoxate.2†	8.114–8.107	8.25E-05	–109.50	1.82	Down
	Creatine†	3.060–3.049	8.25E-05	69.32	1.73	Up
	Glutamate.1†, Pyroglutamate.1†	2.415–2.402	8.25E-05	71.47	1.72	Up
	Isocitrate.1	2.564–2.551	8.25E-05	–68.36	1.71	Down
	Histidine.1†	7.165–7.145	7.51E-04	83.75	1.67	Up
	Carnitine.1†	2.476–2.464	8.25E-05	–64.95	1.63	Down
	Pyridoxine.1	2.485–2.476	8.25E-05	–62.29	1.60	Down
	Tyrosine.1†	7.180–7.165	8.25E-05	–86.67	1.58	Down
	N-Methylhydantoin.1, N,N-Dimethylglycine.1, Trimethylamine.1	2.907–2.897	8.25E-05	–59.07	1.53	Down
	Carnitine.2†, 4-Pyridoxate.3†	2.464–2.453	8.25E-05	–56.71	1.51	Down
	Glutamate.2†, Pyroglutamate.2†, Succinate.1†	2.402–2.390	8.25E-05	55.08	1.50	Up
	Levulinate.2	2.789–2.771	8.25E-05	–57.44	1.48	Down
	Levulinate.3	2.771–2.754	8.25E-05	–54.01	1.47	Down

Table 2. *Kidney and heart metabolites found to be most significantly correlated to anxiety-like behaviour. Pearson correlations were used to assess the relationship between behaviours indicative of heightened anxiety (i.e., more central squares entered in the open field) and relative concentrations of metabolites found to be significantly altered by stress in a Mann-Whitney U test. Top 15 r values, shown in descending order, correspond to Fig. 5. In hearts, the bottom three entries correspond to additional metabolites shown to have an association with adverse mental health outcomes. Positive correlations indicate that a higher anxiety-like state was linked to lower metabolite concentrations, while negative correlations indicate that a higher anxiety-like state was linked to higher metabolite concentrations. Metabolites for which more than one NMR resonance peak was identified are represented as metabolite.1, metabolite.2, … metabolite.n.* ‡*Indicates metabolites that were significantly correlated to anxious behaviour in both kidney and heart tissues.*

DISCUSSION

The perinatal environment is a critical determinant of lifelong NCD risk (Boubred et al., 2013; Chaby et al., 2015; Gluckman et al., 2010). Here, we linked ELS to chronic cardiorenal metabolic pathologies in adulthood based on (i) organ weights, (ii) affective state, and (iii) altered metabolites and/or metabolic pathways linked to adverse mental health outcomes and metabolic illness, such as cardiorenal syndrome, insulin resistance, diabetes, and obesity. Many metabolites found to be significantly altered by stress belong to metabolic pathways involved in aminoacyl-tRNA biosynthesis, supporting a link between early environmental insults and NCD risk later in life

The findings indicate that ELS can cause cardiorenal remodeling. Changes in heart and kidney weights suggest a permanent reprogramming of physiological, metabolic, and transcriptomic processes manifesting as downstream alterations in cardiorenal phenotype and function (Barker, 1995; Bateson et al., 2004). Indeed, the development of renal pathology is associated with increased kidney weight (Everitt, Porter, & Wyndham, 1982). Absolute kidney weight in animals and humans is attributable to endothelial cell proliferation and intrarenal lipid deposition that impair intrarenal hemodynamics (Sata & Krum, 2010; Whaley-Connell, Pavey, Afroze, & Bakris, 2006). Stress-induced kidney hypertrophy is also correlated with higher blood pressure and subsequent hypertensive renal damage (Chen, Naftilan, & Oparil, 1992). Similarly, cardiac remodeling and hypertrophy are pathologically associated with NCDs such as diabetes, obesity, and CVDs (Gaspar-Pereira et al., 2012). By contrast, relative heart weight is decreased in diabetes due to myocyte loss and inadequate reactive hypertrophy of the remaining cells (Fiordaliso et al., 2000), which is also associated with deteriorated heart contractile function (Ma et al., 2010) and impaired insulin signaling (Jankyova et al., 2012). Thus, the present data

suggest and association between ELS and cardiac atrophy and risk of metabolic disorders such as diabetes.

Eighty-one metabolites present in kidney tissues and 241 metabolites present in heart tissues were significantly altered by ELS. In both heart and kidney, stress most drastically altered pathways involved in aminoacyl-tRNA biosynthesis. Thus, while changes in individual metabolites were not identical across tissue types, aggregate stress-induced metabolic changes ultimately led to a shared cardiorenal phenotype. Accordingly, previous work demonstrated mitochondrial dysfunction, cardiorenal pathologies, and impaired aminoacyl-tRNA biosynthesis in response to environmental insults (Jia, Aroor, Martinez-Lemus, & Sowers, 2015).

Several metabolites that obtained a significant VIP score in both heart and kidney tissues are involved in global hemodynamics. Abnormal levels of metabolites may mediate vasoconstriction and vasodilation, such as uridine and adenosine, and impair hemodynamics and hypertension (Macdonald, Assef, Guiffre, & Lo, 1984) and are risk factors for non-communicable cardiovascular and kidney diseases (Vasan et al., 2001; Yu et al., 2019). Uridine, which has a vasoconstrictive effect, was upregulated in both heart and kidney, while adenosine, an inhibitor of vasoconstriction, was downregulated. Indeed, hypertension is characterized by a sustained increase in total peripheral vascular resistance, suggestive of a primary cause in hypertension (Hall, 2003). In kidney, dimethylamine, a product of the hydrolysis of asymmetric dimethylarginine (Fliser et al., 2005), contributed to group separations. Kidneys are a major extraction site for asymmetric dimethylarginine (Nijveldt et al., 2002) and renal dysfunction promotes accumulation of asymmetric dimethylarginine and reduced dimethylamine (Fliser et al., 2005).

Multiple stress-responsive metabolites are involved in energy metabolism. Creatine, a natural regulator of energy homeostasis (Allen, 2012), was upregulated by stress and correlated strongly with increased anxiety-like behaviours. The Krebs cycle, taking place in the mitochondrial matrix, acts as a nexus for the integration of several catabolic and anabolic pathways. Abnormal levels of metabolites involved in the citric acid cycle, such as malate and malonate, can lead to mitochondrial dysfunction (Einat, Yuan, & Manji, 2005). Stress-induced divergent mitochondrial pathways have been implicated in the regulation of integrated central nervous system function, with aberrant energy metabolism playing a key role in the pathophysiological underpinnings of anxiety disorders (Einat et al., 2005; Finsterer, 2006). Oxidative stress, involved in the pathogenesis of mental health disorders (Bouayed, Rammal, & Soulimani, 2009), cardiovascular and kidney diseases (Cachofeiro et al., 2008), is caused by altered mitochondrial energy pathways leading to overabundance of oxidative stress compounds (Zhang et al., 2011). In both animals and humans, stress-induced anxiety alters levels of Krebs cycle intermediates, which subsequently exacerbates oxidative damage (Andreazza et al., 2008; Rezin, Amboni, Zugno, Quevedo, & Streck, 2009; Thurston & Hauhart, 1989).

In heart tissues, glucuronate, a product of the oxidative cleavage of myo-inositol catalyzed by myo-inositol oxygenase (Prabhu, Arner, Vunta, & Reddy, 2005), was highly significant in contributing to unsupervised and supervised separations. Both glucuronate and myo-inositol are involved in inositol metabolism, supporting the involvement of this biochemical pathway in the mediation of stress-induced metabolic changes. Abnormalities in inositol metabolism have been implicated in insulin resistance and long-term microvascular complications in diabetes (Croze & Soulage, 2013). In renal tissues, myo-inositol depletion has been associated with diabetic nephropathy through the activation of fibronectin (Croze &

Soulage, 2013). Myo-inositol has also been found to decrease in the prefrontal cortex and cerebrospinal fluid in affective disorders (Barkai, Dunner, Gross, Mayo, & Fieve, 1978; Coupland et al., 2005). Interestingly, glucuronate is markedly decreased in the urine of perinatally-stressed rats with atherosclerosis, suggesting a link to atherogenesis in ELS (Barderas et al., 2011).

The open-field observations revealed an anxiogenic effect of ELS. Increased anxiety-like behaviours observed in stressed animals correlated with the relative concentrations of serine and methionine in kidney. Stress downregulated serine, a co-agonist of ionotropic N-methyl-D-aspartic acid receptor activation (Otte et al., 2013) and involved in affective behaviour, with serine-depleted mice exhibiting more anxious behaviour and declined cognitive function (Basu et al., 2009). Conversely, elevated brain serine displayed is linked to anxiety-like behaviours, with chronic dietary serine supplementation also having anxiolytic consequences (Otte et al., 2013). Interestingly, plasma levels correlate with glomerular filtration ratio (Hesaka et al., 2019). The renal reabsorption of serine is sensitive to the presence of CKD, with the combination of plasma serine and urinary dynamics effectively distinguishing CKD from non-CKD (Hesaka et al., 2019).

Stress also upregulated methionine, a sulfur-containing donor of methyl groups (Chaturvedi, Kamat, Kalani, Familtseva, & Tyagi, 2016). Elevated methionine levels have been implicated in the pathogenesis of disorders linked to oxidative stress (Chaturvedi et al., 2016). In mice, a high-methionine diet is associated with oxidative stress in cardiac tissues due to increased levels of lectin-like oxidized low-density lipoprotein receptor-1 (LOX-1) and superoxide dismutase 1 (SOD1) (Chaturvedi et al., 2016). Abnormally high levels of methionine also have anxiogenic effects mediated by oxidative stress (Hassan, Eduardo Barroso Silva,

Mohammadzai, Batista Teixeira da Rocha, & Landeira-Fernandez, 2014). Thus, stress-induced methionine increases may provide a mechanism underlying the comorbidity of cardiorenal and affective disorders.

The increased prevalence of anxiety-like behaviours in stressed animals correlated with low concentrations of lysine in heart tissues. Lysine, a nutritionally essential amino acid (Smriga & Torii, 2003). In both animals and humans, prolonged dietary lysine inadequacy can elevate stress-induced anxiety while lysine fortification can reduce chronic anxiety (Smriga, Ghosh, Mouneimne, Pellett, & Scrimshaw, 2004). In a rural Syrian population, dietary lysine supplementation was found to lower blood cortisol levels and decrease sympathetic arousal in response to stress (Smriga et al., 2004). Anxiogenic consequences of lysine deficiency may be mediated by serotonin alterations in the central amygdala (Smriga, Kameishi, Uneyama, & Torii, 2002), with lysine acting as a partial serotonin receptor 4 antagonist (Smriga & Torii, 2003).

Since abnormal concentrations of lysine have been associated with diabetes (Wang et al., 2011) abnormal altered lysine metabolism may also be a factor in chronic disease etiology.

MSEA was used to identify patterns of metabolite concentration changes in a biologically meaningful framework (Xia & Wishart, 2010b). The most significant pathway altered in heart tissues was methylhistidine metabolism, with 3 metabolite hits, whereas in kidney tissues, this was the case for arginine and proline metabolism, with 9 metabolite hits. Significant pathways in the kidney MSEA, apart from arginine and proline metabolism, included methylhistidine metabolism as well as valine, leucine, and isoleucine degradation. In the heart MSEA, significant pathways included glycine and serine metabolism, methionine metabolism, and arginine and proline metabolism. 3-Methylhistidine, a constituent of actin and myosin released via protein degradation (Rooyackers & Nair, 1997), was upregulated in response to stress. Methylhistidine

metabolism serves as an indicator of muscle myofibrillar protein breakdown (Rooyackers & Nair, 1997), with an increase in 3-methylhistidine release in muscle atrophy (Attaix et al., 2005). Disruptions in methionine, glycine and serine metabolisms support the finding that stressed animals are at a higher risk for developing cardiorenal and affective disorders (Basu et al., 2009; Chaturvedi et al., 2016; Hassan et al., 2014; Hesaka et al., 2019). Furthermore, decreased arginine availability due to perturbed renal biosynthesis is causally implicated in nitric oxide deficiency, which contributes to cardiovascular events and kidney damage (Baylis, 2006).

Consistent with MSEA results and VIP scores, both heart and kidney pathway topology analyses revealed changes in valine, leucine, and isoleucine biosynthesis and degradation. This draws attention to a possible metabolic dysregulation of branched-chain amino acids (BCAAs) in stressed animals. Abnormal BCAA metabolism has been implicated in the pathogenesis of insulin resistance, obesity, and type 2 diabetes mellitus (Lynch & Adams, 2014). Altered concentrations of BCAAs promotes oxidative stress and inflammation of peripheral blood mononuclear cells via mTORC1 activation (Neinast, Murashige, & Arany, 2019; Zhenyukh et al., 2017), thus contributing to the pro-inflammatory and oxidative status observed in many pathophysiological conditions.

Stress also altered the aminoacyl-tRNA biosynthesis pathway, which is central for biosynthesis and kinetics of mRNA translation (Ferro, Liebeton, & Ignatova, 2017; Ibba & Söll, 2000). Accordingly, changes in aminoacyl-tRNA biosynthesis have been causally implicated in the pathogenesis of mitochondrial metabolic and congenital heart diseases (Da et al., 2014; Yao & Fox, 2013). In diabetes, both hyperglycemia and hyperinsulinemia stimulate the accumulation of mutations in mitochondrial tRNAs, the substrates of aminoacyl-tRNA synthetases, by

inducing oxidative stress (Park, Schimmel, & Kim, 2008). Altogether, the present results suggest that multidimensional ELS increases the risk for developing diabetes later in life.

CONCLUSION

The present findings provide novel insights into the mechanisms underlying early life stress-induced disease vulnerability by linking a cardiorenal metabolic stress phenotype to chronic heart and kidney dysfunction and impaired mental health. These changes arguably reflect underlying epigenetic modifications and associated cellular functions that manifest as downstream alterations to the metabolome. Clearly recognizable metabolic biomarkers of disease open new personalized medicine strategies for early detection and diagnosis of chronic NCDs.

CHAPTER 3: MULTIDIMENSIONAL EARLY-LIFE STRESS DRASTICALLY ACCELERATES VISUAL SYSTEM DEVELOPMENT & GLOBAL CEBEBRAL METABOLISM

INTRODUCTION TO EXPERIMENT 2

In order to investigate the effects of multidimensional early-life stress on developmental timing, stressed and control animals were tested for biomarkers of visual system development (the primary model of experience-dependent brain plasticity). Visual development was assessed via eye-opening (P13 to P15) and through two behavioural tests (visual cliff & virtual optomotry system) over the course of the critical period for visual cortical plasticity (P20 to P35). Global mRNA expression profiling was performed on visual cortices of stressed and control animals throughout adolescence and adulthood (P20, P35, and P50). Finally, to assess the effects of multidimensional early postnatal stress on brain metabolism, left and right cerebral tissues from shipped animals and controls were collected at P50 and subjected to global metabolomic profiling by ^{1}H NMR spectroscopy.

MATERIALS AND METHODS

Experimental Design

One hundred twenty-seven male C57BL/6 mice (*Mus musculus*) were used. The use of male mice minimized the potential impact of female hormonal fluctuations (Chrousos, Torpy, & Gold, 1998). Seventy-two of these animals came from an animal cohort bred and raised under consistent laboratory conditions at the local vivarium for at least four generations (Canadian Centre for Behavioural Neuroscience, University of Lethbridge, Lethbridge, AB, Canada). Fifty-five animals had been shipped from Charles River Laboratories (Charles River Laboratories, Inc., Saint-Constant, QC, Canada). These pups and their mothers were shipped from 7:30 am to 7:30 pm on P12. Mice were shipped concurrently to minimize variation in shipping environment. Pups remained with their mother until weaning at 9.6 grams, after which animals were housed in groups of at least two. Mice were housed under a 12:12-h light/dark cycle with light starting at

7:30 am. The room temperature was maintained at 22 °C. Standard mouse chow food and water were provided *ad libitum*. Stressed (n = 55) and control (n = 72) pups were inspected for eye-opening at 3:00 pm from P13 to P15. Visual acuity was assessed in a subset of these animals at 1:00 pm on P20, P28, and P35 using the virtual optomotor system (control, n = 12; stressed, n = 17). Similarly, visual development was assessed in a second subset of animals at 1:00 pm on P20 using the visual cliff test (control, n = 9; stressed, n = 14). Repeated behavioural tests were performed at the same time of day at each time point. To assess the impact of multidimensional early-life transportation stress on brain metabolism, left and right cerebral tissues from these mice were extracted, weighed, and processed for metabolomic profiling by ^{1}H NMR spectroscopy in adulthood (P50). To assess the impact of early-life stress on global mRNA expression profiles, visual cortices were collected from a third subset of animals at P20, P35, and P50 (n = 4/group) for transcriptomic analyses. Brains were collected from a fourth group of mice at P35 for immunohistochemical analyses to assess the effects of early-life stress on the abundance of biomarkers indicative of changes in the developmental trajectory of the primary visual cortex (n = 6/group).

Stress Procedure

Mice assigned to the shipment experience underwent a 12-h trip including 3.25-h of ground transportation and a 5-h flight as air freight on P12. Outdoor temperatures during transportation ranged from 20 to 25 °C.

Eye-Opening Observations

From P13 to P15, pups (control, n = 72; stressed, n = 55) were inspected for eye-opening daily at 3:00 pm. Eye-opening was defined as the initial break in the membrane sealing the lids of both eyes.

Behavioural Testing

Visual Cliff

The visual cliff apparatus was used to assess depth perception in offspring on P20 (Dräger & Hubel, 1978; Fox, 1965; Gibson & Walk, 1960; Nagy & Misanin, 1970; Sloane, Shea, Procter, & Dewsbury, 1978). The apparatus consisted of a clear, open-topped Plexiglass box (41.0 x 41.2 cm square x 30.4 cm high) positioned on the edge of a second box so that half of its base was in contact with a second box (the "shallow region") and half was suspended 30.4 cm above the table (the "deep region"). The border between the shallow and deep regions was referred to as "the cliff." A sheet of checkered fabric was placed between the two boxes and lined the table surrounding them. Each animal was placed facing the cliff at the centre of the shallow region furthest from the cliff and filmed for five minutes. The video recordings were analyzed for the total time spent in the deep region as a measure of cliff avoidance.

Virtual Optomotry System

The virtual reality-based optomotry system was used to assess visual acuity on P20, P28 and P35 (Prusky, West, & Douglas, 2000). Briefly, the animal was placed on an elevated platform surrounded by four computer monitors (43.2 x 43.2 cm). A camera imaged the animal from above, thus allowing for the observation of the animal's behaviour in response to a visual stimulus.

The visual stimulus consisted of a virtual cylinder covered by a sinusoidal grating of variable phase, contrast and spatial frequency. The phase of a sinusoidal grating was defined as the relative position of a sine wave within the receptive field, measured in degrees, while the spatial frequency of a visual stimulus refers to the level of detail present in that stimulus per degree of visual angle. Images with a lower spatial frequency therefore appear as a global pattern of light, while images with higher spatial frequencies feature details such as edges. This

sinusoidal grating was projected onto the monitors surrounding the animal using software (OptoMotry; CerebralMechanics, www.cerebralmechanics.com/CerebralMechanics_Inc./OptoMotry.html) running on an Apple Power Macintosh computer. From the point-of-view of the animals, the monitors appeared as large windows through which they could view the rotating sinusoidal grating. Animals were allowed to move freely on the elevated platform. The position of the animal's head was manually tracked throughout the duration of the testing period, and the resulting coordinates were used to automatically adjust the spatial frequency of the grating in response to the animal's point-of-view. Thus, the center of the cylinder was always defined as the position of the mouse's head, and the effective spatial frequency was calibrated accordingly.

A trial began when the center of the animal's head was identified after being placed in the apparatus. A rotating sinusoidal grating (12 degrees/s) then appeared, and it was judged whether the animal made slow, reflexive tracking movements with its head, neck, and body in such a manner as to track the rotating grating. Large repositioning and grooming movements were ignored, and the trial was restarted if it was not clear whether the animal was tracking the visual stimulus, or if the animal was clearly not tracking the stimulus. Each new trial was accompanied by a reversal in the direction of the grating's rotation.

Spatial frequency thresholds were obtained using a staircase method in which the spatial frequency of the sinusoidal grating was increased systematically until the animals were no longer able to track the stimulus. Specifically, the distance between vertical bars, or "step size," was halved after each reversal in direction, and the experiment was terminated when the step size became smaller than the hardware resolution (0.003 cycles/degree). The maximum spatial

frequency capable of eliciting head tracking for each animal was determined and will be referred to as the animal's "visual acuity."

Transcriptomic Analyses

Tissue Collection

Mice ($n = 4$/group) received an intraperitoneal overdose of sodium pentobarbital (150 mg/kg; Euthansol; Merck, QC, Canada). The brains were rapidly removed, and visual cortices dissected and flash-frozen (−80 °C) for global mRNA expression profiling. Norgen Biotek's Fatty Tissue RNA Purification Kit (Cat# 36200, Norgen Biotek, ON, Canada) was used to extract total RNA from visual cortices.

mRNA Analyses

mRNA analyses were performed using an Illumina GAIIx genomic analyzer (Illumina 462 Inc., San Diego, CA, USA) with multiplex. Every library was sequenced across 3 separate lanes, with base calling and demultiplexing performed using Illumina CASAVA 1.8.1 under default settings and Mouse - GRCm38 (Ensembl) used as a reference. Sequence and annotation information were downloaded from iGENOME (Illumina). Data from raw counts were uploaded onto R, where initial data exploration and outlier detection were performed using arrayQualityMetrics and DESeq2 bioconductor packages. Raw counts initially underwent normalization and variance stabilization as described in the DESeq2 manual. Hierarchical clustering analysis of transcriptional profiles was performed based on the top 100 most variable genes selected from a subset of highly-expressed genes (i.e., higher than the median expression). Clustering analysis was performed using the heatmap.2 function from the gplots package with the default clustering algorithm, with gene expression values displayed as heatmaps. Similarities between samples were also visualized as PCA plots generated using the

plotPCA function implemented in DESeq2. Outlier detection and transcriptional profile quality control was performed using the arrayQualityMetrics package.

Immunohistochemical Analyses

Tissue Collection

Brains were collected at P35 (n = 6/group) for immunohistochemical analysis. Animals were placed under 4% anesthesia immediately prior to receiving an intraperitoneal overdose of pentobarbital (150 mg/kg, Euthansol; CDMV Inc., Saint-Hyacinthe, QC, Canada). Mice were then intracardially perfused with 1M phosphate-buffered saline (PBS) and 4% paraformaldehyde (PFA; Sigma-Aldrich, St. Louis, MO), respectively. Brains were extracted and stored in 4% PFA for 24 hours at 4ºC, after which they were cryoprotected in a 30% sucrose solution at 4ºC (Fisher Scientific, Ottawa, ON). Brains were sectioned on a freezing microtome (AO Scientific Instruments, Buffalo, NY) at 40 µm.

Immunofluorescent Staining

Coronal brain sections collected at P35 underwent immunofluorescent staining for perineuronal nets (PNNs). For each brain, a 2:12 series of free-floating coronal sections was washed 6 times in 0.5% PBST for 7 minutes per wash. Tissue sections were subsequently incubated with Lectin from *Wisteria floribunda* in 1% BSA in 1M PBS for 18 hours at 4ºC (1:100; Sigma-Aldrich, St. Louis, MO). Sections were then washed 6 times in 0.5% PBST for 7 minutes per wash, incubated with Streptavidin, Alexa Fluor 633 conjugate in 1% BSA in 1.0 M PBS for 2 hours (1:2000; Fisher Scientific, Ottawa, ON), and 1% DAPI was added to the solution 20 minutes prior to the end of the incubation with secondary antibody (1:1000). Tissue sections were rinsed 6 times in 1.0 M PBS for 7 minutes per rinse and mounted on microscope slides with a fluorescent mounting medium.

All steps were done at room temperature unless otherwise specified. Specificity of the PNN antibody has been confirmed in mouse tissue (Brückner et al., 2000). The dilutions were further optimized, and non-specific labelling was controlled for by incubating sections with 1.0 M PBS instead of primary antibody. All negative controls resulted in the absence of immunoreactivity.

Stereological Cell Counts

Cell counting was performed by an experimenter blind to the treatment groups. Images were analyzed for cell number in the primary visual cortex (area V1) using the optical fractionator method (Bousquet et al., 2011; Glaser & Glaser, 2000). Sections were analyzed using the Stereo Investigator software (MicroBrightfield, Colchester, VT) integrated with a Zeiss Axio Imager M1 microscope (Carl Zeiss AG, Oberkochen, Germany) and a PCO SensiCam camera (PCO AG, Kelheim, Germany). The boundaries of the primary visual cortex were identified using the Allen Mouse Brain Atlas (Dong, 2008). After tracing the primary visual cortex using a 2.5x objective, a point grid was overlaid onto each section. Stereological cell counts were subsequently performed using a 40x objective. The counting variables were as follows: distance between counting frames, 150 x 150 μm; counting frame size, 70 x 70 μm; dissector height, 25 μm; guard zone thickness, 15%. Cells were counted only if they did not intersect forbidden lines.

Metabolomic Analyses

Sample Collection and Preparation

Mice received an intraperitoneal overdose of sodium pentobarbital (150 mg/kg; Euthansol; Merck, QC, Canada). Left and right cerebral tissues were extracted, weighed, and stored at –80 ^{o}C. To isolate water-soluble metabolites for NMR analysis, tissues were thawed at room temperature and subjected to methanol-based protein precipitation as well as chloroform-

based lipid extraction (Bligh et al., 1959). Specifically, deionized H_2O (4.85 mL/g), 99% methanol (4 mL/g; Sigma-Aldrich, MO, USA), and chloroform (4 mL/g; Sigma-Aldrich, MO, USA) were added to each tissue sample. Samples were homogenized and centrifuged at 1000 g for 15 minutes at 4 ºC. After centrifugation, 750 µL aliquots of supernatant were transferred to 2.0-mL centrifuge tubes and allowed to evaporate completely in a well-ventilated fume hood. Subsequently, 600 µL of phosphate buffer was added to each sample. The phosphate buffer was prepared as a 4:1 ratio of KH_2-PO_4:K_2HPO_4 in a 4:1 H_2O:D_2O solution to a final concentration of 0.5 M, with the D_2O containing 0.05% by weight trimethylsilyl propanoic acid (TSP) as a chemical shift reference. The overall buffer pH was titrated to 7.4 using 3 M HCl. To prevent bacterial growth, 0.02% w/v of sodium azide was added to the buffer solution. The samples were centrifuged at 12 000 g for 5 minutes at 4 ºC to precipitate any particulate matter, and 550 µL of the supernatant was transferred to a 5-mm NMR tube for NMR analysis.

NMR Data Acquisition and Processing

Data were acquired using a 700 MHz Bruker Avance III HD spectrometer (Bruker, ON, Canada). Spectra were obtained using a Bruker triple resonance TBO-Z probe with the outer coil tuned to the nuclei of ^{1}H, ^{31}P and ^{2}H and the inner coil tuned to the ^{13}C nucleus. The standard Bruker 1-D NOESY gradient water suppression pulse sequence ‘noesygppr1d’ was used with a mixing time of 10 ms. Each sample was acquired with 128 K data points, a sweep width of 20.5136 ppm, and a recycle delay of 4 s. Tissue samples were run for 512 scans to a total acquisition size of 128 k. The resulting spectra were then zero filled to 256 k, line-broadened by 0.3 Hz, transformed to the frequency domain, phased, and baseline-corrected. Spectral processing was performed using the Bruker Topspin software (version 3.2, patch level 6), after which spectra were exported to MATLAB (MathWorks, MA, USA) for spectral binning, data

normalization, and scaling. Spectra were binned using Dynamic Adaptive Binning (Anderson et al., 2011), manually inspected for binning errors, and corrected if any errors were found. Each spectrum had the area corresponding to water removed, after which the dataset was normalized using the Constant Sum method (Paxman et al., 2018) to remove effects of imperfect water signal suppression. The dataset was then Pareto-scaled (mean-centered and divided by the square root of each variable's standard deviation). All peaks were referenced to TSP (0.00δ).

Metabolite Identification

The Chenomx 8.2 NMR Suite (Chenomx Inc., AB, Canada) was used to identify metabolites present in tissue spectra. Metabolite identities were validated using the Human Metabolome Database (Wishart et al., 2012; Wishart, Knox, et al., 2008; Wishart et al., 2007).

Statistical Analyses

Spectral bins were first analyzed for all comparison groups and classified as either significant or non-significant using a decision tree algorithm (Goodpaster et al., 2010) and a Mann-Whitney U test (Emwas et al., 2013). Three hundred and twenty-one bins were initially included in the left cerebrum analyses and 353 spectral bins were included in the right cerebrum analyses. All *p*-values obtained from these analyses were Bonferroni-Holm corrected for multiple comparisons. Variation in spectral data was visualized using Principle Component Analysis (PCA) using Metaboanalyst (Xia, Broadhurst, Wilson, & Wishart, 2013; Xia, Mandal, Sinelnikov, Broadhurst, & Wishart, 2012; Xia et al., 2009; Xia et al., 2015; Xia, Sinelnikov, & Wishart, 2011; Xia & Wishart, 2002; Xia & Wishart, 2010a, 2010b, 2011, 2016).

MSEA and Pathway Topology Analysis were performed using Metaboanalyst to identify biochemical pathways altered in response to multidimensional ELS. Metabolic pathway analysis identified the most relevant pathways (Xia & Wishart, 2010a) based on the KEGG pathway

database (*Mus musculus*) and the Over Representation Analysis (Paxman et al., 2018) selected, using a hypergeometric test.

Statistical computations pertaining to eye-opening, visual behaviour, and immunohistochemistry were performed using SPSS (version 26.0, SPSS Inc., IL, USA). Mean values ± SEM were calculated for each measure. Visual cliff and immunohistochemical data were analyzed using independent samples *t* tests. Virtual optomotry system and eye-opening data were analyzed using two-way mixed ANOVAs, with Group (stressed and control) as the between-subjects factor and Time (P13, P14, and P15 for eye-opening; P20, P28, and P35 for virtual optomotry system data) as the within-subjects factor. Greenhouse-Geisser corrected *p*-values and Bonferroni corrections were utilized where appropriate. For eye-opening, the average number of eyes open per animal (from 0 to 2) was recorded. A *p*-value of less than 0.05 was chosen as the significance level.

For mRNA analyses, raw count data underwent normalization and regularized *log* transformation using statistical routines implemented in the DESeq2 bioconductor package (Love, Huber, & Anders, 2014) using default settings as described in the DESeq2 user manual. Pairwise comparisons between experimental groups were also performed using DESeq2. mRNAs with false discovery rate adjusted (FDA) *p*-values <0.1 were considered differentially expressed. All results are shown as the means ± standard error of the mean (±SEM).

Data pertaining to visual cliff avoidance in stressed animals relative to controls were then related to metabolic outcomes using the Pearson *r* correlations.

RESULTS

Exploratory Statistical Analyses

The left and right cerebral analyses included 321 and 353 spectral bins, respectively. A MW test was applied to each comparison group to identify which features (bins) led to univariate statistical differences between the groups. These analyses revealed 247 (76.9% of all spectral bins) and 305 (86.4% of all spectral bins) significantly altered features in left and right cerebral tissues, respectively. Unsupervised multivariate PCA tests were initially performed using all features. In left cerebral tissues, separation of the groups was observed in the PCA scores plot, with principal components 1 and 2 accounting for 55.1% and 20.7% of the total variance, respectively (Figure 8A). Separation of the groups was also observed in the PCA scores plot of right cerebral tissues, with principle components 1 and 2 accounting for 76.7% and 7.7% of the total variance, respectively (Figure 8B).

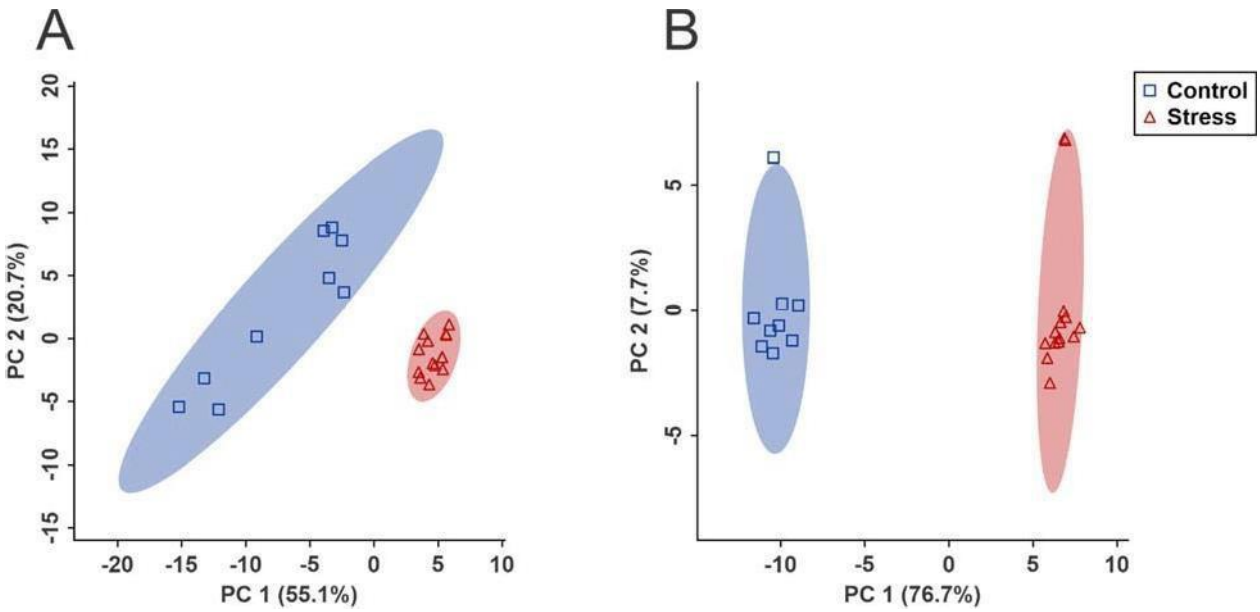

Figure 8. *PCA scores plots showing statistically significant unsupervised separation between adult mice exposed to early life stress and controls for left (**A**) and right (**B**) cerebra. Each triangle or square represents one individual under study, plotted using all cerebrum metabolites. The x- and y-axes show principal components 1 and 2, respectively. The percentages shown in brackets along each axis indicate the amount of data variance explained by that component.*

Supervised and unsupervised multivariate statistical tests were then performed using the bins identified as significant from the MW test. In both left and right cerebral tissues, the unsupervised PCA scores plots showed clear group separation, with principle component 1 being equal to 61.9% and 84.0% of the total variance and principle component 2 being equal to 17.8% and 4.8% of the total variance, respectively (Figures 9A and 9B). The heat maps presented in Figure 9 depict the relative concentrations of metabolites altered as a result of exposure to early postnatal transportation stress, providing a graphical indication of whether the metabolites were upregulated or downregulated with respect to the control group in left (Figure 9C) and right (Figure 9D) cerebral tissues. The dendrograms above the heat maps illustrate the results of unsupervised hierarchical clustering analysis, which was able to correctly classify animals according to their treatment group (Figures 9C and 9D).

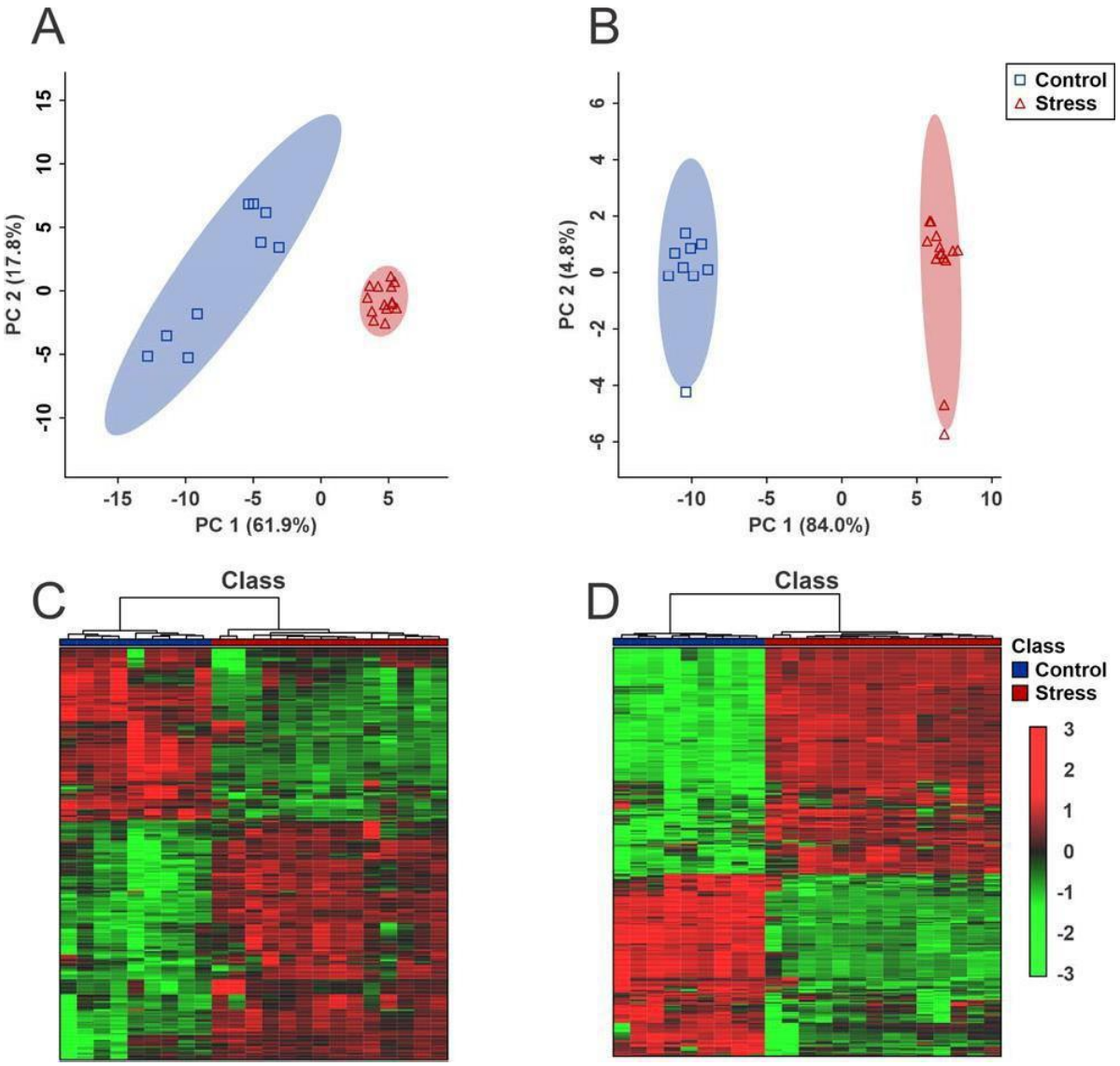

Figure 9. *PCA (**A, B**) scores plots and heat maps (**C, D**) showing statistically significant separation between adult mice exposed to early postnatal stress and controls for both left (**A, C**) and right (**B, D**) cerebra, plotted using a list of metabolites found to be statistically significant by a Mann-Whitney U-test. For the PCA plots (**A, B**), each triangle or square represents one individual under study. The x- and y-axes show principal components 1 and 2, respectively, with the percentages shown in brackets along each axis indicating the amount of data variance explained by that component. For the heat maps (**C, D**), the x- and y-axes show the class and individual spectral bins, respectively. These heat maps visually indicate either upregulation or downregulation of the metabolites presented in Table 3. The dendrogram at the top of each heat map illustrates the results of the unsupervised hierarchical clustering analysis.*

Percent differences reflect the degree of stress-induced changes in cerebral metabolites (Table 3). In left cerebral tissues, uracil, 2-aminoadipate, and adenosine had the largest changes relative concentration, with percent differences reaching 503.57, 68.96, and –55.10, respectively (Table 3). In right cerebral tissues, inosine, nicotinate, and methylmalonate had the largest changes in relative concentration, with percent differences reaching –108.20, –98.94, and –98.38, respectively (Table 3). In left cerebral tissues, 27/48 (56.3%) unique, significantly altered metabolites (as determined by the MW test) were up-regulated in stressed animals compared to controls, with the remaining metabolites being down-regulated (Supplemental Table 3). In right cerebral tissues, 31/63 (49.2%) unique, significantly altered metabolites were down-regulated in stressed animals compared to controls, with the remainder being up-regulated (Supplemental Table 3). Twenty-four unique, significantly altered metabolites were upregulated in both left and right cerebral tissues, while 19 unique, significantly altered metabolites were downregulated in both cerebral hemispheres (Supplemental Table 3).

Functional Analyses

A genome-wide network model of mouse metabolism was used to investigate metabolite sets altered as a result of multidimensional transportation stress (Figures 10 and 11). In left cerebral tissues, early postnatal stress exposure most significantly affected β-alanine metabolism ($p<0.001$), aspartate metabolism ($p<0.001$), as well as ammonia recycling ($p<0.01$) (Figure 10A). Additionally, numerous energy metabolism systems were altered, including pathways in aminoacyl-tRNA biosynthesis ($p<0.001$), alanine, aspartate, and glutamate metabolism ($p<0.001$), valine, leucine, and isoleucine biosynthesis ($p<0.01$), phenylalanine, tyrosine, and tryptophan biosynthesis ($p<0.01$), and D-glutamine and D-glutamate metabolism ($p<0.01$) (Figure 10B). In right cerebral tissues, early postnatal transportation stress most significantly

altered aspartate metabolism (p<0.001), β-alanine metabolism (p<0.01), as well as phenylalanine and tyrosine metabolism (p<0.01) (Figure 11A). Pathway topology analyses (Figure 11B) revealed significant effects on aminoacyl-tRNA biosynthesis (p<0.001), alanine, aspartate, and glutamate metabolism (p<0.001), histidine metabolism (p<0.001), and valine, leucine, and isoleucine biosynthesis (p<0.05).

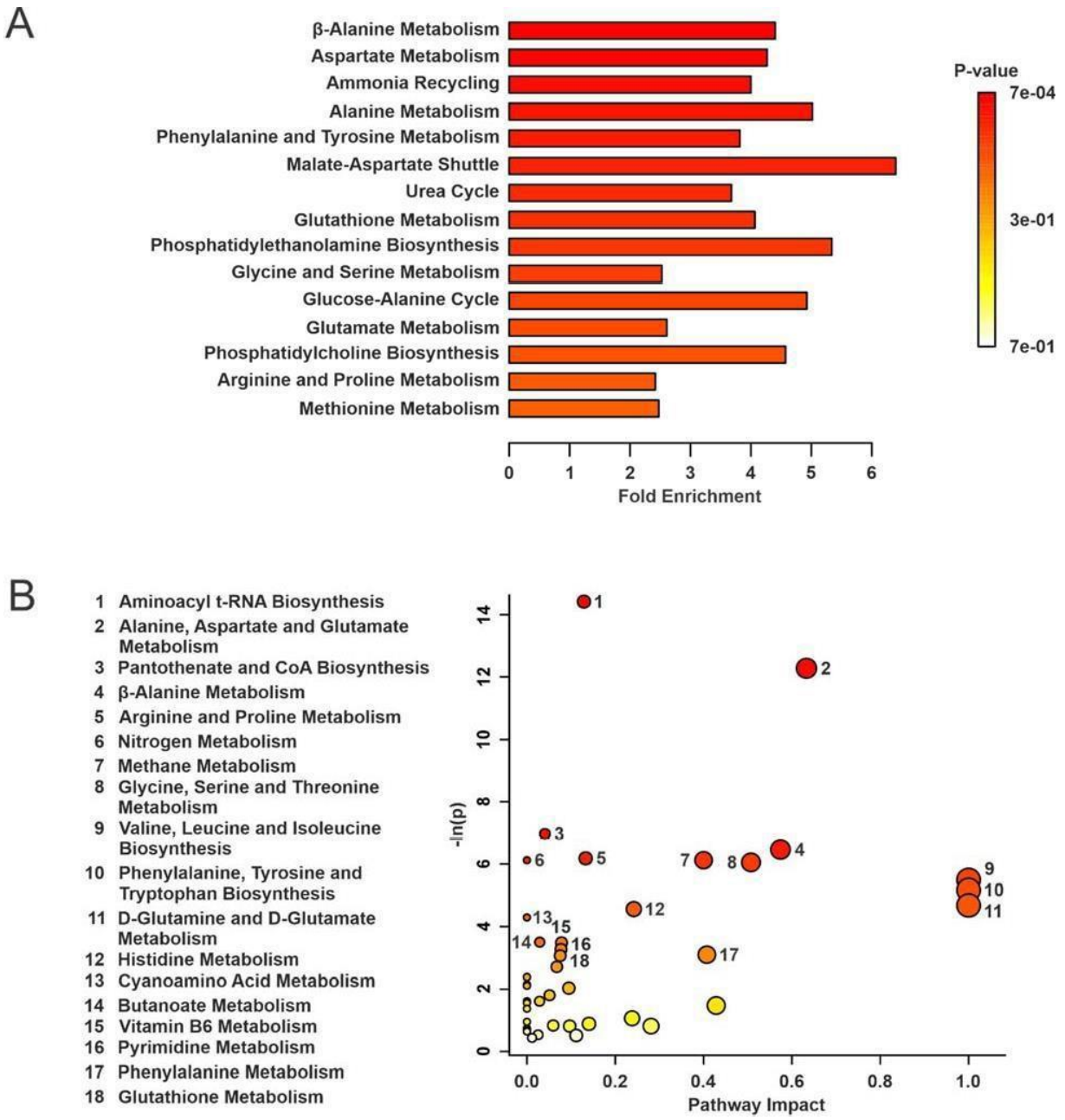

Figure 10. *(**A**) MSEA plot in adult mice exposed to early postnatal stress. (**B**) Metabolomic Pathway Analysis showing all matched pathways according to p-values from pathway enrichment analysis and pathway impact values in left cerebra of adult animals. A higher value on the y-axis indicates a lower p-value. The x-axis gives the Pathway Impact. Only metabolic pathways with $p < 0.05$ are labeled. This figure was created using the lists of metabolites identified as significant in a Mann-Whitney U test.*

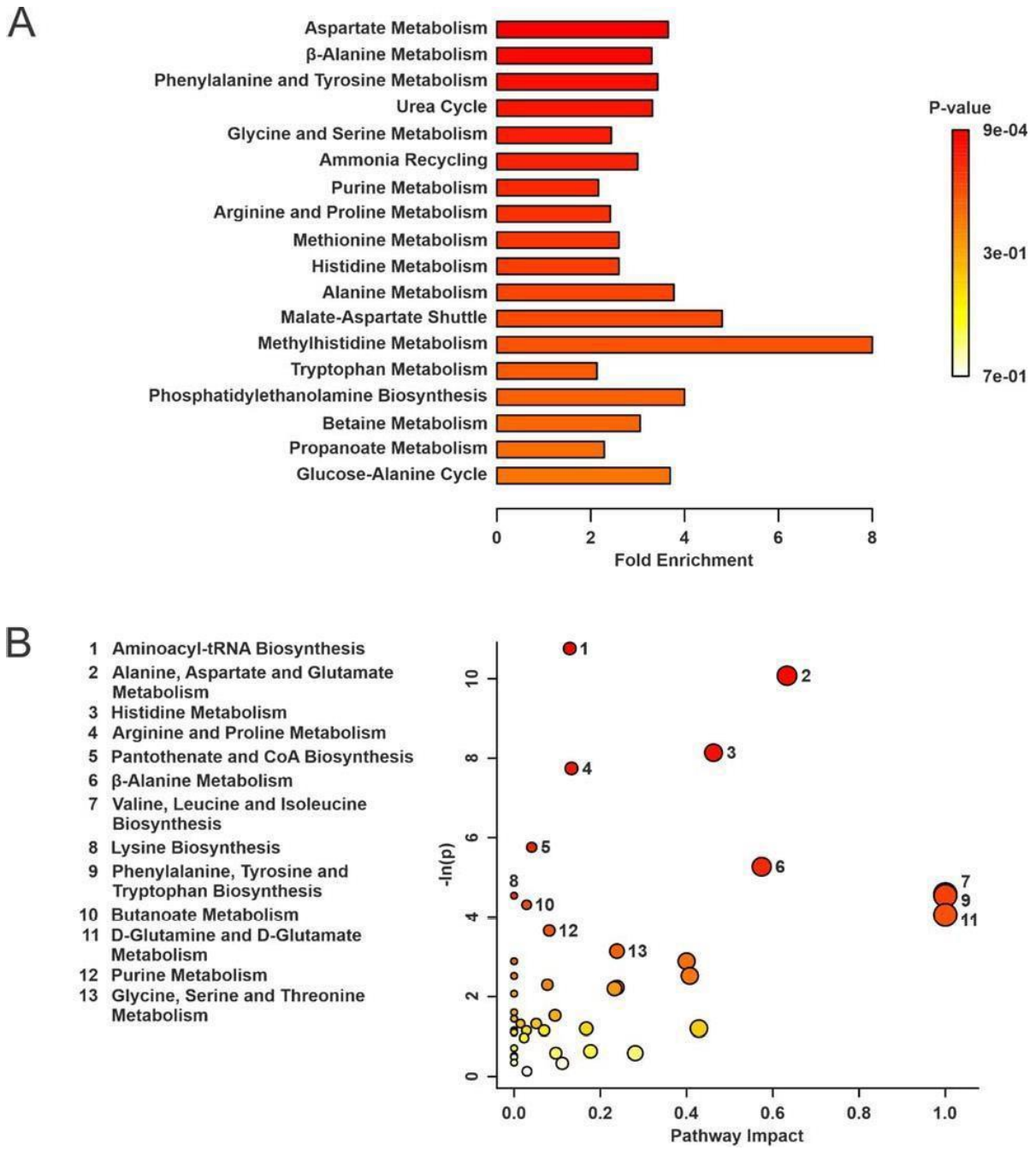

Figure 11. *(**A**) MSEA plot in adult mice exposed to early postnatal stress. (**B**) Metabolomic Pathway Analysis showing all matched pathways according to p-values from pathway enrichment analysis and pathway impact values in right cerebra of adult animals. A higher value on the y-axis indicates a lower p-value. The x-axis gives the Pathway Impact. Only metabolic pathways with $p < 0.05$ are labeled. This figure was created using the lists of metabolites identified as significant in a Mann-Whitney U test.*

Behavioural Phenotype

Visual Cliff

The distinct metabolic profiles of multidimensionally stressed and control groups were correlated with precocious visual behaviour in adolescent animals. Specifically, behavioural profiles suggest a precocious maturation of depth perception in stressed animals compared to non-stressed controls, as reflected by increased visual cliff avoidance at the start of the critical period for visual cortical plasticity (P20). Stressed (M 36.5, SD 27.7) mice exhibited a significant decrease in the time spent in the deep side of the visual cliff relative to control (M 106.6, SD 43.7) animals [$t(21) = 4.730$, $p<0.001$] (Figure 6B). Pearson r correlations revealed 172 (53.6% of all spectral bins) and 279 (79.0% of all spectral bins) altered features significantly correlated with increased visual cliff avoidance in left and right cerebral tissues, respectively (Supplemental Table 4). In both left and right cerebral tissues, the relationship between the time spent in the deep side of the visual cliff and the relative concentrations of several metabolites revealed either significant positive or negative correlations between metabolite levels and visual cliff avoidance. Notably, the relationship between the time spent in the deep side of the visual cliff and the relative concentrations of aspartate, glutamate, and tyrosine indicated a negative correlation for aspartate [$r = –0.78$, $p<0.001$] and positive correlations for glutamate [$r = 0.75$, $p<0. 001$] and tyrosine [$r = 0.73$, $p<0.001$] in left cerebral tissues (Figures 12A, 12B, 12C and Table 4).

Similarly, the relationship between the time spent in the deep side and the relative concentrations of inosine, N-acetylaspartate, and β-alanine indicated a negative correlation for β-alanine [$r = –0.76$, $p<0.001$] and positive correlations for inosine [$r = 0.75$, $p<0.001$] and N-acetylaspartate [$r = 0.77$, $p<0.001$] in right cerebral tissues (Figures 12D, 12E, 12F, and Table 4).

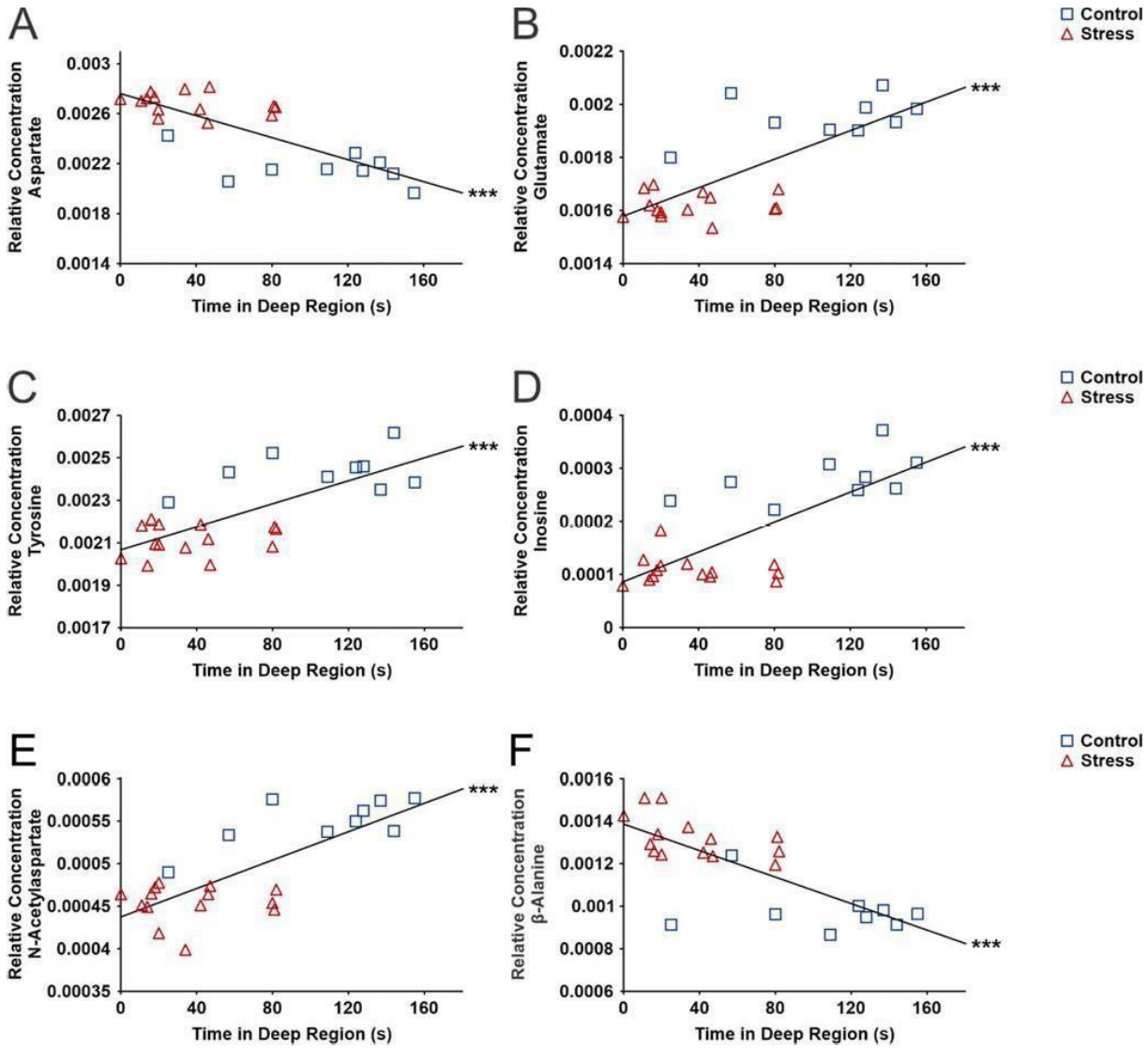

Figure 12. *Pearson correlations to assess the relationship between precocious development of depth perception (i.e., time spent in the deep region of the visual cliff apparatus) and the relative concentrations of (**A**)aspartate, (**B**) glutamate, (**C**) tyrosine, (**D**) inosine, (**E**) N-acetylaspartate, and (**F**) β-alanine in either left (**A, B, C**) or right (**D, E, F**) cerebra. There were negative correlations between the time spent in the deep region and aspartate (r = –0.78, p = 0.000012) and β-alanine (r = –0.76, p = 0.000027), indicating that precocious visual development was linked to higher aspartate and β-alanine concentrations. There were positive correlations between the time spent in the deep region and glutamate (r = 0.75, p = 0. 000043), tyrosine (r = 0.73, p = 0.000077), inosine (r = 0.75, p = 0.000044), and N-acetylaspartate (r = 0.77, p = 0.000020), indicating that precocious visual development was linked to lower glutamate, tyrosine, inosine, and N-acetylaspartate concentrations.*

Virtual Optomotor System

During development (P20, P28, P35), a statistically significant main effect of Age was found for visual acuity, with older mice displaying an increase in visual acuity relative to younger mice (Figure 13D; $F(1.493, 40.311) = 8.131$, $p<0.01$). Further pairwise comparisons revealed that visual acuity significantly increased from P20 to P28 ($p<0.05$) and from P20 to P35 ($p<0.01$). A significant main effect of Group was also found for visual acuity ($F(1, 27) = 149.933$, $p<0.001$), indicating that stressed animals displayed increased visual acuity relative to controls.

Eye-Opening Phenotype

A statistically significant interaction between Age and Group was found during development (P13 to P15), indicating that stressed animals displayed precocious eye opening relative to controls ($F(1.650, 206.214) = 23.339$, $p<0.001$). A statistically significant simple main effect of Age was found for eye opening, with older mice displaying a higher number of eyes open relative to younger animals in both stressed (Figure 13A; $F(1.296, 69.976) = 5.252$, $p<0.05$) and control ($F(1.670, 118.588) = 45.631$, $p<0.001$) groups. Further pairwise comparisons revealed that more eyes were open in P14 compared to P13 in both stressed ($p<0.05$) and non-stressed ($p<0.001$) animals as well as in P15 compared to P13 in both stressed ($p<0.05$) and non-stressed ($p<0.001$) animals. A significant simple main effect of Group was also found for eye-opening, with stressed animals displaying accelerated eye-opening relative to controls at P13 ($F(1, 125) = 59.767$, $p<0.001$), P14 ($F(1, 125) = 16.751$, $p<0.001$), and P15 ($F(1, 125) = 11.705$, $p<0.001$).

Immunohistochemical Analyses

Multidimensional early-life stress led to an increased abundance of PNN-expressing cells (as indicated by WFA-staining) in the primary visual cortex of adolescent animals (Figure 13C). Specifically, the number of PNN-expressing cells in the primary visual cortex was significantly higher in stressed animals relative to non-stressed controls at the closure of the critical period for visual cortical plasticity [$t(10) = -3.095$, $p<0.05$].

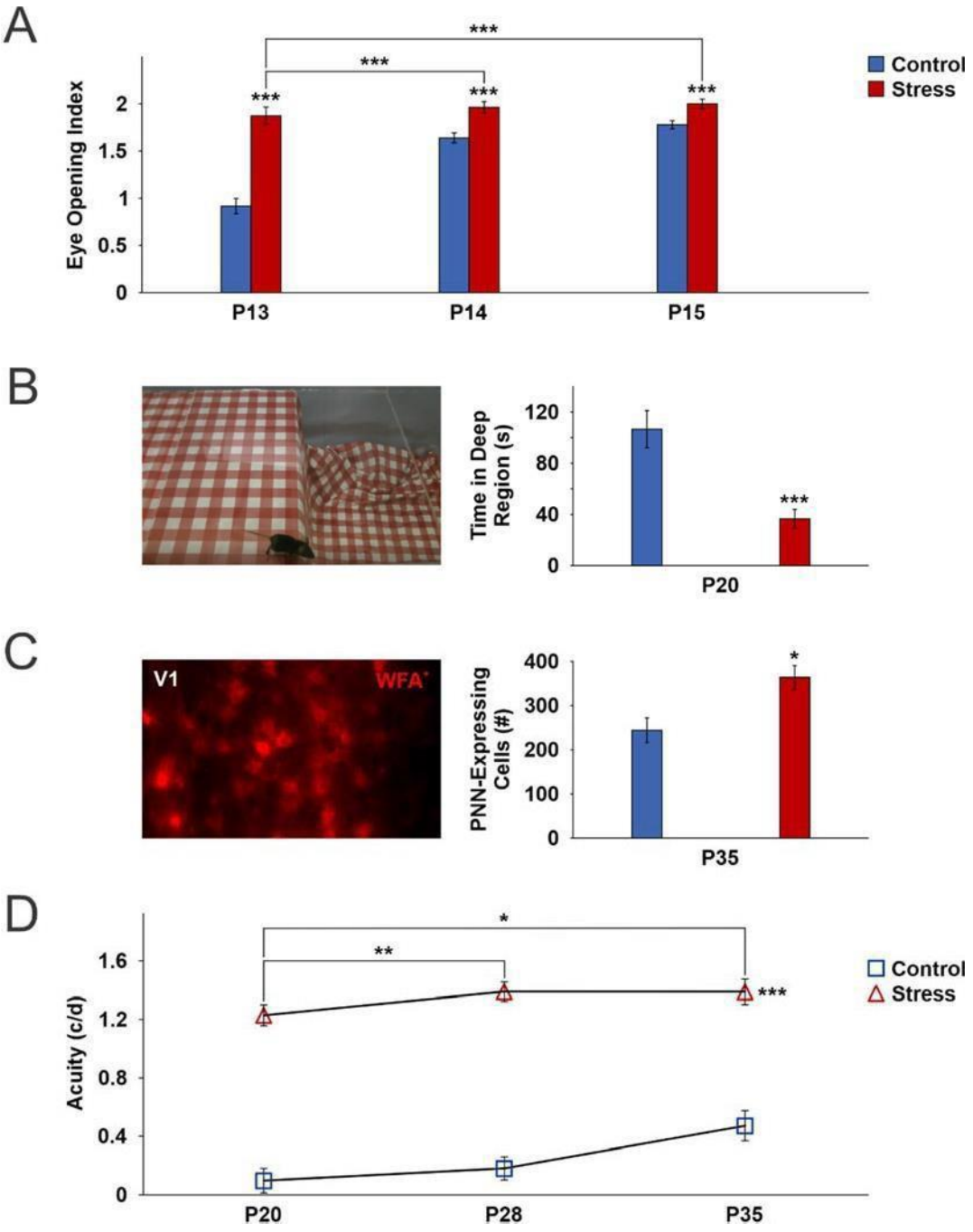

Figure 13. *Multidimensional stress induces precocious development of the visual system. (**A**) Eye Opening Index throughout early adolescence showing accelerated eye-opening in multidimensionally-stressed animals at P13, P14 and P15. (**B**) Photograph of a mouse in the shallow region of the visual cliff apparatus, observed to measure the precocious development of depth perception. Stressed animals spent significantly less time in the deep region of the apparatus, indicating increased perception of the visual cliff. (**C**) Photograph of WFA^+ cells, indicating the presence of PNNs, in the primary visual cortex of an adolescent mouse. Stressed animals showed an increased abundance of PNN-expressing cells at the closure of the critical period for visual system development relative to non-stressed controls. (**D**) Stressed animals showed improved visual performance relative to non-stressed controls in the visuospatial testing box as measured by the optokinetic reflex. Asterisks indicate significances: *p < 0.05, **p < 0.01, p < 0.001. Error bars represent ± SEM.*

Transcriptomic Analyses

The main mRNAs that were differentially regulated by multidimensional early-life stress are summarized in Figure 14 and Table 5. After adjusting *p*-values using the Benjamini and Hochberg correction (Benjamini, Drai, Elmer, Kafkafi, & Golani, 2001), global mRNA expression profiles revealed that 13 mRNAs (P20: 3, P35: 7, P50: 3) were differentially expressed in response to early-life stress. These included Mgat5b (FDR $p<0.05$), Faim2 (FDR $p<0.01$), and Hlf (FDR $p<0.05$). Other mRNAs that approached significance included Lin7b (FDR $p = 0.099$), Gas6 (FDR $p = 0.099$), and L1cam (FDR $p = 0.063$) (upregulated due to stress) as well as Dusp1 (FDR $p = 0.099$) and Vhl (FDR $p = 0.010$) (downregulated due to stress). Importantly, exposure to multidimensional early-life stress dynamically regulates mRNA expression across development, with unique mRNAs altered in response to stress at P20, P35, and P50.

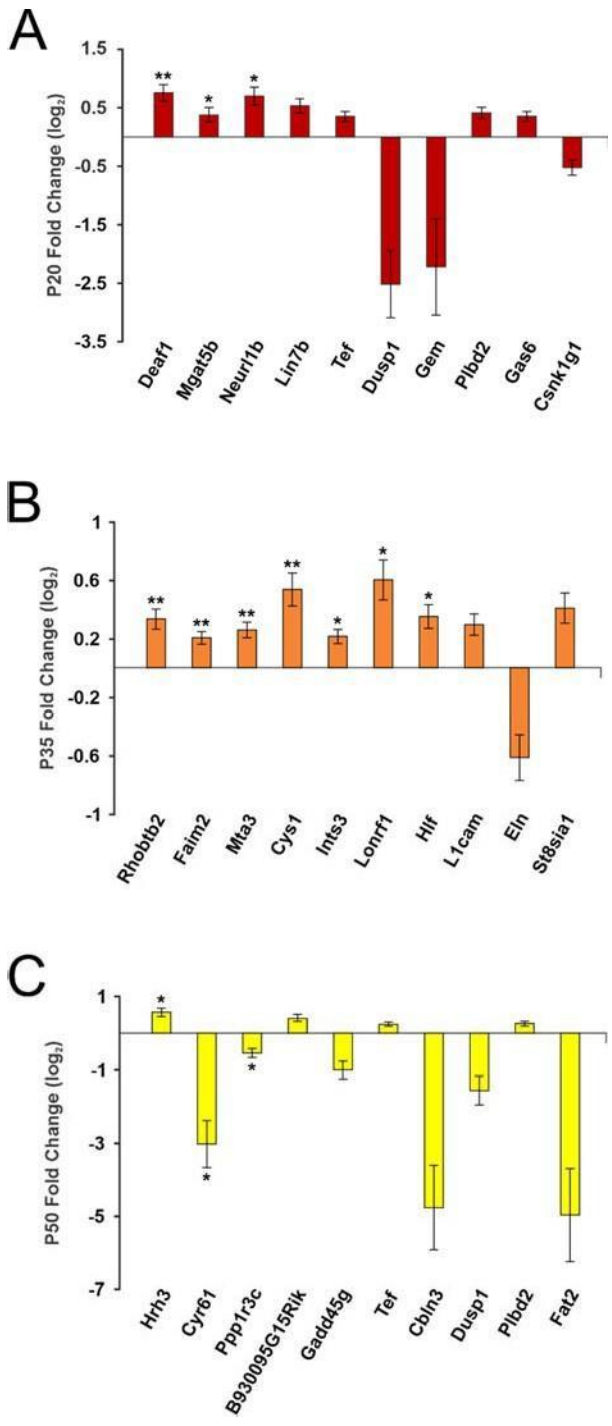

Figure 14. *Multidimensional early postnatal stress programs mRNA expression profiles across development. Fold changes (log_2) of mRNA in P20 (**A**), P35 (**B**), and P50 (**C**) stressed animals in reference to controls. Note that early postnatal stress led to up- or down-regulation of unique mRNA transcripts across development. Asterisks denote significances (FDR-adjusted; *p < 0.05, **p < 0.01). Error bars represent ± SEM.*

Region	Metabolite	NMR Chemical Shift Range of Bin (ppm)	Mann-Whitney U Test	Percent Difference	Regulation by Stress
Left Cerebrum	Uracil.1*	5.253–5.248	1.53E-02	503.57	Up
	Uracil.2*	5.258–5.253	1.53E-02	420.13	Up
	Uracil.3*	5.414–5.406	1.82E-02	200.28	Up
	Singlet 3.055 ppm	3.060–3.049	8.25E-05	–72.52	Down
	2-Aminoadipate.1*	2.243–2.234	8.25E-05	68.96	Up
	Agmatine.1*, Phenylalanine.1*, Taurine.1*	3.268–3.249	8.25E-05	62.38	Up
	Adenosine.1*	8.268–8.259	8.25E-05	–55.10	Down
	Uracil.4*	5.820–5.814	8.25E-05	54.35	Up
	Adenosine.2*	6.119–6.108	8.25E-05	–52.74	Down
	Uracil.5*	5.809–5.803	8.25E-05	51.82	Up
	Adenosine.3*	6.108–6.097	1.07E-04	–51.29	Down
	Adenosine.4*	8.378–8.354	8.25E-05	–48.99	Down
	Nicotinurate.1*	8.561–8.547	8.25E-05	44.55	Up
	Histidine.1*	7.166–7.155	8.25E-05	44.49	Up
	Glutamate.1*	2.358–2.348	8.25E-05	–44.31	Down
	Glutamate.2*	2.348–2.336	8.25E-05	–43.76	Down
	Adenosine.5*	4.457–4.449	8.25E-05	–43.51	Down
	Formate*	8.475–8.453	8.25E-05	–43.31	Down
	Choline.1*	3.492–3.480	1.38E-04	42.05	Up
	Ethanolamine.1*, Homoserine.1*, Uridine.1*	3.818–3.811	8.25E-05	41.81	Up
Right Cerebrum	Inosine.1	6.119–6.108	8.25E-05	–108.20	Down
	Inosine.2	6.108–6.097	8.25E-05	–106.69	Down
	Adenosine.1*, Inosine.3	8.378–8.354	8.25E-05	–102.02	Down
	Nicotinate.1	8.268–8.259	8.25E-05	–98.94	Down
	Methylmalonate.1	1.194–1.185	8.25E-05	–98.38	Down

Right Cerebrum	Uracil.1*	5.820–5.814	8.25E-05	91.81	Up
	Uracil.2*	5.809–5.803	8.25E-05	90.99	Up
	Inosine.4	6.097–6.088	8.25E-05	–87.98	Down
	Phenylalanine.1*	7.440–7.429	8.25E-05	86.76	Up
	Leucine.1*	0.980–0.948	8.25E-05	86.52	Up
	Phenylalanine.2*	7.352–7.337	8.25E-05	85.08	Up
	Phenylalanine.3*	7.429–7.418	8.25E-05	82.90	Up
	3-Phenylpropionate.1*, Phenylalanine.4*	7.337–7.324	8.25E-05	82.12	Up
	Tryptophan.1	7.166–7.155	8.25E-05	80.51	Up
	N-Acetylaspartate.1*	7.992–7.946	8.25E-05	–79.16	Down
	Guanosine.1	4.457–4.449	8.25E-05	–78.45	Down
	Tryptophan.2	7.210–7.199	8.25E-05	78.38	Up
	Adenosine.2*	6.088–6.074	1.07E-04	–76.58	Down
	Homocysteine.1	1.056–1.046	8.25E-05	76.53	Up
	Valine.1*	1.046–1.035	8.25E-05	76.26	Up

Table 3. *Left and right cerebrum metabolites found to be most significantly altered by stress in a Mann-Whitney U test. Metabolite regulation is shown as a function of relative concentration in high early postnatal stress individuals. Metabolites for which more than one NMR resonance peak was identified as significant are represented as metabolite.1, metabolite.2, … metabolite.n.* *Indicates metabolites that were significantly altered by stress in both left and right cerebra.*

Region	Metabolite	*r*	*P*	Correlation
Left Cerebrum	Aspartate.1†	–0.78	0.000012	Negative
	Aspartate.3†	–0.76	0.000028	Negative
	Agmatine.1†, Phenylalanine.1†, Taurine.1†	–0.76	0.000029	Negative
	Myo-Inositol.1†	0.75	0.000033	Positive
	Glutamate.12†	0.75	0.000043	Positive
	Glutamate.10†	0.74	0.000058	Positive
	Glutamate.7†	0.73	0.000067	Positive
	Agmatine.4†	–0.73	0.000070	Negative
	Aspartate.2†	–0.73	0.000074	Negative
	Tyrosine.2†	0.73	0.000077	Positive
	2-Aminobutyrate.2, Leucine.2†	–0.72	0.000097	Negative
	Isoleucine.1†	–0.72	0.000106	Negative
	2-Aminoadipate.1†	–0.71	0.000128	Negative
	Aspartate.5†	–0.71	0.000140	Negative
	Glutamate.14†	0.71	0.000158	Positive
	Agmatine.2†	–0.71	0.000161	Negative
	Ethanolamine.1†, Homoserine.1†, Uridine.1†	–0.71	0.000164	Negative
	Glutamate.15†	0.71	0.000168	Positive
	Glutamate.8†	0.70	0.000179	Positive
	Adenosine.4†	0.70	0.000182	Positive
Right Cerebrum	Aspartate.9†	–0.80	0.000005	Negative
	Aspartate.5†, Tyramine.5	–0.80	0.000006	Negative
	Aspartate.4†	–0.79	0.000006	Negative
	Uridine.3†	–0.79	0.000007	Negative
	Aspartate.1†	–0.79	0.000007	Negative
	Aspartate.6†, Uridine.1†	–0.79	0.000007	Negative
	Aspartate.3†	–0.79	0.000007	Negative
	Aspartate.7†	–0.79	0.000008	Negative
	Aspartate.2†, Tyramine.3	–0.78	0.000010	Negative
	Tyramine.6	–0.77	0.000015	Negative

Right Cerebrum	Methylmalonate.2	0.77	0.000018	Positive
	N-Acetylaspartate.14†	0.77	0.000020	Positive
	β-Alanine.1†	–0.76	0.000027	Negative
	Aspartate.8†, Uridine.5†	–0.76	0.000028	Negative
	Homoserine.13†	–0.76	0.000029	Negative
	Histidine.6†	–0.75	0.000033	Negative
	Nicotinate.2	0.75	0.000038	Positive
	Creatinine.1†	0.75	0.000038	Positive
	Histidine.8†	–0.75	0.000039	Negative
	Adenosine.12†, Tyrosine.2†	0.75	0.000039	Positive

Table 4. *Left and right cerebrum metabolites found to be most significantly correlated to precocious visual behaviour. Pearson correlations were used to assess the relationship between behaviours indicative of precocious visual behaviour (i.e., less time spent in the deep region of the visual cliff apparatus) and relative concentrations of metabolites found to be significantly altered by stress in a Mann-Whitney U test. Top 20 r values, shown in descending order, correspond to Fig. 4. Positive correlations indicate that precocious development of depth perception was linked to lower metabolite concentrations, while negative correlations indicate that precocious development of depth perception was linked to higher metabolite concentrations. Metabolites for which more than one NMR resonance peak was identified are represented as metabolite.1, metabolite.2, … metabolite.n. †Indicates metabolites that were significantly correlated to precocious visual behaviour in both left and right cerebra.*

Age	mRNA	Fold Change (log_2)	Standard Error	Wald Statistic	*P*	Adjusted *p*
P20	Deaf1	0.757	0.142	28.233	7.401E-07	9.127E-03
P20	Mgat5b‡	0.383	0.121	24.716	4.295E-06	2.648E-02
P20	Neurl1b	0.703	0.152	23.259	8.900E-06	3.659E-02
P20	Garem1	–0.755	0.171	19.978	4.590E-05	9.907E-02
P20	Col8a1	1.545	0.354	19.850	4.893E-05	9.907E-02
P20	Lin7b	0.533	0.124	19.544	5.703E-05	9.907E-02
P20	Csnk1g1	–0.519	0.130	19.158	6.918E-05	9.907E-02
P20	Hrh3‡	0.737	0.171	19.070	7.229E-05	9.907E-02
P20	Tef‡	0.352	0.087	18.708	8.664E-05	9.907E-02
P20	Dusp1	–2.513	0.578	18.646	8.933E-05	9.907E-02
P20	Plbd2	0.414	0.097	18.504	9.593E-05	9.907E-02
P20	Gem	–2.222	0.825	18.348	1.037E-04	9.907E-02
P20	Gas6	0.356	0.084	18.334	1.044E-04	9.907E-02
P35	Rhobtb2	0.332	0.069	4.822	1.423E-06	6.191E-03
P35	Mta3	0.257	0.053	4.821	1.431E-06	6.191E-03
P35	Cys1	0.535	0.113	4.724	2.315E-06	6.191E-03
P35	Faim2	0.204	0.043	4.701	2.590E-06	6.191E-03
P35	Lonrf1	0.600	0.137	4.389	1.137E-05	1.824E-02
P35	Ints3	0.213	0.048	4.388	1.145E-05	1.824E-02
P35	Hlf	0.349	0.081	4.288	1.804E-05	2.464E-02
P35	L1cam	0.295	0.073	4.043	5.276E-05	6.305E-02
P35	St8sia1	0.407	0.103	3.943	8.042E-05	7.440E-02
P35	Eln	–0.616	0.156	–3.940	8.165E-05	7.440E-02
P35	Mgat5b‡	0.316	0.080	3.928	8.559E-05	7.440E-02
P35	Atg9a	0.251	0.065	3.879	1.047E-04	8.247E-02
P35	Sstr3	–0.347	0.090	–3.863	1.121E-04	8.247E-02
P35	Hbb-bs	–1.261	0.331	–3.807	1.407E-04	9.612E-02

P35	Vhl	–0.257	0.068	–3.774	1.605E-04	9.994E-02
P35	Ahsa2	0.395	0.105	3.764	1.672E-04	9.994E-02
P50	Hrh3‡	0.567	0.116	4.907	9.252E-07	1.654E-02
P50	Cyr61	–3.023	0.643	–4.700	2.599E-06	2.324E-02
P50	Ppp1r3c	–0.545	0.121	–4.489	7.170E-06	4.273E-02
P50	B930095G15Rik	0.416	0.096	4.348	1.375E-05	6.145E-02
P50	Cbln3	–4.762	1.155	–4.123	3.742E-05	9.917E-02
P50	Tef‡	0.243	0.059	4.122	3.761E-05	9.917E-02
P50	Gadd45g	–1.005	0.244	–4.114	3.883E-05	9.917E-02

Table 5. *mRNA expression fold change (log_2) with raw and adjusted p-values. Included are FDR-adjusted values with $p < 0.1$ in order of smallest adjusted p-values. ‡Indicates mRNA transcripts that were differentially expressed in more than one time-point.*

DISCUSSION

The perinatal environment plays a critical role in shaping development and lifelong health (Heim & Binder, 2012; Hertzman, 1999). Here, we linked ELS to altered programming of cerebral development based on (i) the occurrence of precocious visual functioning, (ii) cellular expression of immunofluorescent developmental biomarkers, and (iii) altered metabolites and/or metabolic pathways linked to an aberrant developmental phenotype and associated topographical desynchronization of brain development. Many metabolites found to be significantly altered by stress belong to metabolic pathways involved in aminoacyl-tRNA biosynthesis, supporting a link between early environmental insults and abnormal developmental trajectories.

The findings indicate that ELS leads to the occurrence of accelerated visual functioning. The precocious development of depth perception (indicated by stressed animals exhibiting a preference for the "shallow side" of the visual cliff apparatus) as well as the precocious development of visual acuity (indicated by improved performance on the virtual optomotry system throughout the critical period for visual cortical plasticity) and the accelerated eye opening observed in shipped animals suggest a permanent reprogramming of developmental processes manifesting as downstream alterations in visual phenotype and function. Indeed, aberrant developmental trajectories in response to ELS have been well-documented, and have been postulated as a possible mechanism underlying stress-induced adverse health outcomes in adulthood (Belsky, Ruttle, Boyce, Armstrong, & Essex, 2015; Cameron, Eagleson, Fox, Hensch, & Levitt, 2017; Cowan, Stylianakis, & Richardson, 2019).

Precocious visual behaviours throughout the critical period for visual system development in stressed animals were accompanied by abundance of PNN-expressing cells in the primary visual cortex at P35, the age of visual critical period closure in the mouse (Espinosa & Stryker, 2012; Gordon & Stryker, 1996). Throughout the brain, PV-positive interneurons playa

critical role in the proper sequential timing of critical periods (Hensch, 2005). These cells mature at divergent rates throughout the brain, exerting temporal control over the flow of information to pyramidal neurons (Condé, Lund, & Lewis, 1996; Ferrer & Soriano, 1994). At the closure of a critical period, these PV-positive cells and their proximal neurites are enclosed by chondroitin sulfate proteoglycan-containing PNNs (Hensch, 2005). Along with myelin-associated proteins, these chondroitin sulfate proteoglycans bind to the Nogo receptor (Dickendesher et al., 2012) which then act along with immune cells to inhibit neurite growth and plasticity (Atwal et al., 2008; Bochner et al., 2014). Thus, PNNs act as a structural molecular "brake" to critical period plasticity, and the appearance of PNNs indicates a closure of the critical period for visual system development (Gogolla, Caroni, Lüthi, & Herry, 2009; Nabel & Morishita, 2013). Altogether, these behavioural and immunohistochemical findings indicate that the visual cortices of stressed animals exhibited an abnormal, accelerated cellular developmental trajectory along with precocious visual behaviours at the functional level.

Recent evidence has suggested that the mistiming of critical periods can derail development and has causally implicated aberrant developmental trajectories in the pathophysiology of several diseases. The disruption of PV-positive interneurons and their associated PNNs may contribute to the circuit instability characterizing mental health impairments (Do, Cuenod, & Hensch, 2015). These events have been implicated in schizophrenia, autism, and other psychiatric disorders (Do et al., 2015; LeBlanc & Fagiolini, 2011; Marín, 2012). Previously, early life stressors such as parental separation (Brenhouse & Andersen, 2011) and social isolation (Harte, Powell, Swerdlow, Geyer, & Reynolds, 2007; Schiavone et al., 2009) were shown to lead to PV circuit abnormalities in hippocampal and prefrontal cortical regions by impacting the efficacy of molecular "triggers" and "brakes" of

developmental critical periods. An as example, the limbic system has proven to be especially sensitive to adverse early-life experiences, with both rats (Callaghan & Richardson, 2011) and mice (Bath et al., 2016) showing an accelerated transition to enduring, mature fear memories coinciding with the premature appearance of PNNs in the amygdala (Gogolla et al., 2009). These shifts in developmental timing result in limited critical period windows of opportunity to potentially correct derailed circuitry as a result of stress, thus further contributing to the adverse effects of early-life stress on physical and mental health outcomes.

Two hundred forty-seven spectral bins present in left cerebral tissues and 305 bins present in right cerebral tissues were significantly altered by ELS. In both left and right cerebral tissues, stress most drastically altered pathways involved in aminoacyl-tRNA biosynthesis. Thus, while there was some lateralization in the specific metabolites altered across cerebral hemispheres, aggregate stress-induced metabolic changes ultimately led to a shared cerebral phenotype. Accordingly, previous work demonstrated abnormal brain development, functional diversification, and impaired aminoacyl-tRNA biosynthesis in response to early adverse experiences (Mehler & Mattick, 2007).

Several metabolites that underwent a significant change in percent difference are involved in mediating plasticity at both the cellular and behavioural levels. Abnormal levels of metabolites involved in gating synaptic plasticity, such as adenosine and inosine, may disrupt the sequential timing of developmental critical periods (Reh, 2015), thus contributing to a topographical desynchronization of brain development and subsequent risk of stress-induced adverse mental health outcomes. Adenosine, which was downregulated in left and right adult cerebral tissues, is known to play an important role in the regulation of neuronal excitability as well as low-frequency synaptic transmission by activating membrane receptors (de Mendonça &

Ribeiro, 1996; Flajolet et al., 2008; Moore, Nicoll, & Schmitz, 2003). Inosine, which has been shown to induce the expression neuronal growth associated proteins and axon extension in models of focal brain injury (Benowitz, Goldberg, Madsen, Soni, & Irwin, 1999; Chen, Goldberg, Kolb, Lanser, & Benowitz, 2002; Kolb, Teskey, & Gibb, 2010; Smith et al., 2007), was also downregulated in adult cerebral tissues. These results suggest that, in addition to shifting the critical period for visual system plasticity forward, ELS may also attenuate adult neuroplasticity in at least some brain regions.

Behavioural observations on the visual cliff revealed that ELS resulted in the precocious development of depth perception, as reflected by an increased preference for the shallow region. Precocious visual behaviours seen in stressed animals correlated with the relative concentrations of aspartate, glutamate, and tyrosine in left cerebral tissues as well as inosine, N-acetylaspartate, and β-alanine in right cerebral tissues. In both left and right cerebral hemispheres this correlation was strongest with aspartate, with upregulated relative concentrations of cerebral aspartate in postnatally stressed animals. Aspartate has been shown to modulate N-methyl-D-aspartate receptor (NMDAR)-dependent signaling (Billard, 2012) – specifically, aspartate acts as an endogenous NMDAR agonist by triggering currents through its interaction with each of the two NR2A-D receptor subunits (Errico et al., 2011). Interestingly, increased aspartate levels in the brain have been shown to rescue hippocampal age-related deterioration of synaptic plasticity in mice (Errico et al., 2011), suggesting a global cerebral desynchronization of synaptic plasticity neuromodulators, with some significantly increased and others significantly decreased in response to stress.

MSEA was used to identify patterns of metabolite concentration changes in a biologically meaningful framework (Xia & Wishart, 2010b). The most significant pathway altered in left

cerebral tissues was β-alanine metabolism, with 7 metabolite hits, whereas in right cerebral tissues, the most significant pathway altered was aspartate metabolism, with 8 metabolite hits. Significant pathways in the left cerebrum MSEA, apart from β-alanine metabolism, included aspartate metabolism, the malate aspartate shuttle, and glutamate metabolism. In the right cerebrum MSEA, other significant pathways included β-alanine metabolism as well as the malate-aspartate shuttle. Ammonia recycling was significantly altered in both hemispheres, with 6 metabolite hits in both left and right cerebral tissues.

β-Alanine, a structural hybrid between α- and γ-amino acid neurotransmitters (Tiedje, Stevens, Barnes, & Weaver, 2010), was upregulated in response to stress. Previously, β-alanine was found to be elevated during the early and late phase of memory retrieval in the Morris water maze, suggesting that this metabolite may play a role in learning and memory (Sase, Dahanayaka, Höger, Wu, & Lubec, 2013).

Glutamate metabolism was altered in shipped animals. Glutamate, an endogenous metabotropic glutamate receptor (mGluR) agonist (Reid, Daw, Gregory, & Flavin, 1996), was significantly downregulated in the cerebra of adult animals exposed to postnatal stress. In the primary visual cortex, cAMP levels are increased by stimulation of mGluRs, which correlate strongly with visual plasticity. Because glutamate is an mGluR agonist, it is integral in modulating the developmental critical period for the visual system (Fagiolini & Hensch, 2000; Hensch, 2005; Reid et al., 1996).

Multiple metabolites altered in response to stress are involved in energy metabolism. Aberrant energy metabolism contributes substantially to the association between disrupted PV-positive circuits throughout development and later adverse health outcomes. Indeed, a characteristic feature of fast-spiking PV-positive cells is their high metabolic demand, which

results in an abundance of reactive oxygen species (Buzsáki, Kaila, & Raichle, 2007). The malate-aspartate shuttle, a key mechanism for the transfer of reducing agents (NADH) from the cytosol into the mitochondria for oxidative phosphorylation (Fitzpatrick, Cooper, & Hertz, 1988; Hindfelt, Plum, & Duffy, 1977; Ratnakumari & Murthy, 1989), was significantly altered in response to ELS, suggesting the presence of abnormal stress-related mitochondrial energy metabolism. Glutamate is a critical component of this shuttle, and the depletion of cerebral glutamate pools by ammonia may be responsible for malate-aspartate shuttle disruption in the brain (Hindfelt et al., 1977). This concept gained further support when the addition of glutamate and ammonia to primary cultures of neurons and astrocytes was found to normalize the malate-aspartate shuttle (Murthy & Hertz, 1988). Thus, abnormalities in ammonia-mediated cerebral glutamate levels represent an important type of dysregulation in energy metabolism and provide key insights to the mechanisms linking abnormal glutamatergic signaling to stress-associated adverse health outcomes (Rao & Norenberg, 2001).

Consistent with MSEA results and metabolite percent differences, pathway topology analyses for both left and right cerebral tissues revealed changes in D-glutamine and D-glutamate metabolism. Additionally, a significantly altered pathway with one of the highest impact values was valine, leucine, and isoleucine degradation. In agreement with previous studies on the metabolomics of ELS (Paxman et al., 2018), this draws attention to a possible metabolic dysregulation of BCAAs in stressed animals. Abnormal BCAA metabolism has been implicated in the pathogenesis of several chronic conditions including insulin resistance, diabetes, and obesity (Lynch & Adams, 2014), and may play a mechanistic role in the association between ELS and an increased incidence of chronic disease risk in later life.

Stress also altered the aminoacyl-tRNA biosynthesis pathway, which is central for biosynthesis and kinetics of mRNA translation (Ferro et al., 2017; Ibba & Söll, 2000). Normally, mischarged tRNAs are cleaved by aminoacyl-tRNA synthetases via the actions of a domain distinct from the aminoacylation domain (Lee et al., 2006; Mehler & Mattick, 2007). Dysregulating of aminoacyl-tRNA synthetases results in increased mischarged tRNAs as well as an intracellular accumulation of misfolded proteins in neurons (Lee et al., 2006; Mehler & Mattick, 2007). Therefore, aberrant aminoacyl-tRNA biosynthesis may compromise the fidelity of cerebral protein translation as well as structural and functional neuronal differentiation (Liu, Shue, Ewalt, & Schimmel, 2004; Maas, Kim, & Rich, 2001; Mehler & Mattick, 2007; Schimmel & de Pouplana, 2000).

Although many alterations in metabolic pathways were shared across hemispheres, MSEA and pathway topology analyses revealed lateralized changes in neurometabolic phenotype. For example, aspartate metabolism was the most significantly altered pathway in right cerebral tissues, while β-alanine metabolism was the most significantly altered pathway in left cerebral tissues. Thus, while many of the pathways altered were shared across cerebral hemispheres, the degree to which these pathways were changed was not identical. Interestingly, previous research has reported a stress-induced asymmetrical allocation of NMDA-associated receptor subunits in rodent homogenates of right and left hippocampal tissues, and has suggested that the asymmetrical allocation of these subunits may affect hippocampal synaptic plasticity (Coplan et al., 2010). As aspartate is a known modulator of NMDAR-dependent signaling (Billard, 2012), these lateralized changes in aspartate metabolism may reflect lateralized effects of early adverse experiences on brain plasticity.

The mechanisms underlying the association between early adverse experiences and lifelong disease risk involve complex gene-environment interactions (Meaney, 2010). In animals, gene expression is modulated by transcriptional and translational initiation, which are also controlled through epigenetic processes such as the modification of chromatic structure of the control of mRNA translation (Bird, 2007). Importantly, epigenetic changes brought about by environmental insults are a key mechanism linking stress to long-term alterations in transcriptional regulation and organismal phenotype. Interestingly, epigenetic alterations following exposure to early-life stress are known to cause long-term transcriptional changes in the brain. For instance, adverse early-life experiences have been found to disrupt serotonin transporter mRNA expression, thus highlighting the importance of transcriptomic processes in the dysregulation of serotonergic systems modulating stress-related neuropsychiatric disorders (Gardner, Hale, Lightman, Plotsky, & Lowry, 2009).

Accordingly, epigenetic and transcriptomic regulation play a key role in the lifelong effects of early experience-dependent brain plasticity. Indeed, several mRNAs that were differentially expressed in stressed visual cortices are recognized mediators of brain development and neurodevelopmental disorders, including Deaf1 in memory deficits and anxiety-like behaviours (Mehregan, Najmabadi, & Kahrizi, 2016), Faim2 in obsessive compulsive disorder (Gazzellone et al., 2016; Pauls, Abramovitch, Rauch, & Geller, 2014; Stewart et al., 2013) and Hrh3 in schizophrenia (Dempster et al., 2011; Narayan et al., 2008; Wei et al., 2012). Altogether, these results suggest multidimensional early-life stress may program changes in mRNA expression that predispose an organism to adverse mental health outcomes later in life.

CONCLUSION

The present findings provide novel insights into the mechanisms underlying perinatal stress-induced disease vulnerability by linking an adverse early-life environment to aberrant cerebral development and metabolism. These changes reflect underlying transcriptomic modifications and associated cellular functions that manifest as downstream alterations to the metabolome and behaviour, and suggest that migration stress may have long-term physiological consequences in mammals. Further insights into the mechanisms underlying early-life stress-induced disease prevalence along with clearly recognizable metabolic biomarkers of psychiatric disorders open new personalized medicine strategies for early detection and prevention of experience-dependent adverse health outcomes.

CHAPTER 4: GENERAL DISCUSSION AND CONCLUSIONS

GENERAL DISCUSSION

SUMMARY OF FINDINGS

The present findings provide novel mechanistic insights into the effects of a multidimensional early-life stressor on metabolism, developmental trajectories, and behavioural outcomes. Here, ^{1}H NMR spectroscopy was utilized to investigate the effects of perinatal transportation stress on (1) cardiorenal and (2) global cerebral metabolism. Compared to other methods, NMR spectroscopy is an ideal starting point for global, untargeted metabolomic analyses of tissues with limited availability. As it is a non-destructive technique, tissue samples can easily be saved and further processed for additional analyses using techniques such as gas chromatography – mass spectrometry (GC-MS), liquid chromatography – mass spectrometry (LC-MS), and thin-layer chromatography/gas chromatography – flame ionization detection (TLC/GC-FID). Furthermore, metabolomic analyses using ^{1}H NMR is high-throughput process, with minimal sample preparation and rapid data collection (Bouatra et al., 2013; Dame et al., 2015; Psychogios et al., 2011; Wishart, Lewis, et al., 2008).

Currently, much of the metabolomics literature is focused on the analysis of urine and blood plasma. These biofluids are non-invasive/easy to obtain and provide valuable insights into the mechanisms underlying prognostic and diagnostic outcomes of myriad disease states. Nevertheless, metabolomic analyses utilizing tissues and organ systems implicated in adverse disease states provide valuable insights into the *direct* mechanisms underlying system-specific pathologies. In the first study presented (Chapter 2), a multidimensional stressor, early-life transportation stress, was successfully utilized to study experience-dependent biological signatures induced by early-life stress as downstream cardiorenal metabolomic changes using ^{1}H NMR spectroscopy in a murine model. Similarly, ^{1}H NMR was successfully used to investigate the effects of multidimensional early-life transportation stress on global cerebral metabolic

profiles in rodents (Chapter 3). In both studies, we accurately differentiated between stressed and non-stressed experimental groups based on a subset of significantly-altered metabolites and metabolic pathways, which were then correlated to anxious (Chapter 2) and precocious visual (Chapter 3) behavioural phenotypes as well as dynamic changes in mRNA expression across development and an increased abundance of PNN-expressing cells in late adolescence. These analyses provide novel insights into the direct impacts of adverse environmental events on cardiorenal and cerebral tissues, and further support the previously-established association between adverse early-life experiences, aberrant developmental processes, and increased lifelong NCD risk (Barouki et al., 2012).

Cardiorenal and global cerebral metabolomic profiles exhibited overlapping stress-induced metabolomic changes. In both cardiorenal and cerebral tissues, stressed animals showed significant stress-induced alterations in pathways regulating energy metabolism. Metabolic pathway analysis revealed significant changes in citric acid cycle metabolism in heart and kidney tissues, while cerebral tissues underwent significant changes in glutamate metabolism, ammonia recycling, and the malate-aspartate shuttle. Thus, early-life stress resulted in permanent dysregulation of mitochondrial energy metabolism that persisted across disparate organ systems. Similarly, stressed animals displayed dysregulations in BCAA metabolism in both cardiorenal and cerebral tissues, and the most significantly-altered pathway in response to stress across organ systems was aminoacyl-tRNA synthesis, suggesting that early-life stress results in shared metabolic phenotypes across organ systems. Notably, several seemingly unrelated chronic adverse health outcomes – such as cardiorenal pathologies and affective disorders – show striking comorbidities. These findings draw attention to metabolic pathways that may link these

comorbid conditions and provide insight into potential mechanisms underlying well-documented experience-dependent adverse health outcomes.

STUDY LIMITATIONS

The present experiments utilized transportation stress to investigate the effects of early-life stress on offspring development, metabolism, and behaviour. While many stress studies in the literature focus on the physiological consequences of a single stressor at a single point in time, this rarely reflects early-life adverse environments outside the laboratory. Rather, individuals exposed to early adverse environments are often exposed to *multidimensional* stressors. The experimental design utilized in Chapters 2 and 3 reflects this. Furthermore, while animals are often shipped between facilities for use in scientific research, the physiological effects of rodent transportation have seldom been explored. Here, we compared animals shipped from a common animal supplier to animals bred in-house for at least 5 generations to investigate the effects of shipment stress within the context of its usual occurrence. While this experimental design provides novel insights into the effects of multidimensional transportation stress on animal metabolism, development, and behaviour, and while all animals were shipped concurrently to minimize variation in shipping environment, it was not possible to control precisely the individual environmental variables comprising animal shipment. Thus, additional research is needed to parse out the individual effects of the independent environmental variables comprising the multidimensional stress treatment (e.g., temperatures, vibrations, changes to the light-dark cycle).

Additional techniques including Mass Spectroscopy (MS), Gas Chromatography – Mass Spectrometry (GC-MS), and Liquid Chromatography – Mass Spectrometry (LC-MS) may be

used to assess the cardiorenal and cerebral metabolome from different perspectives. While these experiments utilized ^{1}H NMR spectroscopy-based metabolomic profiling, NMR spectroscopy is an ideal starting point for global, untargeted metabolomic analyses. Sample processing and analysis using this approach is efficient, high-throughput, and non-destructive, meaning samples can be further processed and later analyzed using disparate approaches. Furthermore, each of these separate approaches isolates and identifies an overlapping but predominantly unique portion of the tissue metabolome (Zhang, Sun, Wang, Han, & Wang, 2012).

In Chapter 3, water-soluble metabolites were extracted from left and right cerebral tissues for ^{1}H NMR analyses. While this approach allowed for the investigation of (1) global cerebral metabolic changes in response to stress and (2) lateralization in stress-induced metabolic changes, metabolomic processing of individual brain regions would allow for the acute assessment of plasticity-related metabolic changes across brain regions. Altogether, these metabolomic, behavioural, and immunohistochemical findings indicate a stress-induced acceleration of visual system development. However, further research is needed to determine the effects of stress on other brain regions, and to determine whether a topographical desynchronization of brain development underlies the association between early adverse experiences and lifelong adverse health outcomes.

CONSIDERATIONS FOR FUTURE WORK

There are several implications for future research presented by the current findings. Future studies should aim to include females in the analysis, as well-documented sex differences in stress responses have previously been established (Ježová, Juránková, Mosnárová, & Kriška, 1996; Kudielka & Kirschbaum, 2005; Tilbrook, Turner, & Clarke, 2000). Additional research

into the effects of early-life stress on the timing of developmental critical periods in other brain regions is also needed, as the results presented here focus only on stress-induced changes in the developmental trajectory of the visual system. Finally, these findings suggest that the shipment of animals may represent a confound in the life sciences. Future experiments that replicate these results using carefully controlled multidimensional stressors would be invaluable in pinpointing the effects of these independent variables on animal physiology, development, and behaviour.

REFERENCES

Allen, P. J. (2012). Creatine metabolism and psychiatric disorders: Does creatine supplementation have therapeutic value? *Neuroscience & Biobehavioral Reviews, 36*(5), 1442-1462.

Anderson, P. E., Mahle, D. A., Doom, T. E., Reo, N. V., DelRaso, N. J., & Raymer, M. L. (2011). Dynamic adaptive binning: an improved quantification technique for NMR spectroscopic data. *Metabolomics, 7*(2), 179-190.

Andreazza, A. C., Kauer-Sant'Anna, M., Frey, B. N., Bond, D. J., Kapczinski, F., Young, L. T., & Yatham, L. N. (2008). Oxidative stress markers in bipolar disorder: a meta-analysis. *Journal of affective disorders, 111*(2-3), 135-144.

Attaix, D., Ventadour, S., Codran, A., Béchet, D., Taillandier, D., & Combaret, L. (2005). The ubiquitin–proteasome system and skeletal muscle wasting. *Essays in biochemistry, 41*, 173-186.

Atwal, J. K., Pinkston-Gosse, J., Syken, J., Stawicki, S., Wu, Y., Shatz, C., & Tessier-Lavigne, M. J. S. (2008). PirB is a functional receptor for myelin inhibitors of axonal regeneration. *322*(5903), 967-970.

Baigent, C., Burbury, K., & Wheeler, D. (2000). Premature cardiovascular disease in chronic renal failure. *The Lancet, 356*(9224), 147-152.

Bale, T. L., Baram, T. Z., Brown, A. S., Goldstein, J. M., Insel, T. R., McCarthy, M. M., . . . Susser, E. S. J. B. p. (2010). Early life programming and neurodevelopmental disorders. *68*(4), 314-319.

Barderas, M. G., Laborde, C. M., Posada, M., de la Cuesta, F., Zubiri, I., Vivanco, F., & Alvarez-Llamas, G. (2011). Metabolomic profiling for identification of novel potential biomarkers in cardiovascular diseases. *BioMed Research International, 2011*.

Barkai, A. I., Dunner, D., Gross, H. A., Mayo, P., & Fieve, R. (1978). Reduced myo-inositol levels in cerebrospinal fluid from patients with affective disorder. *Biological psychiatry*.

Barker, D. J. (1995). Fetal origins of coronary heart disease. *Bmj, 311*(6998), 171-174.

Barouki, R., Gluckman, P. D., Grandjean, P., Hanson, M., & Heindel, J. J. J. E. H. (2012). Developmental origins of non-communicable disease: implications for research and public health. *11*(1), 42.

Basu, A. C., Tsai, G. E., Ma, C.-L., Ehmsen, J. T., Mustafa, A. K., Han, L., . . . Lange, N. (2009). Targeted disruption of serine racemase affects glutamatergic neurotransmission and behavior. *Molecular psychiatry, 14*(7), 719.

Bateson, P., Barker, D., Clutton-Brock, T., Deb, D., D'udine, B., Foley, R. A., . . . Lahr, M. M. (2004). Developmental plasticity and human health. *Nature, 430*(6998), 419.

Bath, K., Manzano-Nieves, G., Goodwill, H. J. H., & behavior. (2016). Early life stress accelerates behavioral and neural maturation of the hippocampus in male mice. *82*, 64-71.

Baylis, C. (2006). Arginine, arginine analogs and nitric oxide production in chronic kidney disease. *Nature Reviews Nephrology, 2*(4), 209.

Beaglehole, R., & Yach, D. (2003). Globalisation and the prevention and control of non-communicable disease: the neglected chronic diseases of adults. *The Lancet, 362*(9387), 903-908.

Beckonert, O., Keun, H. C., Ebbels, T. M., Bundy, J., Holmes, E., Lindon, J. C., & Nicholson, J. K. (2007). Metabolic profiling, metabolomic and metabonomic procedures for NMR spectroscopy of urine, plasma, serum and tissue extracts. *Nature protocols, 2*(11), 2692.

Cameron, J. L., Eagleson, K. L., Fox, N. A., Hensch, T. K., & Levitt, P. J. J. o. N. (2017). Social origins of developmental risk for mental and physical illness. *37*(45), 10783-10791.

Cancedda, L., Putignano, E., Sale, A., Viegi, A., Berardi, N., & Maffei, L. J. J. o. N. (2004). Acceleration of visual system development by environmental enrichment. *24*(20), 4840-4848.

Chaby, L., Cavigelli, S. A., Hirrlinger, A., Caruso, M., & Braithwaite, V. (2015). Chronic unpredictable stress during adolescence causes long-term anxiety. *Behavioural brain research, 278*, 492-495.

Chaddha, A., Robinson, E. A., Kline-Rogers, E., Alexandris-Souphis, T., & Rubenfire, M. (2016). Mental health and cardiovascular disease. *The American journal of medicine, 129*(11), 1145-1148.

Chaturvedi, P., Kamat, P. K., Kalani, A., Familtseva, A., & Tyagi, S. C. (2016). High methionine diet poses cardiac threat: a molecular insight. *Journal of cellular physiology, 231*(7), 1554-1561.

Chauvet-Gelinier, J.-C., & Bonin, B. (2017). Stress, anxiety and depression in heart disease patients: A major challenge for cardiac rehabilitation. *Annals of physical and rehabilitation medicine, 60*(1), 6-12.

Chen, P., Goldberg, D. E., Kolb, B., Lanser, M., & Benowitz, L. I. J. P. o. t. N. A. o. S. (2002). Inosine induces axonal rewiring and improves behavioral outcome after stroke. *99*(13), 9031-9036.

Chen, Y.-F., Naftilan, A. J., & Oparil, S. (1992). Androgen-dependent angiotensinogen and renin messenger RNA expression in hypertensive rats. *Hypertension, 19*(5), 456-463.

Chrousos, G. (2000). The role of stress and the hypothalamic–pituitary–adrenal axis in the

pathogenesis of the metabolic syndrome: neuro-endocrine and target tissue-related causes. *International Journal of Obesity, 24*(S2), S50.

Chrousos, G. P., Torpy, D. J., & Gold, P. W. (1998). Interactions between the hypothalamic-pituitary-adrenal axis and the female reproductive system: clinical implications. *Annals of internal medicine, 129*(3), 229-240.

Collins, A. J., Li, S., Gilbertson, D. T., Liu, J., Chen, S.-C., & Herzog, C. A. (2003). Chronic kidney disease and cardiovascular disease in the Medicare population: Management of comorbidities in kidney disease in the 21st century: Anemia and bone disease. *Kidney International, 64*, S24-S31.

Condé, F., Lund, J. S., & Lewis, D. A. J. D. b. r. (1996). The hierarchical development of monkey visual cortical regions as revealed by the maturation of parvalbumin-immunoreactive neurons. *96*(1-2), 261-276.

Coplan, J. D., Mathew, S. J., Abdallah, C. G., Mao, X., Kral, J. G., Smith, E. L., ... & Gorman, J. M. (2010). Early-life stress and neurometabolites of the hippocampus. *Brain research, 1358*, 191-199.

Cottrell, E. C., & Seckl, J. J. F. i. b. n. (2009). Prenatal stress, glucocorticoids and the programming of adult disease. *3*, 19.

Coupland, N. J., Ogilvie, C. J., Hegadoren, K. M., Seres, P., Hanstock, C. C., & Allen, P. S. (2005). Decreased prefrontal Myo-inositol in major depressive disorder. *Biological psychiatry, 57*(12), 1526-1534.

Cowan, C. S., Stylianakis, A. A., & Richardson, R. J. D. c. n. (2019). Early-life stress, microbiota, and brain development: probiotics reverse the effects of maternal separation on neural circuits underpinning fear expression and extinction in infant rats. *37*, 100627.

Cravedi, P., & Remuzzi, G. (2008). Treating the kidney to cure the heart: New strategies to prevent cardiovascular risk in chronic kidney disease. *Kidney International, 74*, S2-S3.

Crowley, J. C., & Katz, L. C. J. N. n. (1999). Development of ocular dominance columns in the absence of retinal input. *2*(12), 1125.

Croze, M. L., & Soulage, C. O. (2013). Potential role and therapeutic interests of myo-inositol in metabolic diseases. *Biochimie, 95*(10), 1811-1827.

Da, M., Feng, Y., Xu, J., Hu, Y., Lin, Y., Ni, B., . . . Mo, X. (2014). Association of aminoacyl-tRNA synthetases gene polymorphisms with the risk of congenital heart disease in the Chinese Han population. *PloS one, 9*(10), e110072.

Dame, Z. T., Aziat, F., Mandal, R., Krishnamurthy, R., Bouatra, S., Borzouie, S., . . . Lin, H. J. M. (2015). The human saliva metabolome. *11*(6), 1864-1883.

Danese, A., Pariante, C. M., Caspi, A., Taylor, A., & Poulton, R. J. P. o. t. N. A. o. S. (2007). Childhood maltreatment predicts adult inflammation in a life-course study. *104*(4), 1319-1324.

de Mendonça, A., & Ribeiro, J. J. L. s. (1996). Adenosine and neuronal plasticity. *60*(4-5), 245-251.

Dempster, E. L., Pidsley, R., Schalkwyk, L. C., Owens, S., Georgiades, A., Kane, F., . . . Toulopoulou, T. J. H. m. g. (2011). Disease-associated epigenetic changes in monozygotic twins discordant for schizophrenia and bipolar disorder. *20*(24), 4786-4796.

Dickendesher, T. L., Baldwin, K. T., Mironova, Y. A., Koriyama, Y., Raiker, S. J., Askew, K. L., . . . Liepmann, C. D. J. N. n. (2012). NgR1 and NgR3 are receptors for chondroitin sulfate proteoglycans. *15*(5), 703.

Do, K. Q., Cuenod, M., & Hensch, T. K. J. S. b. (2015). Targeting oxidative stress and aberrant critical period plasticity in the developmental trajectory to schizophrenia. *41*(4), 835-846.

Dobbing, J. (1972). Vulnerable periods of brain development. In *Lipids, malnutrition and the developing brain* (pp. 9-29): Associated Scientific Publishers, Amsterdam.

Dong, H. W. (2008). *The Allen reference atlas: A digital color brain atlas of the C57Bl/6J male mouse*: John Wiley & Sons Inc.

Dräger, U. C., & Hubel, D. H. J. J. o. C. N. (1978). Studies of visual function and its decay in mice with hereditary retinal degeneration. *180*(1), 85-114.

Einat, H., Yuan, P., & Manji, H. K. (2005). Increased anxiety-like behaviors and mitochondrial dysfunction in mice with targeted mutation of the Bcl-2 gene: further support for the involvement of mitochondrial function in anxiety disorders. *Behavioural brain research, 165*(2), 172-180.

Emwas, A.-H. M., Salek, R. M., Griffin, J. L., & Merzaban, J. (2013). NMR-based metabolomics in human disease diagnosis: applications, limitations, and recommendations. *Metabolomics, 9*(5), 1048-1072.

Epel, E. S., Blackburn, E. H., Lin, J., Dhabhar, F. S., Adler, N. E., Morrow, J. D., & Cawthon,R. M. J. P. o. t. N. A. o. S. (2004). Accelerated telomere shortening in response to lifestress. *101*(49), 17312-17315.

Erickson, Z. T., Falkenberg, E. A., & Metz, G. A. (2014). Lifespan psychomotor behaviour profiles of multigenerational prenatal stress and artificial food dye effects in rats. *PloS one, 9*(6), e92132.

Errico, F., Nisticò, R., Napolitano, F., Mazzola, C., Astone, D., Pisapia, T., . . . Usiello, A. J. N. o. a. (2011). Increased D-aspartate brain content rescues hippocampal age-related synaptic plasticity deterioration of mice. *32*(12), 2229-2243.

Espinosa, J. S., & Stryker, M. P. J. N. (2012). Development and plasticity of the primary visual cortex. *75*(2), 230-249.

Evans, G. W., & Kim, P. J. P. S. (2007). Childhood poverty and health: Cumulative risk exposure and stress dysregulation. *18*(11), 953-957.

Everitt, A. V., Porter, B. D., & Wyndham, J. R. (1982). Effects of caloric intake and dietary composition on the development of proteinuria, age-associated renal disease and longevity in the male rat. *Gerontology, 28*(3), 168-175.

Everson-Rose, S. A., & Lewis, T. T. (2005). Psychosocial factors and cardiovascular diseases. *Annu. Rev. Public Health, 26*, 469-500.

Fagiolini, M., & Hensch, T. K. J. N. (2000). Inhibitory threshold for critical-period activation in primary visual cortex. *404*(6774), 183.

Fagiolini, M., Jensen, C. L., & Champagne, F. A. J. C. o. i. n. (2009). Epigenetic influences on brain development and plasticity. *19*(2), 207-212.

Ferrer, I., & Soriano, E. J. B. r. D. b. r. (1994). The development of parvalbumin-immunoreactivity in the neocortex of the mouse. *81*(2), 247-259.

Ferro, I., Liebeton, K., & Ignatova, Z. (2017). Growth-rate dependent regulation of tRNA level and charging in Bacillus licheniformis. *Journal of molecular biology, 429*(20), 3102-3112.

Fiehn, O. (2002). Metabolomics—the link between genotypes and phenotypes. In *Functional genomics* (pp. 155-171): Springer.

Finsterer, J. (2006). Central nervous system manifestations of mitochondrial disorders. *Acta Neurologica Scandinavica, 114*(4), 217-238.

Fiordaliso, F., Li, B., Latini, R., Sonnenblick, E. H., Anversa, P., Leri, A., & Kajstura, J. (2000). Myocyte death in streptozotocin-induced diabetes in rats is angiotensin II-dependent. *Laboratory investigation, 80*(4), 513.

Fitzpatrick, S. M., Cooper, A. J., & Hertz, L. J. J. o. n. (1988). Effects of Ammonia and β-Methylene-dl-Aspartate on the Oxidation of Glucose and Pyruvate by Neurons and Astrocytes in Primary Culture. *51*(4), 1197-1203.

Flajolet, M., Wang, Z., Futter, M., Shen, W., Nuangchamnong, N., Bendor, J., . . . Greengard, P. J. N. n. (2008). FGF acts as a co-transmitter through adenosine A 2A receptor to regulate synaptic plasticity. *11*(12), 1402.

Fliser, D., Kronenberg, F., Kielstein, J. T., Morath, C., Bode-Böger, S. M., Haller, H., & Ritz, E. (2005). Asymmetric dimethylarginine and progression of chronic kidney disease: the

mild to moderate kidney disease study. *Journal of the American Society of Nephrology, 16*(8), 2456-2461.

Fox, M. J. A. b. (1965). The visual cliff test for the study of visual depth perception in the mouse. *13*(2-3), 232-IN233.

Gale, C. R., O'Callaghan, F. J., Godfrey, K. M., Law, C. M., & Martyn, C. N. J. B. (2004). Critical periods of brain growth and cognitive function in children. *127*(2), 321-329.

Gardner, K. L., Hale, M. W., Lightman, S. L., Plotsky, P. M., & Lowry, C. A. J. B. r. (2009). Adverse early life experience and social stress during adulthood interact to increase serotonin transporter mRNA expression. *1305*, 47-63.

Gaspar-Pereira, S., Fullard, N., Townsend, P. A., Banks, P. S., Ellis, E. L., Fox, C., . . . Bauer, R. (2012). The NF-κB subunit c-Rel stimulates cardiac hypertrophy and fibrosis. *The American journal of pathology, 180*(3), 929-939.

Gazzellone, M. J., Zarrei, M., Burton, C. L., Walker, S., Uddin, M., Shaheen, S., . . . Colasanto, M. J. J. o. n. d. (2016). Uncovering obsessive-compulsive disorder risk genes in a pediatric cohort by high-resolution analysis of copy number variation. *8*(1), 36.

Gibson, E. J., & Walk, R. D. J. S. A. (1960). The "visual cliff".

Glaser, J.R., & Glaser, E. M. J. J. o. c. n. (2000). Stereology, morphometry, and mapping: the whole is greater than the sum of its parts. *20*(1), 115-126.

Gluckman, P. D., Hanson, M. A., & Mitchell, M. D. (2010). Developmental origins of health and disease: reducing the burden of chronic disease in the next generation. *Genome medicine, 2*(2), 14.

Go, A. S., Chertow, G. M., Fan, D., McCulloch, C. E., & Hsu, C.-y. (2004). Chronic kidney disease and the risks of death, cardiovascular events, and hospitalization. *New England Journal of Medicine, 351*(13), 1296-1305.

Gogolla, N., Caroni, P., Lüthi, A., & Herry, C. J. S. (2009). Perineuronal nets protect fear memories from erasure. *325*(5945), 1258-1261.

Goodpaster, A. M., Romick-Rosendale, L. E., & Kennedy, M. A. (2010). Statistical significance analysis of nuclear magnetic resonance-based metabonomics data. *Analytical biochemistry, 401*(1), 134-143.

Gordon, J. A., & Stryker, M. P. J. J. o. N. (1996). Experience-dependent plasticity of binocular responses in the primary visual cortex of the mouse. *16*(10), 3274-3286.

Greenland, P., Knoll, M. D., Stamler, J., Neaton, J. D., Dyer, A. R., Garside, D. B., & Wilson, P. W. (2003). Major risk factors as antecedents of fatal and nonfatal coronary heart disease events. *Jama, 290*(7), 891-897.

Habib, S. H., & Saha, S. (2010). Burden of non-communicable disease: global overview. *Diabetes & Metabolic Syndrome: Clinical Research & Reviews, 4*(1), 41-47.

Hall, J. E. (2003). The kidney, hypertension, and obesity. *Hypertension, 41*(3), 625-633.

Hamilton, H. L. (1952). Sensitive periods during development. *Annals of the New York Academy of Sciences, 55*(1), 177-187.

Harte, M. K., Powell, S., Swerdlow, N., Geyer, M., & Reynolds, G. J. J. o. n. t. (2007). Deficits in parvalbumin and calbindin immunoreactive cells in the hippocampus of isolation reared rats. *114*(7), 893-898.

Hassan, W., Eduardo Barroso Silva, C., Mohammadzai, I. U., Batista Teixeira da Rocha, J., & Landeira-Fernandez, J. (2014). Association of oxidative stress to the genesis of anxiety: implications for possible therapeutic interventions. *Current neuropharmacology, 12*(2), 120-139.

Heim, C., & Binder, E. B. J. E. n. (2012). Current research trends in early life stress and depression: Review of human studies on sensitive periods, gene–environment interactions, and epigenetics. *233*(1), 102-111.

Hensch, T. K. J. A. R. N. (2004). Critical period regulation. *27*, 549-579.

Hensch, T. K. J. C. t. i. d. b. (2005). Critical period mechanisms in developing visual cortex. *69*, 215-237.

Hensch, T. K. J. N. R. N. (2005). Critical period plasticity in local cortical circuits. *6*(11), 877.

Hershkovitz, D., Burbea, Z., Skorecki, K., & Brenner, B. M. (2007). Fetal programming of adult kidney disease: cellular and molecular mechanisms. *Clinical Journal of the American Society of Nephrology, 2*(2), 334-342.

Hertzman, C. J. A. o. t. N. Y. A. o. S. (1999). The biological embedding of early experience and its effects on health in adulthood. *896*(1), 85-95.

Hesaka, A., Sakai, S., Hamase, K., Ikeda, T., Matsui, R., Mita, M., . . . Kimura, T. (2019). D-Serine reflects kidney function and diseases. *Scientific reports, 9*(1), 5104.

Hill, N. R., Fatoba, S. T., Oke, J. L., Hirst, J. A., O'Callaghan, C. A., Lasserson, D. S., & Hobbs, F. R. (2016). Global prevalence of chronic kidney disease–a systematic review and meta-analysis. *PloS one, 11*(7), e0158765.

Hindfelt, B., Plum, F., & Duffy, T. E. J. T. J. o. c. i. (1977). Effect of acute ammonia intoxication on cerebral metabolism in rats with portacaval shunts. *59*(3), 386-396.

Hoeijmakers, L., Lucassen, P. J., & Korosi, A. J. F. i. m. n. (2015). The interplay of early-life stress, nutrition, and immune activation programs adult hippocampal structure and

function. *7*, 103.

Hubel, D. H., & Wiesel, T. N. J. T. J. o. p. (1968). Receptive fields and functional architecture of monkey striate cortex. *195*(1), 215-243.

Ibba, M., & Söll, D. (2000). Aminoacyl-tRNA synthesis. *Annual review of biochemistry, 69*(1), 617-650.

Idris, N. S., Uiterwaal, C. S., van der Schouw, Y. T., van Abeelen, A. F., Roseboom, T. J., de Jong, P. A., . . . Elias, S. G. (2013). Famine in childhood and postmenopausal coronary artery calcification: a cohort study. *BMJ open, 3*(11), e003818.

Ismail, F. Y., Fatemi, A., & Johnston, M. V. J. E. J. o. P. N. (2017). Cerebral plasticity: windows of opportunity in the developing brain. *21*(1), 23-48.

Jankyova, S., Kmecova, J., Cernecka, H., Mesarosova, L., Musil, P., Brnoliakova, Z., . . . Klimas, J. (2012). Glucose and blood pressure lowering effects of Pycnogenol® are inefficient to prevent prolongation of QT interval in experimental diabetic cardiomyopathy. *Pathology-Research and Practice, 208*(8), 452-457.

Ježová, D., Juránková, E., Mosnárová, A., & Kriška, M. J. A. n. e. (1996). Neuroendocrine response during stress with relation to gender differences.

Jia, G., Aroor, A. R., Martinez-Lemus, L. A., & Sowers, J. R. (2015). Mitochondrial functional impairment in response to environmental toxins in the cardiorenal metabolic syndrome. *Archives of toxicology, 89*(2), 147-153.

Johnson, S. B., Riley, A. W., Granger, D. A., & Riis, J. J. P. (2013). The science of early life toxic stress for pediatric practice and advocacy. *131*(2), 319-327.

Kerr, D. S., Campbell, L. W., Applegate, M. D., Brodish, A., & Landfield, P. W. J. J. o. N. (1991). Chronic stress-induced acceleration of electrophysiologic and morphometric biomarkers of hippocampal aging. *11*(5), 1316-1324.

Kiss, D., Ambeskovic, M., Montina, T., & Metz, G. A. (2016). Stress transgenerationally programs metabolic pathways linked to altered mental health. *Cellular and molecular life sciences, 73*(23), 4547-4557.

Kolb, B., Teskey, C., & Gibb, R. J. F. i. h. n. (2010). Factors influencing cerebral plasticity in the normal and injured brain. *4*, 204.

Konstam, V., Moser, D. K., & De Jong, M. J. (2005). Depression and anxiety in heart failure. *Journal of cardiac failure, 11*(6), 455-463.

Kozela, M., Bobak, M., Besala, A., Micek, A., Kubinova, R., Malyutina, S., . . . Peasey, A. (2016). The association of depressive symptoms with cardiovascular and all-cause mortality in Central and Eastern Europe: prospective results of the HAPIEE study. *European journal of preventive cardiology, 23*(17), 1839-1847.

Kudielka, B. M., & Kirschbaum, C. J. B. p. (2005). Sex differences in HPA axis responses to stress: a review. *69*(1), 113-132.

Langley-Evans, S. C. (2013). Fetal programming of CVD and renal disease: animal models and mechanistic considerations. *Proceedings of the Nutrition Society, 72*(3), 317-325.

LeBlanc, J. J., & Fagiolini, M. J. N. p. (2011). Autism: a "critical period" disorder? , *2011*.

Lee, J. W., Beebe, K., Nangle, L. A., Jang, J., Longo-Guess, C. M., Cook, S. A., . . .Ackerman, S. L. J. N. (2006). Editing-defective tRNA synthetase causes protein misfolding and neurodegeneration. *443*(7107), 50.

Licher, S., Heshmatollah, A., van der Willik, K. D., Stricker, B. H. C., Ruiter, R., de Roos, E. W., . . . Fani, L. (2019). Lifetime risk and multimorbidity of non-communicable diseases and disease-free life expectancy in the general population: A population-based cohort study. *PLoS medicine, 16*(2), e1002741.

Liu, J., Shue, E., Ewalt, K. L., & Schimmel, P. J. N. a. r. (2004). A new γ-interferon-inducible promoter and splice variants of an anti-angiogenic human tRNA synthetase. *32*(2), 719-727.

Love, M. I., Huber, W., & Anders, S. J. G. b. (2014). Moderated estimation of fold change and dispersion for RNA-seq data with DESeq2. *15*(12), 550.

Lynch, C. J., & Adams, S. H. (2014). Branched-chain amino acids in metabolic signalling and insulin resistance. *Nature Reviews Endocrinology, 10*(12), 723.

Ma, H., Jones, K. R., Guo, R., Xu, P., Shen, Y., & Ren, J. (2010). Cisplatin compromises myocardial contractile function and mitochondrial ultrastructure: role of endoplasmic reticulum stress. *Clinical and Experimental Pharmacology and Physiology, 37*(4), 460-465.

Maas, S., Kim, Y.-G., & Rich, A. J. M. G. (2001). Genomic clustering of tRNA-specific adenosine deaminase ADAT1 and two tRNA synthetases. *12*(5), 387-393.

Macdonald, G., Assef, R., Guiffre, A., & Lo, E. (1984). Vasoconstrictor effects of uridine and its nucleotides and their inhibition by adenosine. *Clinical and Experimental Pharmacology and Physiology, 11*(4), 381-384.

Maher, B. (2008). Personal genomes: The case of the missing heritability. *Nature News, 456*(7218), 18-21.

Marín, O. J. N. R. N. (2012). Interneuron dysfunction in psychiatric disorders. *13*(2), 107.

McEwen, B. S., & Gianaros, P. J. J. A. r. o. m. (2011). Stress-and allostasis-induced brain plasticity. *62*, 431-445.

McEwen, B. S., & Magarinos, A. M. (2001). Stress and hippocampal plasticity: implications for the pathophysiology of affective disorders. *Human Psychopharmacology: Clinical and Experimental, 16*(S1), S7-S19.

Meaney, M. J. J. C. d. (2010). Epigenetics and the biological definition of gene× environment interactions. *81*(1), 41-79.

Mehler, M. F., & Mattick, J. S. J. P. r. (2007). Noncoding RNAs and RNA editing in brain development, functional diversification, and neurological disease. *87*(3), 799-823.

Mehregan, H., Najmabadi, H., & Kahrizi, K. (2016). Genetic studies in intellectual disability and behavioral impairment.

Moore, K. A., Nicoll, R. A., & Schmitz, D. J. P. o. t. N. A. o. S. (2003). Adenosine gates synaptic plasticity at hippocampal mossy fiber synapses. *100*(24), 14397-14402.

Moser, D. K., Dracup, K., Evangelista, L. S., Zambroski, C. H., Lennie, T. A., Chung, M. L., . . . Heo, S. (2010). Comparison of prevalence of symptoms of depression, anxiety, and hostility in elderly patients with heart failure, myocardial infarction, and a coronary artery bypass graft. *Heart & Lung: The Journal of Acute and Critical Care, 39*(5), 378-385.

Muntner, P., He, J., Hamm, L., Loria, C., & Whelton, P. K. (2002). Renal insufficiency and subsequent death resulting from cardiovascular disease in the United States. *Journal of the American Society of Nephrology, 13*(3), 745-753.

Murthy, C. R., & Hertz, L. J. N. r. (1988). Pyruvate decarboxylation in astrocytes and in neurons in primary cultures in the presence and the absence of ammonia. *13*(1), 57-61.

Nabel, E. M., & Morishita, H. J. F. i. p. (2013). Regulating critical period plasticity: insight from the visual system to fear circuitry for therapeutic interventions. *4*, 146.

Nagy, Z. M., Misanin, J. R. J. J. o. c., & psychology, p. (1970). Visual perception in the retinal degenerate C3H mouse. *72*(2), 306.

Naninck, E. F., Hoeijmakers, L., Kakava-Georgiadou, N., Meesters, A., Lazic, S. E., Lucassen, P. J., & Korosi, A. J. H. (2015). Chronic early life stress alters developmental and adult neurogenesis and impairs cognitive function in mice. *25*(3), 309-328.

Napoli, C., Casamassimi, A., Crudele, V., Infante, T., & Abbondanza, C. (2011). Kidney and heart interactions during cardiorenal syndrome: a molecular and clinical pathogenic framework. *Future cardiology, 7*(4), 485-497.

Narayan, S., Tang, B., Head, S. R., Gilmartin, T. J., Sutcliffe, J. G., Dean, B., & Thomas, E. A. J. B. r. (2008). Molecular profiles of schizophrenia in the CNS at different stages of illness. *1239*, 235-248.

Neinast, M., Murashige, D., & Arany, Z. (2019). Branched chain amino acids. *Annual review of physiology, 81*, 139-164.

Nicholson, J. K., Lindon, J. C., & Holmes, E. (1999). 'Metabonomics': understanding the metabolic responses of living systems to pathophysiological stimuli via multivariate statistical analysis of biological NMR spectroscopic data. *Xenobiotica, 29*(11), 1181-1189.

Nijveldt, R. J., van Leeuwen, P. A., van Guldener, C., Stehouwer, C. D., Rauwerda, J. A., & Teerlink, T. (2002). Net renal extraction of asymmetrical (ADMA) and symmetrical (SDMA) dimethylarginine in fasting humans. *Nephrology Dialysis Transplantation, 17*(11), 1999-2002.

Nowicki, S., Searcy, W., & Peters, S. J. J. o. C. P. A. (2002). Brain development, song learning and mate choice in birds: a review and experimental test of the" nutritional stress hypothesis". *188*(11-12), 1003-1014.

Organization, W. H. (2018). World health statistics 2018: monitoring health for the SDGs, sustainable development goals.

Otte, D.-M., de Arellano, M. L. B., Bilkei-Gorzo, A., Albayram, Ö., Imbeault, S., Jeung, H., . . . Zimmer, A. (2013). Effects of chronic D-serine elevation on animal models of depression and anxiety-related behavior. *PloS one, 8*(6), e67131.

Pace, T. W., Mletzko, T. C., Alagbe, O., Musselman, D. L., Nemeroff, C. B., Miller, A. H., & Heim, C. M. J. A. J. o. P. (2006). Increased stress-induced inflammatory responses in male patients with major depression and increased early life stress. *163*(9), 1630-1633.

Painter, R. C., de Rooij, S. R., Bossuyt, P. M., Simmers, T. A., Osmond, C., Barker, D. J., . . . Roseboom, T. J. J. T. A. j. o. c. n. (2006). Early onset of coronary artery disease after prenatal exposure to the Dutch famine–. *84*(2), 322-327.

Park, S. G., Schimmel, P., & Kim, S. (2008). Aminoacyl tRNA synthetases and their connections to disease. *Proceedings of the National Academy of Sciences, 105*(32), 11043-11049.

Pauls, D. L., Abramovitch, A., Rauch, S. L., & Geller, D. A. J. N. R. N. (2014). Obsessive– compulsive disorder: an integrative genetic and neurobiological perspective. *15*(6), 410.

Paxman, E. J., Boora, N. S., Kiss, D., Laplante, D. P., King, S., Montina, T., & Metz, G. A. (2018). Prenatal maternal stress from a natural disaster alters urinary metabolomic profiles in Project Ice Storm participants. *Scientific reports, 8*(1), 12932.

Pinto, L. H., & Enroth-Cugell, C. J. M. G. (2000). Tests of the mouse visual system. *11*(7), 531-536.

Portrait, F., Teeuwiszen, E., & Deeg, D. (2011). Early life undernutrition and chronic diseases at

older ages: the effects of the Dutch famine on cardiovascular diseases and diabetes. *Social science & medicine, 73*(5), 711-718.

Post, R. M. (1992). Transduction of psychosocial stress into the neurobiology of recurrent affective disorder. *The American journal of psychiatry, 149*(8), 999.

Prabhu, K. S., Arner, R. J., Vunta, H., & Reddy, C. C. (2005). Up-regulation of human myo-inositol oxygenase by hyperosmotic stress in renal proximal tubular epithelial cells. *Journal of Biological Chemistry, 280*(20), 19895-19901.

Prusky, G. T., West, P. W., & Douglas, R. M. J. V. r. (2000). Behavioral assessment of visual acuity in mice and rats. *40*(16), 2201-2209.

Psychogios, N., Hau, D. D., Peng, J., Guo, A. C., Mandal, R., Bouatra, S., . . . Gautam, B. J. P. o. (2011). The human serum metabolome. *6*(2), e16957.

Rao, K. R., & Norenberg, M. J. M. B. D. (2001). Cerebral energy metabolism in hepatic encephalopathy and hyperammonemia. *16*(1-2), 67-78.

Ratnakumari, L., & Murthy, C. R. J. N. r. (1989). Activities of pyruvate dehydrogenase,enzymes of citric acid cycle, and aminotransferases in the subcellular fractions of cerebral cortex in normal and hyperammonemic rats. *14*(3), 221-228.

Reh, R. K. (2015). *A Rapid Peak in Gamma Power Signals Critical Period Plasticity in the Developing Mouse Visual Cortex.*

Reid, S. N., Daw, N. W., Gregory, D. S., & Flavin, H. J. J. o. N. (1996). cAMP levels increased by activation of metabotropic glutamate receptors correlate with visual plasticity. *16*(23), 7619-7626.

Rezin, G. T., Amboni, G., Zugno, A. I., Quevedo, J., & Streck, E. L. (2009). Mitochondrial dysfunction and psychiatric disorders. *Neurochemical research, 34*(6), 1021.

Rice, D., & Barone Jr, S. J. E. h. p. (2000). Critical periods of vulnerability for the developing nervous system: evidence from humans and animal models. *108*(suppl 3), 511-533.

Rooyackers, O. E., & Nair, K. S. (1997). Hormonal regulation of human muscle protein metabolism. *Annual review of nutrition, 17*(1), 457-485.

Roseboom, T. J., van der Meulen, J. H., Osmond, C., Barker, D. J., Ravelli, A. C.,Schroeder-Tanka, J. M., . . . Bleker, O. P. J. H. (2000). Coronary heart disease after prenatal exposure to the Dutch famine, 1944–45. *84*(6), 595-598.

Roseboom, T. J., Van Der Meulen, J. H., Ravelli, A. C., Osmond, C., Barker, D. J., Bleker, O. P. J. T. R., & Genetics, H. (2001). Effects of prenatal exposure to the Dutch famine on adult disease in later life: an overview. *4*(5), 293-298.

Sase, A., Dahanayaka, S., Höger, H., Wu, G., & Lubec, G. J. B. b. r. (2013). Changes of

hippocampal beta-alanine and citrulline levels are paralleling early and late phase of retrieval in the Morris Water Maze. *249*, 104-108.

Sata, Y., & Krum, H. (2010). The future of pharmacological therapy for heart failure. *Circulation Journal*, 1004130687-1004130687.

Saxbe, D. E., Negriff, S., Susman, E. J., Trickett, P. K. J. D., & psychopathology. (2015). Attenuated hypothalamic–pituitary–adrenal axis functioning predicts accelerated pubertal development in girls 1 year later. *27*(3), 819-828.

Schiavone, S., Sorce, S., Dubois-Dauphin, M., Jaquet, V., Colaianna, M., Zotti, M., . . . Krause, K.-H. J. B. p. (2009). Involvement of NOX2 in the development of behavioral and pathologic alterations in isolated rats. *66*(4), 384-392.

Schimmel, P., & de Pouplana, L. s. R. J. T. i. b. s. (2000). Footprints of aminoacyl-tRNA synthetases are everywhere. *25*(5), 207-209.

Shonkoff, J. P., Garner, A. S., Siegel, B. S., Dobbins, M. I., Earls, M. F., McGuinn, L., . . . Pediatrics, D. C. J. (2012). The lifelong effects of early childhood adversity and toxic stress. *129*(1), e232-e246.

Singer, B., & Ryff, C. D. J. A. o. t. N. y. A. o. S. (1999). Hierarchies of life histories and associated health risks. *896*(1), 96-115.

Sloane, S. A., Shea, S. L., Procter, M. M., Dewsbury, D. A. J. A. l., & behavior. (1978). Visual cliff performance in 10 species of muroid rodents. *6*(2), 244-248.

Smith, J. M., Lunga, P., Story, D., Harris, N., Le Belle, J., James, M. F., . . . Fawcett, J. W. J. B. (2007). Inosine promotes recovery of skilled motor function in a model of focal brain injury. *130*(4), 915-925.

Smriga, M., Ghosh, S., Mouneimne, Y., Pellett, P. L., & Scrimshaw, N. S. (2004). Lysine fortification reduces anxiety and lessens stress in family members in economically weak communities in Northwest Syria. *Proceedings of the National Academy of Sciences, 101*(22), 8285-8288.

Smriga, M., Kameishi, M., Uneyama, H., & Torii, K. (2002). Dietary L-lysine deficiency increases stress-induced anxiety and fecal excretion in rats. *The Journal of nutrition, 132*(12), 3744-3746.

Smriga, M., & Torii, K. (2003). L-Lysine acts like a partial serotonin receptor 4 antagonist and inhibits serotonin-mediated intestinal pathologies and anxiety in rats. *Proceedings of the National Academy of Sciences, 100*(26), 15370-15375.

Steptoe, A., & Kivimäki, M. (2012). Stress and cardiovascular disease. *Nature Reviews Cardiology, 9*(6), 360.

Stewart, S. E., Yu, D., Scharf, J. M., Neale, B. M., Fagerness, J. A., Mathews, C. A., . . . Osiecki, L. J. M. p. (2013). Genome-wide association study of obsessive-compulsive disorder. *18*(7), 788.

Stockard, C. R. J. A. J. o. A. (1921). Developmental rate and structural expression: an experimental study of twins,'double monsters' and single deformities, and the interaction among embryonic organs during their origin and development. *28*(2), 115-277.

Sur, M., & Leamey, C. A. J. N. R. N. (2001). Development and plasticity of cortical areas and networks. *2*(4), 251.

Sur, M., & Rubenstein, J. L. J. S. (2005). Patterning and plasticity of the cerebral cortex. *310*(5749), 805-810.

Szymańska, E., Saccenti, E., Smilde, A. K., & Westerhuis, J. A. (2012). Double-check: validation of diagnostic statistics for PLS-DA models in metabolomics studies. *Metabolomics, 8*(1), 3-16.

Tain, Y.-L., & Hsu, C.-N. (2017). Developmental origins of chronic kidney disease: should we focus on early life? *International journal of molecular sciences, 18*(2), 381.

Taylor, R. (1983). Prevention and control of non-communicable diseases in Pacific Island nations: prospects and constraints. *Medical journal of Australia, 2*(8), 389-394.

Thornburg, K., & Louey, S. (2005). Fetal roots of cardiac disease. *Heart, 91*(7), 867-868.

Thurston, J. H., & Hauhart, R. E. (1989). Effect of momentary stress on brain energy metabolism in weanling mice: apparent use of lactate as cerebral metabolic fuel concomitant with a decrease in brain glucose utilization. *Metabolic brain disease, 4*(3), 177-186.

Tiedje, K., Stevens, K., Barnes, S., & Weaver, D. J. N. i. (2010). β-Alanine as a small molecule neurotransmitter. *57*(3), 177-188.

Tilbrook, A. J., Turner, A. I., & Clarke, I. J. J. R. o. r. (2000). Effects of stress on reproduction in non-rodent mammals: the role of glucocorticoids and sex differences. *5*(2), 105-113.

Tropea, D., Van Wart, A., & Sur, M. J. P. T. o. t. R. S. B. B. S. (2008). Molecular mechanisms of experience-dependent plasticity in visual cortex. *364*(1515), 341-355.

Vasan, R. S., Larson, M. G., Leip, E. P., Evans, J. C., O'donnell, C. J., Kannel, W. B., & Levy, D. (2001). Impact of high-normal blood pressure on the risk of cardiovascular disease. *New England Journal of Medicine, 345*(18), 1291-1297.

Vieau, D. (2011). Perinatal nutritional programming of health and metabolic adult disease. *World journal of diabetes, 2*(9), 133.

Wang, G., Walker, S. O., Hong, X., Bartell, T. R., & Wang, X. J. J. o. A. H. (2013). Epigenetics

and early life origins of chronic noncommunicable diseases. *52*(2), S14-S21.

Wang, T. J., Larson, M. G., Vasan, R. S., Cheng, S., Rhee, E. P., McCabe, E., . . . Fernandez, C. (2011). Metabolite profiles and the risk of developing diabetes. *Nature medicine, 17*(4), 448.

Wang, X.-M. (2013). Early life programming and metabolic syndrome. *World Journal of Pediatrics, 9*(1), 5-8.

Wei, Z., Wang, L., Zhang, M., Xuan, J., Wang, Y., Liu, B., . . . Li, T. J. J. o. p. (2012). A pharmacogenetic study of risperidone on histamine H3 receptor gene (HRH3) in Chinese Han schizophrenia patients. *26*(6), 813-818.

Weiss, M. J. S., & Wagner, S. H. J. A. J. o. P. M. (1998). What explains the negative consequences of adverse childhood experiences on adult health. *14*(4), 356-360.

Westerhuis, J. A., Hoefsloot, H. C., Smit, S., Vis, D. J., Smilde, A. K., van Velzen, E. J., . . . van Dorsten, F. A. (2008). Assessment of PLSDA cross validation. *Metabolomics, 4*(1), 81-89.

Whaley-Connell, A., Pavey, B. S., Afroze, A., & Bakris, G. L. (2006). Obesity and insulin resistance as risk factors for chronic kidney disease. *Journal of the cardiometabolic syndrome, 1*(3), 209-216.

Wiesel, T. N., & Hubel, D. H. J. J. o. n. (1963). Single-cell responses in striate cortex of kittens deprived of vision in one eye. *26*(6), 1003-1017.

Wishart, D. S. (2008). Quantitative metabolomics using NMR. *TrAC trends in analytical chemistry, 27*(3), 228-237.

Wishart, D. S., Jewison, T., Guo, A. C., Wilson, M., Knox, C., Liu, Y., . . . Dong, E. (2012). HMDB 3.0—the human metabolome database in 2013. *Nucleic acids research, 41*(D1), D801-D807.

Wishart, D. S., Knox, C., Guo, A. C., Eisner, R., Young, N., Gautam, B., . . . Bouatra, S. (2008). HMDB: a knowledgebase for the human metabolome. *Nucleic acids research, 37*(suppl_1), D603-D610.

Wishart, D. S., Lewis, M. J., Morrissey, J. A., Flegel, M. D., Jeroncic, K., Xiong, Y., . . . Tzur, D. J. J. o. C. B. (2008). The human cerebrospinal fluid metabolome. *871*(2), 164-173.

Wishart, D. S., Tzur, D., Knox, C., Eisner, R., Guo, A. C., Young, N., . . . Sawhney, S. (2007). HMDB: the human metabolome database. *Nucleic acids research, 35*(suppl_1), D521-D526.

Xia, J., Broadhurst, D. I., Wilson, M., & Wishart, D. S. (2013). Translational biomarker discovery in clinical metabolomics: an introductory tutorial. *Metabolomics, 9*(2), 280-

299.

Xia, J., Mandal, R., Sinelnikov, I. V., Broadhurst, D., & Wishart, D. S. (2012). MetaboAnalyst 2.0—a comprehensive server for metabolomic data analysis. *Nucleic acids research, 40*(W1), W127-W133.

Xia, J., Psychogios, N., Young, N., & Wishart, D. S. (2009). MetaboAnalyst: a web server for metabolomic data analysis and interpretation. *Nucleic acids research, 37*(suppl_2), W652-W660.

Xia, J., Sinelnikov, I. V., Han, B., & Wishart, D. S. (2015). MetaboAnalyst 3.0—making metabolomics more meaningful. *Nucleic acids research, 43*(W1), W251-W257.

Xia, J., Sinelnikov, I. V., & Wishart, D. S. (2011). MetATT: a web-based metabolomics tool for analyzing time-series and two-factor datasets. *Bioinformatics, 27*(17), 2455-2456.

Xia, J., & Wishart, D. (2002). Current Protocols in Bioinformatics. Baxevanis AD, Petsko GA, Stein LD, Stormo GD, editors Hoboken. *NJ, USA: John Wiley & Sons, Inc. doi, 10*, 0471250953.

Xia, J., & Wishart, D. S. (2010a). MetPA: a web-based metabolomics tool for pathway analysis and visualization. *Bioinformatics, 26*(18), 2342-2344.

Xia, J., & Wishart, D. S. (2010b). MSEA: a web-based tool to identify biologically meaningful patterns in quantitative metabolomic data. *Nucleic acids research, 38*(suppl_2), W71-W77.

Xia, J., & Wishart, D. S. (2011). Web-based inference of biological patterns, functions and pathways from metabolomic data using MetaboAnalyst. *Nature protocols, 6*(6), 743.

Xia, J., & Wishart, D. S. (2016). Using MetaboAnalyst 3.0 for comprehensive metabolomics data analysis. *Current protocols in bioinformatics, 55*(1), 14.10. 11-14.10. 91.

Yao, P., & Fox, P. L. (2013). Aminoacyl-tRNA synthetases in medicine and disease. *EMBO molecular medicine, 5*(3), 332-343.

Yu, Z., Rebholz, C. M., Wong, E., Chen, Y., Matsushita, K., Coresh, J., & Grams, M. E. (2019). Association Between Hypertension and Kidney Function Decline: The Atherosclerosis Risk in Communities (ARIC) Study. *American Journal of Kidney Diseases*.

Zhang, A., Sun, H., Wang, P., Han, Y., & Wang, X. J. A. (2012). Modern analytical techniques in metabolomics analysis. *137*(2), 293-300.

Zhang, Y., Filiou, M. D., Reckow, S., Gormanns, P., Maccarrone, G., Kessler, M. S., . . . Landgraf, R. (2011). Proteomic and metabolomic profiling of a trait anxiety mouse model implicate affected pathways. *Molecular & Cellular Proteomics, 10*(12), M111. 008110.

Zhenyukh, O., Civantos, E., Ruiz-Ortega, M., Sánchez, M. S., Vázquez, C., Peiró, C., . . . Mas, S. (2017). High concentration of branched-chain amino acids promotes oxidative stress, inflammation and migration of human peripheral blood mononuclear cells via mTORC1 activation. *Free Radical Biology and Medicine*, *104*, 165-177.

APPENDIX A: SUPPLEMENTAL TABLES FOR CHAPTERS 2 AND 3

Organ	Metabolite	NMR Chemical Shift Range of Bin (ppm)	Mann-Whitney U Test	Percent Difference	VIP Score	Regulation by Stress
Kidney	Dimethylamine.1†	2.771–2.756	8.25E-05	–86.21	3.00	Down
	Uridine.1†	4.344–4.320	1.82E-02	40.14	1.61	Up
	Malate.1†	2.653–2.639	1.38E-04	28.94	1.58	Up
	Methionine.1	2.639–2.630	1.07E-04	27.16	1.54	Up
	Fumarate†	6.533–6.519	1.82E-03	–34.74	1.54	Down
	Valine.1†	2.326–2.248	8.25E-05	–24.00	1.51	Down
	Tyrosine.1†	3.051–2.980	1.38E-04	–20.13	1.36	Down
	Phenylalanine.1	7.813–7.801	1.18E-03	–24.54	1.34	Down
	Tyrosine.2†	2.870–2.854	1.82E-03	–24.50	1.31	Down
	Inosine.1†	4.466–4.441	1.82E-02	–34.38	1.31	Up
	Carnitine.1†, Malate.2†, Pyroglutamate.1†	2.476–2.429	8.25E-05	18.03	1.28	Up
	Inosine.2†	6.817–6.806	2.53E-02	29.34	1.28	Up
	Phenylalanine.2	7.453–7.415	1.18E-03	–19.81	1.28	Down
	Valine.2†	1.058–1.029	1.82E-03	–19.24	1.26	Down
	3-Hydroxybutyrate.1	0.901–0.886	1.47E-03	22.37	1.25	Up
	Aspartate.1†	2.722–2.709	1.38E-04	–17.36	1.25	Down
	Phenylalanine.3	7.354–7.321	1.18E-03	–18.58	1.23	Down
	Acetate.1	1.967–1.873	5.97E-04	–17.93	1.23	Down
	Dimethylamine.2†	2.738–2.722	8.25E-05	–15.33	1.18	Down
	Aspartate.2†	2.697–2.686	8.25E-05	–15.24	1.17	Down
	Inosine.3†	4.295–4.274	8.94E-03	21.37	1.16	Up
	Glutamate.1†, Methionine.2	2.168–2.098	1.38E-04	14.77	1.14	Up
	Leucine.1†, Valine.3†	0.984–0.948	2.25E-03	–15.86	1.12	Down
	Lactate.1†	1.215–1.206	5.97E-04	16.31	1.11	Up
	Serine.1†	3.960–3.952	1.07E-04	–13.37	1.10	Down
	Phenylalanine.4	7.403–7.362	7.51E-04	–16.05	1.08	Down

Kidney	Tyrosine.3†	3.095–3.051	4.72E-04	–13.27	1.04	Down
	Valine.4†	1.029–0.984	1.82E-03	–13.61	1.02	Down
	Aspartate.3†	2.709–2.697	1.78E-04	–12.04	1.01	Down
	3-Hydroxybutyrate.2	1.206–1.197	2.25E-03	14.67	1.01	Up
	Choline.1†	3.220–3.189	1.47E-03	14.33	1.00	Up
	Azelate, Isoleucine.1, Methylmalonate†	1.303–1.231	1.53E-02	19.43	0.99	Up
	Alanine†	1.501–1.475	2.77E-03	–12.96	0.98	Down
	Malate.3†	2.664–2.653	6.14E-03	16.26	0.97	Up
	Aspartate.4†	2.814–2.780	4.72E-04	–11.88	0.97	Down
	Tyrosine.4†	7.220–7.178	1.18E-03	–12.78	0.97	Down
	Choline.2†	4.093–4.054	9.42E-04	12.19	0.93	Up
	Aspartate.5†	2.835–2.814	7.51E-04	–11.43	0.93	Down
	Niacinamide.1†, S-Adenosylhomocysteine†	8.290–8.248	7.42E-03	16.23	0.91	Up
	Inosine.4†	8.374–8.351	4.15E-03	26.84	0.90	Up
	Leucine.2†	0.948–0.938	2.25E-03	–11.36	0.90	Down
	Arginine, Cadaverine, Leucine.3†	1.768–1.637	1.82E-03	–10.67	0.89	Down
	Carnitine.2†, Glutamate.2†, Malate.4†, Pyroglutamate.2†, Succinate†	2.430–2.390	1.07E-02	13.50	0.89	Up
	τ-Methylhistidine†	8.021–8.013	2.53E-02	15.86	0.88	Up
	Creatine Phosphate	3.933–3.923	1.53E-02	12.99	0.84	Up
	Tyrosine.5†	6.933–6.895	1.82E-03	–10.39	0.82	Down
	Caffeine	7.937–7.913	6.14E-03	–10.24	0.79	Down
	Choline.3†	3.539–3.512	1.82E-03	8.86	0.75	Up
	Inosine.5†	6.118–6.092	6.14E-03	22.51	0.74	Up
	Malate.5†	2.676–2.664	4.72E-02	15.62	0.73	Up
	Glucose.1†	3.901–3.880	1.07E-02	–9.10	0.73	Down
	2-Aminoadipate†	3.758–3.725	2.77E-03	–8.46	0.73	Down

Kidney	Creatine†, Serine.2†, Tyrosine.6†	3.952–3.945	1.82E-03	–7.54	0.72	Down
	Lactate.2†	4.158–4.093	8.94E-03	8.22	0.69	Up
	Uracil†	5.824–5.811	4.72E-02	–11.18	0.68	Down
	Choline.4†	4.054–4.039	2.53E-02	11.14	0.68	Up
	Serine.3†	3.972–3.960	1.82E-03	–7.01	0.68	Down
	Cystine	3.370–3.361	5.06E-03	–7.49	0.67	Down
	Tyrosine.7†	7.169–7.150	3.48E-02	–8.99	0.67	Down
	Serine.4†	4.011–3.981	4.15E-03	–6.92	0.65	Down
	Isoleucine.2	3.699–3.662	1.53E-02	6.76	0.60	Up
	Glucose.2†	3.907–3.901	2.25E-03	–6.56	0.59	Down
	Formate†	8.469–8.457	8.94E-03	–7.65	0.58	Down
	Histidine†	8.082–8.063	3.48E-02	–7.28	0.58	Down
	Serine.5†	3.981–3.972	7.42E-03	–5.91	0.57	Down
	Proline.1	3.354–3.321	4.06E-02	6.85	0.55	Up
	Lactate.3†	1.355–1.317	2.98E-02	6.90	0.53	Up
	Choline.5†	3.179–3.171	1.82E-02	5.00	0.53	Up
	Acetate.2	2.012–1.967	8.94E-03	–4.90	0.52	Down
	Glucose.3†	3.512–3.499	1.07E-02	–8.34	0.51	Down
	Niacinamide.2†	8.964–8.941	3.48E-02	5.79	0.51	Up
	Choline.6†	3.189–3.179	2.53E-02	4.65	0.50	Up
	Ethanolamine†	3.130–3.095	1.53E-02	4.26	0.50	Up
	Proline.2	3.321–3.303	2.53E-02	5.47	0.49	Up
	Uridine.2†	7.888–7.875	3.48E-02	10.73	0.44	Up
	Glutamate.3†	2.098–2.024	2.98E-02	3.76	0.43	Up
	4-Pyridoxate†	7.899–7.888	4.06E-02	10.99	0.38	Up
	Tyrosine.8†	3.171–3.161	2.98E-02	–2.92	0.35	Down
	Myo-Inositol†, Threonine†, Valine.5†	3.611–3.591	2.53E-02	–3.46	0.34	Down
	Glycerol†	3.638–3.611	1.53E-02	3.57	0.26	Up
	Glucose.4†	3.725–3.712	4.72E-02	–3.11	0.23	Down

Heart	Glucuronate.1	4.675–4.663	7.51E-04	–149.75	3.41	Down
	Glucuronate.2	4.663–4.652	7.51E-04	–143.00	2.95	Down
	Adenosine.1	4.437–4.321	7.51E-04	–83.06	2.80	Down
	Uridine.1†	7.930–7.921	8.25E-05	137.40	2.66	Up
	2-Aminoadipate.1†, Levulinate.1, Thymol.1, Valine.1†	2.242–2.234	8.25E-05	–122.46	2.45	Down
	4-Pyridoxate.1†	7.938–7.930	8.25E-05	–131.59	2.13	Down
	Uridine.2†	8.079–8.069	8.25E-05	94.58	2.03	Up
	4-Pyridoxate.2†	8.114–8.107	8.25E-05	–109.50	1.82	Down
	Creatine†	3.060–3.049	8.25E-05	69.32	1.73	Up
	Glutamate.1†, Pyroglutamate.1†	2.415–2.402	8.25E-05	71.47	1.72	Up
	Isocitrate.1	2.564–2.551	8.25E-05	–68.36	1.71	Down
	Histidine.1†	7.165–7.145	7.51E-04	83.75	1.67	Up
	Carnitine.1†	2.476–2.464	8.25E-05	–64.95	1.63	Down
	Pyridoxine.1	2.485–2.476	8.25E-05	–62.29	1.60	Down
	Tyrosine.1†	7.180–7.165	8.25E-05	–86.67	1.58	Down
	N-Methylhydantoin.1, N,N-Dimethylglycine.1, Trimethylamine.1	2.907–2.897	8.25E-05	–59.07	1.53	Down
	Carnitine.2†, 4-Pyridoxate.3†	2.464–2.453	8.25E-05	–56.71	1.51	Down
	Glutamate.2†, Pyroglutamate.2†, Succinate.1†	2.402–2.390	8.25E-05	55.08	1.50	Up
	Levulinate.2	2.789–2.771	8.25E-05	–57.44	1.48	Down
	Levulinate.3	2.771–2.754	8.25E-05	–54.01	1.47	Down
	Anserine.1	2.958–2.946	8.25E-05	–53.23	1.45	Down
	N-Methylhydantoin.2, N,N-Dimethylglycine.2, Tyramine.1	2.917–2.907	8.25E-05	–53.84	1.44	Down
	Threonine.1†	4.209–4.204	7.51E-04	–61.86	1.44	Down
	Threonine.2†	4.270–4.264	9.42E-04	–59.97	1.43	Down

Heart	Anserine.2, N-Methylhydantoin.3	2.946–2.940	8.25E-05	–51.29	1.42	Down
	Trimethylamine.2	2.868–2.861	8.25E-05	–52.81	1.40	Down
	Threonine.3†	4.241–4.234	5.97E-04	–59.59	1.39	Down
	S-Adenosylhomocysteine.1†	2.166–2.153	8.25E-05	–47.72	1.39	Down
	Isocitrate.2	2.572–2.564	8.25E-05	–47.07	1.39	Down
	Levulinate.4	2.754–2.732	1.38E-04	–51.78	1.39	Down
	O-Phosphocholine.1, Threonine.4†	4.234–4.226	7.51E-04	–59.96	1.39	Down
	Threonine.5†	4.257–4.247	7.51E-04	–57.66	1.37	Down
	3-Hydroxykynurenine.1, Pyroglutamate.3†	4.192–4.187	8.25E-05	50.50	1.34	Up
	O-Phosphocholine.2, Threonine.6†	4.226–4.209	7.51E-04	–54.20	1.34	Down
	Anserine.3, Isocitrate.3	2.968–2.958	8.25E-05	–45.46	1.34	Down
	2-Oxoisocaproate.1, Homocysteine.1, Methylamine	2.633–2.625	1.07E-04	–47.49	1.33	Down
	Cholate.1	1.198–1.181	8.25E-05	–45.05	1.32	Down
	3-Hydroxyphenylacetate.1	3.492–3.482	8.25E-05	41.27	1.31	Up
	S-Adenosylhomocysteine.2†	3.109–3.060	1.78E-04	–46.11	1.30	Down
	Pyroglutamate.4†	2.514–2.507	8.25E-05	43.04	1.30	Up
	Carnitine.3†	2.453–2.439	8.25E-05	–42.45	1.29	Down
	Isocitrate.4	2.979–2.968	8.25E-05	–42.40	1.29	Down
	S-Adenosylhomocysteine.3†	2.192–2.166	8.25E-05	–39.98	1.29	Down
	Isocitrate.5	2.586–2.572	1.07E-04	–43.54	1.29	Down
	Formate†	8.471–8.459	5.97E-04	–47.10	1.27	Down
	S-Adenosylhomocysteine.4†	2.153–2.145	8.25E-05	–41.42	1.26	Down
	Glutamate.3†, Pyroglutamate.5†	2.035–2.025	8.25E-05	40.53	1.26	Up
	Threonine.7†	4.247–4.241	7.51E-04	–49.97	1.26	Down
	4-Pyridoxate.4†, Carnitine.4†	2.439–2.429	8.25E-05	–40.43	1.26	Down

Heart	Glutamate.4†, Pyroglutamate.6†	2.045–2.035	8.25E-05	38.99	1.25	Up
	Isocitrate.6	2.551–2.543	1.07E-04	–39.47	1.22	Down
	Threonine.8†	4.264–4.257	1.18E-03	–47.47	1.20	Down
	Thymol.2	3.134–3.122	8.25E-05	–36.91	1.19	Down
	Malonate.1	3.122–3.109	1.07E-04	–37.84	1.19	Down
	Cholate.2	1.181–1.168	1.38E-04	–38.78	1.19	Down
	Isocitrate.7	2.988–2.979	8.25E-05	–35.84	1.18	Down
	Glycerol.1†, Guanidoacetate.1	3.786–3.782	1.38E-04	–36.89	1.17	Down
	Singlet 4.068 ppm	4.072–4.064	8.25E-05	34.84	1.17	Up
	S-Adenosylhomocysteine.5†	2.141–2.129	8.25E-05	–35.95	1.16	Down
	2-Aminoadipate.2†, Levulinate.5, Thymol.3, Valine.2†	2.251–2.242	1.78E-04	–36.12	1.15	Down
	Pyroglutamate.7†, Succinate.2†	2.429–2.415	8.25E-05	36.11	1.14	Up
	Thymol.4	3.171–3.143	8.25E-05	–32.27	1.12	Down
	Isocitrate.8	3.003–2.988	8.25E-05	–32.32	1.11	Down
	Glucarate.1	4.163–4.146	7.51E-04	–40.76	1.10	Down
	Malonate.2, Thymol.5	3.179–3.171	8.25E-05	–30.70	1.10	Down
	Adenosine.2	4.314–4.306	7.51E-04	–40.26	1.10	Down
	Pyroglutamate.8†	2.525–2.514	8.25E-05	32.80	1.10	Up
	Anserine.4, N-Methylhydantoin.4, N,N-Dimethylglycine.3	2.940–2.934	8.25E-05	–30.66	1.08	Down
	Glucarate.2	4.167–4.163	9.42E-04	–38.89	1.08	Down
	Glutamate.5†, Pyroglutamate.9†	2.025–2.015	8.25E-05	30.71	1.07	Up
	Homogentisate	3.504–3.492	1.18E-03	–38.93	1.06	Down
	3-Hydroxykynurenine.2, Pyroglutamate.10†	4.187–4.180	1.38E-04	35.49	1.05	Up
	Cholate.3	1.168–1.157	3.72E-04	–32.40	1.05	Down

Heart	3-Hydroxyphenylacetate.2, Homovanillate	3.482–3.468	8.25E-05	28.32	1.02	Up
	Theophylline.1	3.384–3.374	1.38E-04	–26.57	1.00	Down
	Adenosine.3, Threonine.9†	4.306–4.300	7.51E-04	–33.87	0.99	Down
	Glycerol.2†	3.646–3.639	1.38E-04	–27.17	0.99	Down
	Pyridoxine.2	2.492–2.485	4.72E-04	–28.72	0.99	Down
	Adenosine.4	4.449–4.437	9.42E-04	–33.81	0.98	Down
	Isocitrate.9	3.015–3.003	2.92E-04	–27.25	0.98	Down
	Adenosine.5	4.466–4.456	9.42E-04	–33.48	0.97	Down
	Glucarate.3, N-Methylhydantoin.5	4.090–4.086	5.97E-04	–31.39	0.97	Down
	Methylmalonate.1†	1.241–1.222	4.72E-04	–29.03	0.96	Down
	3,4-Dihydroxybenzeneacetate.1	3.391–3.384	8.25E-05	–23.79	0.96	Down
	Glucarate.4, N-Methylhydantoin.6	4.106–4.090	7.51E-04	–30.65	0.95	Down
	Adenosine.6, Threonine.10†	4.279–4.270	7.51E-04	–31.19	0.95	Down
	Tyramine.2	3.253–3.248	1.38E-04	–25.06	0.95	Down
	3-Methylglutarate.1	0.923–0.896	7.51E-04	–28.54	0.94	Down
	2-Oxoisocaproate.2, Homocysteine.2	2.641–2.633	4.72E-04	–27.11	0.94	Down
	Adenosine.7, Threonine.11†	4.300–4.295	7.51E-04	–29.02	0.92	Down
	Adenosine.8, Threonine.12†	4.295–4.290	7.51E-04	–28.28	0.92	Down
	Glutamate.6†, Pyroglutamate.11†	2.056–2.045	8.25E-05	21.62	0.91	Up
	Adenosine.9	8.277–8.274	1.78E-04	–24.74	0.91	Down
	Carnitine.5†, O-Phosphocholine.3	3.248–3.241	1.07E-04	–21.78	0.90	Down
	Galactitol.1	3.683–3.677	8.25E-05	–21.57	0.90	Down
	Adenosine.10	4.321–4.314	1.47E-03	–29.35	0.90	Down
	Pyroglutamate.12†	2.673–2.669	4.72E-04	28.67	0.89	Up
	Ethanolamine.1†, Guanidoacetate.2	3.820–3.812	1.78E-04	–22.35	0.88	Down

Heart	Tyramine.3	3.257–3.253	8.25E-05	–20.36	0.88	Down
	Thymol.6	3.143–3.134	1.07E-04	–20.62	0.87	Down
	Glucuronate.3	3.512–3.504	1.82E-02	–32.47	0.86	Down
	O-Phosphoethanolamine	4.039–4.032	5.97E-04	–25.83	0.86	Down
	Choline.1†, Malonate.3	3.189–3.179	1.38E-04	–19.87	0.85	Down
	3-Hydroxyisovalerate.1	2.390–2.385	2.92E-04	–20.56	0.85	Down
	Myo-Inositol.1†	4.075–4.072	7.51E-04	–23.92	0.85	Down
	Glycerol.3†, Guanidoacetate.3	3.796–3.790	1.78E-04	–20.27	0.85	Down
	Homocysteine.3, S-Adenosylhomocysteine.6†	2.107–2.098	1.38E-04	–19.60	0.84	Down
	1,7-Dimethylxanthine.1	3.344–3.338	1.47E-03	–24.88	0.84	Down
	4-Carboxyglutamate.1	3.362–3.359	1.47E-03	–21.78	0.82	Down
	Glucarate.5, N-Methylhydantoin.7	4.086–4.081	1.47E-03	–23.14	0.82	Down
	Kynurenine.1, N,N-Dimethylglycine.4	3.715–3.705	1.47E-03	–24.58	0.82	Down
	2-Hydroxyisovalerate.1	0.794–0.760	4.15E-03	–24.74	0.81	Down
	Galactitol.2, Kynurenine.2	3.705–3.689	7.51E-04	–23.27	0.81	Down
	Aspartate.1†	2.710–2.696	1.18E-03	–20.09	0.80	Down
	2-Hydroxybutyrate.1	0.896–0.866	1.47E-03	–23.01	0.80	Down
	2-Hydroxyisovalerate.2	0.825–0.804	1.28E-02	–25.52	0.80	Down
	3,4-Dihydroxybenzeneacetate.2	3.406–3.391	2.92E-04	–17.20	0.79	Down
	Methylmalonate.2†	1.251–1.241	9.42E-04	–21.92	0.78	Down
	Galactitol.3, Kynurenine.3	3.725–3.719	7.42E-03	–25.06	0.78	Down
	2-Aminoadipate.3†	1.776–1.636	7.51E-04	–18.94	0.78	Down
	Valine.3†	2.329–2.324	7.51E-04	–17.91	0.76	Down
	Myo-Inositol.2†	4.077–4.075	1.82E-03	–21.85	0.76	Down
	Pyroglutamate.13†	2.536–2.525	2.29E-04	19.06	0.76	Up
	4-Carboxyglutamate.2	3.359–3.355	2.92E-04	–18.48	0.76	Down
	Glycylproline.1	1.986–1.978	9.42E-04	–18.87	0.76	Down

Heart	3-Methylxanthine, Glucuronate.4	3.517–3.512	1.47E-03	–21.12	0.75	Down
	Galactitol.4, Kynurenine.4	3.719–3.715	5.97E-04	–19.06	0.75	Down
	Adenosine Monophosphate	4.064–4.039	5.06E-03	–22.20	0.74	Down
	Glucarate.6	4.081–4.077	2.25E-03	–20.15	0.73	Down
	S-Adenosylhomocysteine.7†	2.130–2.119	4.72E-04	–16.53	0.72	Down
	Thymol.7	1.222–1.205	3.40E-03	–20.75	0.72	Down
	1,7-Dimethylxanthine.2	3.338–3.329	4.15E-03	–19.95	0.71	Down
	Choline.2†, O-Phosphocholine.4	3.204–3.189	5.97E-04	–16.04	0.70	Down
	Galactitol.5, Kynurenine.5	3.732–3.728	3.48E-02	–23.03	0.70	Down
	Valine.4†	2.321–2.315	5.97E-04	–14.75	0.69	Down
	Inosine.1†	6.108–6.097	2.25E-03	19.51	0.68	Up
	Tyramine.4	3.266–3.257	6.14E-03	–18.26	0.68	Down
	Tyrosine.2†	3.979–3.970	2.25E-03	–18.30	0.67	Down
	Valine.5†	2.315–2.309	5.97E-04	–14.74	0.67	Down
	Uridine.3†	5.930–5.924	6.14E-03	38.90	0.67	Up
	Ethylmalonate	3.025–3.015	7.51E-04	–13.89	0.66	Down
	2-Aminoadipate.4†, Valine.6†	2.305–2.294	1.82E-03	–16.55	0.66	Down
	Aspartate.2†	2.830–2.823	2.25E-03	–14.99	0.66	Down
	Glycylproline.2	2.004–1.995	2.98E-02	–17.20	0.65	Down
	Valine.7†	2.309–2.305	1.82E-03	–15.38	0.65	Down
	Glycylproline.3	1.995–1.986	4.15E-03	–15.34	0.65	Down
	N-Phenylacetylglycine.1	7.349–7.337	2.77E-03	24.72	0.65	Up
	Taurine.1	3.418–3.406	1.78E-04	12.88	0.64	Up
	Taurine.2	3.289–3.278	2.29E-04	13.05	0.63	Up
	Aspartate.3†	2.823–2.814	4.15E-03	–14.95	0.63	Down
	Adenosine.11	3.884–3.878	3.40E-03	–14.92	0.63	Down
	Adenosine.12	3.888–3.884	2.77E-03	–14.54	0.63	Down
	Taurine.3	3.428–3.418	2.92E-04	12.61	0.62	Up
	Aspartate.4†	2.814–2.798	4.15E-03	–14.55	0.62	Down
	S-Adenosylhomocysteine.8†	2.119–2.107	1.78E-04	–12.03	0.62	Down

Heart	Adenosine.13, Ethanolamine.2†	3.843–3.830	7.42E-03	–14.64	0.61	Down
	Valine.8†	2.324–2.321	2.92E-04	–11.69	0.61	Down
	2-Hydroxyisovalerate.3	0.840–0.825	4.06E-02	–18.32	0.60	Down
	Taurine.4	3.303–3.289	2.92E-04	11.75	0.60	Up
	Theophylline.2	3.374–3.362	6.14E-03	–13.57	0.60	Down
	Hypoxanthine, Niacinamide.1†	8.222–8.203	2.25E-03	15.42	0.60	Up
	Glycine.1	3.577–3.567	1.18E-03	11.91	0.60	Up
	Uridine.4†	5.924–5.915	5.06E-03	45.69	0.59	Up
	Adenosine.14, Ethanolamine.3†	3.830–3.820	8.94E-03	–14.72	0.59	Down
	Serine†	3.878–3.870	2.77E-03	–14.11	0.59	Down
	Lysine.1	1.444–1.431	2.53E-02	–17.89	0.59	Down
	2-Hydroxybutyrate.2, 2-Hydroxyisovalerate.4	0.866–0.852	4.72E-02	–19.38	0.58	Down
	Fumarate†	6.546–6.494	3.48E-02	26.24	0.58	Up
	Myo-Inositol.3†, Valine.9†	3.639–3.627	5.06E-03	–12.89	0.58	Down
	Glutamate.7†, Pyroglutamate.14†	2.065–2.056	2.92E-04	10.03	0.58	Up
	Taurine.5	3.278–3.266	3.72E-04	11.05	0.58	Up
	Niacinamide.2†, Nicotinurate.1	8.268–8.250	1.53E-02	14.16	0.57	Up
	Glycerol.4†	3.782–3.776	9.42E-04	–10.19	0.57	Down
	Niacinamide.3†, Nicotinurate.2	7.610–7.604	4.15E-03	16.89	0.57	Up
	τ-Methylhistidine†	7.811–7.801	1.07E-02	39.24	0.57	Up
	Glycerol.5†, Kynurenine.6	3.758–3.751	4.06E-02	–15.28	0.56	Down
	Thymol.8	1.205–1.198	4.06E-02	–16.58	0.56	Down
	Alanine.1†	1.487–1.476	3.40E-03	12.65	0.55	Up
	Valine.10†	3.617–3.612	6.14E-03	–12.48	0.55	Down
	3-Hydroxyisovalerate.2	2.385–2.379	2.77E-03	–10.58	0.55	Down

Heart	5-Hydroxyindole-3-acetate.1, Theophylline.3	3.597–3.587	6.14E-03	–13.40	0.55	Down
	S-Adenosylhomocysteine.9†	2.098–2.085	1.28E-02	–11.57	0.54	Down
	Alanine.2†	1.500–1.487	3.40E-03	12.19	0.54	Up
	Taurine.6	3.440–3.428	4.72E-04	9.63	0.54	Up
	Choline.3†	3.539–3.517	1.82E-02	–12.89	0.54	Down
	3-Hydroxyisovalerate.3	2.379–2.376	5.97E-04	–9.10	0.54	Down
	Galactitol.6	3.689–3.683	1.53E-02	–12.56	0.54	Down
	Glucuronate.5	3.550–3.539	4.06E-02	–14.58	0.53	Down
	Inosine.2†	6.120–6.108	1.82E-02	14.84	0.53	Up
	Tyrosine.3†	3.970–3.963	2.53E-02	–13.01	0.52	Down
	Homocysteine.4, Malate†	2.656–2.641	2.53E-02	–13.87	0.52	Down
	1,7-Dimethylxanthine.3	3.322–3.313	2.98E-02	–12.84	0.52	Down
	2-Hydroxyisovalerate.5, Ethanolamine.4†, Adenosine.15	3.855–3.851	1.28E-02	–11.33	0.51	Down
	Ethanolamine.5†, Guanidoacetate.4	3.812–3.806	7.51E-04	–8.47	0.51	Down
	Valine.11†	1.046–1.027	5.06E-03	–11.22	0.49	Down
	3-Hydroxy-3-Methylglutarate.1, Lactate.1†	1.354–1.335	2.98E-02	13.24	0.49	Up
	Glycine.2	3.587–3.577	5.06E-03	9.76	0.48	Up
	Tyrosine.4†	3.963–3.960	4.72E-02	–12.01	0.48	Down
	Lysine.2	1.423–1.418	1.53E-02	–11.60	0.47	Down
	Adenosine.16	3.892–3.888	3.48E-02	–10.91	0.47	Down
	Leucine†	0.969–0.959	2.53E-02	9.06	0.46	Up
	Citraconate.1	5.615–5.608	1.82E-02	48.06	0.46	Up
	3-Hydroxy-3-Methylglutarate.2, Lactate.2†	1.335–1.319	4.72E-02	12.11	0.45	Up
	Alanine.3†, N-Phenylacetylglycine.2, O-Acetylcholine.1	3.771–3.766	5.06E-03	7.82	0.45	Up
	Valine.12†	1.027–1.015	1.28E-02	–10.63	0.45	Down

	Aspartate.5†, Dimethylamine.1†	2.721–2.710	1.07E-02	–9.38	0.44	Down
	5-Hydroxyindole-3-acetate.2, Threonine.13†, Valine.13†	3.612–3.603	1.28E-02	–8.36	0.44	Down
	Lysine.3	1.431–1.423	1.82E-02	–12.00	0.44	Down
	Niacinamide.4†, Nicotinurate.3	8.274–8.271	4.72E-02	9.18	0.44	Up
	Glucose.1†	5.261–5.253	4.72E-02	47.89	0.43	Up
	Dimethylamine.2†	2.732–2.721	1.82E-02	–8.83	0.42	Down
	N-Phenylacetylglycine.3	3.677–3.670	7.42E-03	8.41	0.42	Up
	3-Methylglutarate.2, Cholate.4	0.938–0.923	6.14E-03	–8.98	0.42	Down
	Homocysteine.5	2.696–2.690	1.82E-02	–8.17	0.41	Down
	Glucose.2†	5.253–5.245	2.98E-02	50.90	0.40	Up
Heart	2-Hydroxyisovalerate.6	0.852–0.844	2.15E-02	–16.07	0.40	Down
	Aspartate.6†	2.798–2.789	2.15E-02	–8.29	0.40	Down
	Glycerol.6†	3.776–3.771	2.98E-02	–7.47	0.39	Down
	Alanine.4†, N-Phenylacetylglycine.4, O-Acetylcholine.2	3.766–3.758	1.53E-02	6.99	0.39	Up
	Uridine.5†	5.915–5.905	3.40E-03	55.96	0.39	Up
	Histidine.2†	7.197–7.180	8.94E-03	25.77	0.39	Up
	Uracil.1†	5.820–5.811	6.14E-03	59.01	0.38	Up
	Citraconate.2	5.620–5.615	8.94E-03	52.76	0.38	Up
	Glutamate.8†	2.358–2.348	3.48E-02	7.42	0.38	Up
	Maleate.1	6.158–6.154	2.98E-02	22.34	0.38	Up
	Valine.14†	3.627–3.617	2.15E-02	–7.29	0.38	Down
	Citraconate.3	5.624–5.620	2.53E-02	49.09	0.37	Up
	3-Hydroxyisovalerate.4	2.376–2.370	6.14E-03	–5.65	0.36	Down
	O-Acetylcholine.3	3.217–3.204	3.48E-02	7.58	0.36	Up
	N-Phenylacetylglycine.5	7.337–7.324	2.53E-02	18.94	0.36	Up
	2-Hydroxyisovalerate.7	0.804–0.794	2.15E-02	–14.18	0.35	Down
	Glucose.3†, Inosine.3†	3.862–3.860	3.48E-02	6.01	0.35	Up

Heart	Maleate.2	6.154–6.145	4.06E-02	22.98	0.34	Up
	N-Phenylacetylglycine.6	3.662–3.654	3.48E-02	6.89	0.33	Up
	Uracil.2†	5.811–5.797	8.94E-03	66.91	0.33	Up
	Glycerol.7†, Guanidoacetate.5	3.790–3.786	3.48E-02	–4.86	0.32	Down
	Histidine.3†	7.213–7.197	8.94E-03	23.71	0.31	Up
	Inosine.4†	3.905–3.901	2.98E-02	4.62	0.30	Up
	Niacinamide.5†	7.440–7.428	3.48E-02	12.76	0.28	Up
	Uridine.6†	5.937–5.930	5.06E-03	52.96	0.27	Up
	Citraconate.4	5.630–5.624	6.14E-03	65.76	0.24	Up

Table A1. *Kidney and heart metabolites found to be significantly altered by stress in a Mann-Whitney U test. VIP scores, shown in descending order, correspond to Fig. 3A, B. Metabolite regulation is shown as a function of relative concentration in high early postnatal stress individuals. Metabolites for which more than one NMR resonance peak was identified as significant are represented as metabolite.1, metabolite.2, … metabolite.n. †Indicates metabolites that were differentially regulated in both kidney and heart tissues.*

Organ	Metabolite	*r*	*p*	Correlation
Kidney	Methionine.1	–0.66	0.0007	Negative
	Malate.1	–0.64	0.0011	Negative
	Malate.3	–0.61	0.0019	Negative
	Glucose.1	0.60	0.0024	Positive
	2-Aminoadipate‡	0.57	0.0042	Positive
	Cystine	0.56	0.0057	Positive
	Dimethylamine.1	0.54	0.0076	Positive
	Glutamate.1‡, Methionine.2	–0.53	0.0097	Negative
	3-Hydroxybutyrate.1	–0.50	0.0150	Negative
	Glucose.3	0.49	0.0187	Positive
	Serine.1	0.45	0.0293	Positive
	Choline.5‡	–0.45	0.0307	Negative
	Choline.1‡	–0.44	0.0373	Negative
	Alanine‡	0.43	0.0425	Positive
	Glucose.4	0.43	0.0397	Positive
	Malate.5	–0.43	0.0388	Negative
Heart	2-Hydroxybutyrate.1	0.65	0.0009	Positive
	Alanine.3‡, N-Phenylacetylglycine.2, O-Acetylcholine.1	–0.63	0.0012	Negative
	3-Hydroxyisovalerate.2	0.63	0.0014	Positive
	Cholate.1	0.61	0.0019	Positive
	Formate	0.61	0.0018	Positive
	Galactitol.1	0.61	0.0020	Positive
	Methylmalonate.2	0.61	0.0022	Positive
	Thymol.7	0.61	0.0018	Positive
	4-Pyridoxate.1	0.60	0.0025	Positive
	Cholate.3	0.60	0.0025	Positive
	3-Methylglutarate.1	0.60	0.0022	Positive
	Methylmalonate.1	0.59	0.0033	Positive
	Alanine.4‡, N-Phenylacetylglycine.4, O-Acetylcholine.2	–0.59	0.0033	Negative

	Glutamate.8‡	–0.59	0.0033	Negative
	2-Aminoadipate.1‡, Levulinate.1, Thymol.1, Valine.1	0.58	0.0038	Positive
	Isocitrate.1	0.58	0.0038	Positive
	Isocitrate.2	0.58	0.0038	Positive
	Cholate.2	0.58	0.0038	Positive
	Glutamate.1‡, Pyroglutamate.1	–0.57	0.0044	Negative
	Malonate.1	0.57	0.0050	Positive
	Pyroglutamate.7, Succinate.2	–0.57	0.0048	Negative
	Glutamate.6‡, Pyroglutamate.11	–0.56	0.0051	Negative
	Glutamate.7‡, Pyroglutamate.14	–0.56	0.0052	Negative
	Glutamate.4‡, Pyroglutamate.6	–0.56	0.0054	Negative
	S-Adenosylhomocysteine.3	0.56	0.0052	Positive
	Isocitrate.6	0.56	0.0055	Positive
	Theophylline.2	0.56	0.0057	Positive
	Thymol.8	0.56	0.0051	Positive
Heart	3-Hydroxyphenylacetate.1	–0.56	0.0057	Negative
	2-Aminoadipate.3‡	0.55	0.0069	Positive
	Valine.3	0.55	0.0065	Positive
	Glutamate.2‡, Pyroglutamate.2, Succinate.1	–0.55	0.0069	Negative
	2-Hydroxyisovalerate.2	0.54	0.0079	Positive
	3-Methylglutarate.2, Cholate.4	0.54	0.0077	Positive
	Pyroglutamate.4	–0.53	0.0088	Negative
	4-Pyridoxate.2	0.53	0.0093	Positive
	Levulinate.3	0.53	0.0089	Positive
	Levulinate.4	0.53	0.0098	Positive
	Thymol.4	0.53	0.0096	Positive
	Glycylproline.1	0.53	0.0095	Positive
	Lysine.2	0.53	0.0101	Positive
	3-Hydroxykynurenine.1, Pyroglutamate.3	–0.53	0.0100	Negative
	Glutamate.3‡, Pyroglutamate.5	–0.52	0.0106	Negative
	Isocitrate.5	0.52	0.0110	Positive

Heart	Malonate.2, Thymol.5	0.52	0.0110	Positive
	Glycylproline.3	0.52	0.0107	Positive
	Glucuronate.5	0.52	0.0105	Positive
	Creatine	–0.52	0.0114	Negative
	Levulinate.2	0.51	0.0139	Positive
	Thymol.2	0.51	0.0125	Positive
	2-Aminoadipate.2‡, Levulinate.5, Thymol.3, Valine.2	0.51	0.0128	Positive
	Valine.11	0.51	0.0133	Positive
	Singlet 4.068 ppm	–0.50	0.0147	Negative
	Glycerol.2	0.50	0.0141	Positive
	Ethanolamine.5, Guanidoacetate.4	0.50	0.0149	Positive
	Valine.12	0.50	0.0145	Positive
	3-Hydroxykynurenine.2, Pyroglutamate.10	–0.49	0.0168	Negative
	Tyrosine.1	0.49	0.0173	Positive
	S-Adenosylhomocysteine.2	0.49	0.0174	Positive
	Tyramine.2	0.49	0.0180	Positive
	1,7-Dimethylxanthine.1	0.49	0.0173	Positive
	2-Hydroxyisovalerate.1	0.49	0.0173	Positive
	Aspartate.1	0.49	0.0178	Positive
	Lysine.1	0.49	0.0173	Positive
	2-Hydroxybutyrate.2, 2-Hydroxyisovalerate.4	0.49	0.0169	Positive
	Niacinamide.2, Nicotinurate.1	–0.49	0.0183	Negative
	Uridine.1	–0.48	0.0196	Negative
	Uridine.2	–0.48	0.0199	Negative
	Pyroglutamate.8	–0.48	0.0201	Negative
	Anserine.2, N-Methylhydantoin.3	0.48	0.0203	Positive
	Anserine.3, Isocitrate.3	0.48	0.0212	Positive
	2-Oxoisocaproate.1, Homocysteine.1, Methylamine	0.48	0.0205	Positive
	Isocitrate.7	0.48	0.0202	Positive
	2-Oxoisocaproate.2, Homocysteine.2	0.48	0.0208	Positive
	Valine.7	0.48	0.0215	Positive

Heart	Adenosine.16	0.48	0.0213	Positive
	Glutamate.5‡, Pyroglutamate.9	–0.47	0.0225	Negative
	Pyroglutamate.13	–0.47	0.0233	Negative
	Anserine.1	0.47	0.0245	Positive
	Carnitine.5, O-Phosphocholine.3	0.47	0.0227	Positive
	Glycylproline.2	0.47	0.0240	Positive
	Adenosine.12	0.47	0.0231	Positive
	2-Hydroxyisovalerate.3	0.47	0.0235	Positive
	Lysine.3	0.47	0.0249	Positive
	Taurine.1	–0.47	0.0247	Negative
	Taurine.4	–0.46	0.0257	Negative
	Taurine.2	–0.46	0.0266	Negative
	Taurine.3	–0.46	0.0270	Negative
	Isocitrate.4	0.46	0.0262	Positive
	Theophylline.1	0.46	0.0287	Positive
	Adenosine.9	0.46	0.0256	Positive
	1,7-Dimethylxanthine.2	0.46	0.0272	Positive
	Valine.4	0.46	0.0284	Positive
	3-Hydroxyphenylacetate.2, Homovanillate	–0.45	0.0311	Negative
	N-Methylhydantoin.1, N,N-Dimethylglycine.1, Trimethylamine.1	0.45	0.0298	Positive
	Homogentisate	0.45	0.0293	Positive
	3,4-Dihydroxybenzeneacetate.1	0.45	0.0297	Positive
	Tyramine.3	0.45	0.0293	Positive
	Thymol.6	0.45	0.0310	Positive
	Choline.1‡, Malonate.3	0.45	0.0309	Positive
	Homocysteine.3, S-Adenosylhomocysteine.6	0.45	0.0324	Positive
	Glucarate.5, N-Methylhydantoin.7	0.45	0.0315	Positive
	Adenosine.11	0.45	0.0316	Positive
	S-Adenosylhomocysteine.9	0.45	0.0331	Positive
	3,4-Dihydroxybenzeneacetate.2	0.44	0.0354	Positive
	Taurine.5	–0.43	0.0381	Negative

	Trimethylamine.2	0.43	0.0391	Positive
	Isocitrate.8	0.43	0.0415	Positive
	Anserine.4, N-Methylhydantoin.4, N,N-Dimethylglycine.3	0.43	0.0400	Positive
	4-Carboxyglutamate.2	0.43	0.0401	Positive
	3-Methylxanthine, Glucuronate.4	0.43	0.0389	Positive
	Myo-Inositol.3, Valine.9	0.43	0.0392	Positive
Heart	N-Methylhydantoin.2, N,N-Dimethylglycine.2, Tyramine.1	0.42	0.0476	Positive
	Glucarate.2	0.42	0.0488	Positive
	Galactitol.6	0.42	0.0440	Positive
	3-Hydroxyisovalerate.4	0.42	0.0450	Positive
	Aspartate.4	0.41	0.0492	Positive

Table A2. *Kidney and heart metabolites found to be significantly correlated to anxiety-like behaviour. Pearson correlations were used to assess the relationship between behaviours indicative of heightened anxiety (i.e., more central squares entered in the open field) and relative concentrations of metabolites found to be significantly altered by stress in a Mann-Whitney U test. Positive correlations indicate that a higher anxiety-like state was linked to lower metabolite concentrations, while negative correlations indicate that a higher anxiety-like state was linked to higher metabolite concentrations. Metabolites for which more than one NMR resonance peak was identified are represented as metabolite.1, metabolite.2, … metabolite.n.* [‡]*Indicates metabolites that were significantly correlated to anxious behaviour in both kidney and heart tissues.*

Region	Metabolite	NMR Chemical Shift Range of Bin (ppm)	Mann-Whitney U Test	Percent Difference	Regulation by Stress
Left Cerebrum	Uracil.1*	5.253–5.248	1.53E-02	503.57	Up
	Uracil.2*	5.258–5.253	1.53E-02	420.13	Up
	Uracil.3*	5.414–5.406	1.82E-02	200.28	Up
	Singlet 3.055 ppm	3.060–3.049	8.25E-05	–72.52	Down
	2-Aminoadipate.1*	2.243–2.234	8.25E-05	68.96	Up
	Agmatine.1*, Phenylalanine.1*, Taurine.1*	3.268–3.249	8.25E-05	62.38	Up
	Adenosine.1*	8.268–8.259	8.25E-05	–55.10	Down
	Uracil.4*	5.820–5.814	8.25E-05	54.35	Up
	Adenosine.2*	6.119–6.108	8.25E-05	–52.74	Down
	Uracil.5*	5.809–5.803	8.25E-05	51.82	Up
	Adenosine.3*	6.108–6.097	1.07E-04	–51.29	Down
	Adenosine.4*	8.378–8.354	8.25E-05	–48.99	Down
	Nicotinurate.1*	8.561–8.547	8.25E-05	44.55	Up
	Histidine.1*	7.166–7.155	8.25E-05	44.49	Up
	Glutamate.1*	2.358–2.348	8.25E-05	–44.31	Down
	Glutamate.2*	2.348–2.336	8.25E-05	–43.76	Down
	Adenosine.5*	4.457–4.449	8.25E-05	–43.51	Down
	Formate*	8.475–8.453	8.25E-05	–43.31	Down
	Choline.1*	3.492–3.480	1.38E-04	42.05	Up
	Ethanolamine.1*, Homoserine.1*, Uridine.1*	3.818–3.811	8.25E-05	41.81	Up
	Choline.2*	3.480–3.468	1.38E-04	41.70	Up
	2-Oxoglutarate.1*	2.464–2.452	1.47E-03	41.41	Up
	Pyridoxine	2.476–2.464	1.47E-03	41.27	Up
	5,6-Dihydrouracil.1*	2.650–2.643	8.25E-05	40.54	Up
	Agmatine.2*	3.249–3.241	8.25E-05	39.96	Up
	Adenosine.6*	4.449–4.444	8.25E-05	–39.61	Down

Left Cerebrum	Glutamate.3*	2.336–2.328	8.25E-05	–38.98	Down
	Isoleucine.1*	1.251–1.242	8.25E-05	38.70	Up
	Valine.1*	1.046–1.035	8.25E-05	38.58	Up
	Uracil.6*	7.567–7.558	8.25E-05	38.53	Up
	N-Acetylaspartate.1*	7.992–7.952	8.25E-05	–38.24	Down
	2-Oxoglutarate.2*	2.452–2.439	9.42E-04	38.23	Up
	Adenosine.7*	4.398–4.389	8.25E-05	–38.13	Down
	Phenylalanine.2*	7.812–7.806	1.18E-03	38.09	Up
	Adenosine.8*	4.389–4.384	8.25E-05	–37.86	Down
	Adenosine.9*	4.290–4.284	8.25E-05	–37.30	Down
	Carnitine.1*	4.463–4.457	8.25E-05	–37.22	Down
	Adenosine.10*	4.405–4.398	8.25E-05	–37.05	Down
	Fumarate*	6.535–6.518	5.97E-04	–37.03	Down
	Isoleucine.2*, Valine.2*	0.995–0.985	8.25E-05	36.78	Up
	Valine.3*	1.023–1.013	8.25E-05	36.31	Up
	2-Oxoglutarate.3*	2.439–2.429	1.47E-03	36.03	Up
	Uracil.7*	7.576–7.567	8.25E-05	35.85	Up
	Valine.4*	1.056–1.046	8.25E-05	35.81	Up
	N-Acetylaspartate.2*	2.681–2.677	8.25E-05	–35.31	Down
	N-Acetylaspartate.3*	2.687–2.681	8.25E-05	–35.05	Down
	Phenylalanine.3*	7.429–7.418	8.25E-05	34.46	Up
	Glutamate.4*, N-Acetylaspartate.4*, Pyroglutamate.1*	2.035–2.013	8.25E-05	–34.45	Down
	N-Acetylaspartate.5*	4.379–4.373	8.25E-05	–34.15	Down
	Phenylalanine.4*	7.450–7.440	8.25E-05	34.10	Up
	Adenosine.11*	4.410–4.405	8.25E-05	–33.95	Down
	Niacinamide.1*	8.712–8.699	9.42E-04	33.82	Up
	Histidine.2*	8.085–8.069	8.25E-05	33.59	Up
	5,6-Dihydrouracil.2*	2.639–2.633	8.25E-05	33.53	Up
	Phenylalanine.5*	7.440–7.429	8.25E-05	33.28	Up

Left Cerebrum	N-Acetylaspartate.6*, Pyroglutamate.2*	2.514–2.507	3.72E-04	–32.83	Down
	Phenylalanine.6*	3.152–3.143	1.07E-04	32.74	Up
	Isoleucine.3*	1.242–1.233	8.25E-05	32.23	Up
	Phenylalanine.7*	6.929–6.916	8.25E-05	31.75	Up
	Phenylalanine.8*	6.916–6.903	8.25E-05	31.69	Up
	3-Phenylpropionate.1*	7.210–7.199	8.25E-05	30.45	Up
	Adenosine.12*	4.384–4.379	8.25E-05	–30.41	Down
	β-Alanine.1*	3.159–3.152	8.25E-05	30.41	Up
	Nicotinurate.2*	8.699–8.683	2.53E-02	30.33	Up
	Serine.1*	3.996–3.989	8.25E-05	–30.21	Down
	Phenylalanine.9*	7.397–7.389	8.25E-05	29.70	Up
	Glutamate.5*	2.372–2.362	8.25E-05	–29.68	Down
	Histidine.3*	7.199–7.185	8.25E-05	29.08	Up
	Adenosine.13*	4.284–4.274	8.25E-05	–28.95	Down
	Phenylalanine.10*	7.554–7.549	1.07E-04	28.91	Up
	Glutamate.6*, Glycerol.1*	3.772–3.766	8.25E-05	–28.83	Down
	Phenylalanine.11*	7.337–7.324	1.07E-04	28.33	Up
	2-Aminobutyrate.1, Leucine.1*	0.980–0.948	8.25E-05	28.28	Up
	Pyroglutamate.3*	2.533–2.521	4.72E-04	–27.71	Down
	Histidine.4*	3.344–3.338	8.25E-05	27.30	Up
	Phenylalanine.12*	7.352–7.337	1.07E-04	27.29	Up
	Phenylalanine.13*	7.389–7.377	1.38E-04	26.94	Up
	N-Acetylaspartate.7*	2.768–2.759	8.25E-05	–26.81	Down
	Homoserine.2*	2.166–2.129	2.77E-03	26.71	Up
	Adenosine.14*	4.295–4.290	8.25E-05	–26.44	Down
	Alanine.1*, Homoserine.3*	3.794–3.790	1.38E-04	26.43	Up
	Uridine.2*	3.839–3.831	1.78E-04	25.76	Up
	Histidine.5*	3.360–3.353	8.25E-05	25.76	Up
	Glutamate.7*	2.085–2.075	8.25E-05	–25.67	Down
	5,6-Dihydrouracil.3*	2.660–2.650	8.25E-05	25.01	Up

Left Cerebrum	Glutamate.8*	2.321–2.317	8.25E-05	–24.83	Down
	Pyroglutamate.4*	4.193–4.181	6.14E-03	–24.76	Down
	2-Aminobutyrate.2, Leucine.2*	3.731–3.723	8.25E-05	24.65	Up
	Pyroglutamate.5*	4.181–4.166	5.97E-04	–24.59	Down
	Ethanolamine.2*, Homoserine.4*	3.831–3.824	1.38E-04	24.52	Up
	Glutamate.9*, Glycerol.2*	3.766–3.757	8.25E-05	–24.50	Down
	Myo-Inositol.1*	3.370–3.360	1.07E-04	–23.98	Down
	Phenylalanine.14*	7.752–7.729	2.53E-02	23.89	Up
	Phenylalanine.15*	7.377–7.368	2.29E-04	23.16	Up
	Homoserine.5*	2.176–2.166	7.42E-03	23.11	Up
	Serine.2*	3.989–3.980	1.07E-04	–23.03	Down
	Pyroglutamate.6*	2.379–2.372	8.25E-05	–22.88	Down
	Histidine.6*	3.353–3.344	8.25E-05	22.50	Up
	Carnitine.2*	3.232–3.217	1.18E-03	–22.38	Down
	Creatine*, Tyrosine.1*	3.931–3.919	8.25E-05	–21.79	Down
	Pyroglutamate.7*	4.166–4.162	3.72E-04	–21.61	Down
	Glutamate.10*	2.325–2.321	8.25E-05	–21.53	Down
	Pyroglutamate.8*	4.202–4.193	1.28E-02	–21.36	Down
	Aspartate.1*	2.823–2.811	8.25E-05	21.10	Up
	3-Phenylpropionate.2*	7.295–7.283	1.82E-03	21.03	Up
	Ethanolamine.3*, Homoserine.6*	3.824–3.818	8.25E-05	20.67	Up
	Agmatine.3*, Leucine.3*	1.764–1.640	1.38E-04	20.53	Up
	N-Acetylaspartate.8*	4.373–4.368	1.82E-03	–20.35	Down
	O-Phosphocholine.1	4.162–4.159	2.92E-04	–20.24	Down
	N-Acetylaspartate.9*	4.368–4.359	9.42E-04	–19.97	Down
	Ethanolamine.4*	3.143–3.134	1.38E-04	19.93	Up
	Glutamate.11*	2.119–2.107	2.92E-04	–19.70	Down
	Histidine.7*	4.021–4.012	8.25E-05	19.65	Up
	Hypoxanthine*	8.224–8.211	8.25E-05	19.46	Up

Left Cerebrum	Niacinamide.2*	8.238–8.224	8.25E-05	19.09	Up
	Aspartate.2*	2.811–2.798	8.25E-05	19.05	Up
	2-Aminoadipate.2*	3.746–3.737	1.07E-04	18.97	Up
	Aspartate.3*	2.798–2.789	8.25E-05	18.83	Up
	N-Acetylaspartate.10*, Pyroglutamate.9*	2.507–2.498	4.15E-03	–18.66	Down
	Isoleucine.4*	1.004–0.995	1.07E-04	18.53	Up
	Glutamate.12*	2.094–2.085	8.25E-05	–18.42	Down
	Homoserine.7*	1.985–1.975	1.07E-04	18.06	Up
	O-Phosphocholine.2	4.159–4.155	5.97E-04	–18.03	Down
	Choline.3*	3.578–3.567	8.25E-05	17.96	Up
	Histidine.8*	4.025–4.021	8.25E-05	17.82	Up
	Agmatine.4*	2.831–2.823	8.25E-05	17.66	Up
	Taurine.2*	3.407–3.397	1.38E-04	17.40	Up
	Glutamate.13*	2.064–2.056	8.25E-05	–17.34	Down
	Carnitine.3*, Levulinate.1*, Pyroglutamate.10*	2.402–2.391	2.15E-02	–17.15	Down
	N-Acetylaspartate.11*	4.355–4.347	6.14E-03	–16.98	Down
	Homoserine.8*	1.994–1.985	8.25E-05	16.78	Up
	Taurine.3*	3.397–3.391	2.92E-04	16.59	Up
	Adenosine.15*	4.300–4.295	7.51E-04	–16.56	Down
	Creatinine.1*	4.051–4.044	9.42E-04	–16.52	Down
	Glutamate.14*	2.362–2.358	8.25E-05	–16.47	Down
	Adenosine.16*	4.304–4.300	9.42E-04	–16.33	Down
	Histidine.9*	4.007–4.003	8.25E-05	16.20	Up
	Lactate.1*	4.114–4.106	1.07E-04	–16.06	Down
	Homoserine.9*	1.975–1.938	1.38E-04	16.02	Up
	Adenosine.17*	4.320–4.314	1.82E-03	–15.98	Down
	Adenosine.18*	4.314–4.309	1.82E-03	–15.91	Down
	2-Aminobutyrate.3, Isoleucine.5*, Leucine.4*	0.938–0.929	5.97E-04	15.86	Up

Left Cerebrum	2-Aminobutyrate.4, Isoleucine.6*, Leucine.5*	0.948–0.938	1.18E-03	15.83	Up
	2-Aminobutyrate.5, Leucine.6*	3.737–3.731	8.25E-05	15.65	Up
	Serine.3*	4.031–4.025	1.78E-04	–15.60	Down
	Lactate.2*	4.125–4.114	1.07E-04	–15.37	Down
	Homoserine.10*	3.855–3.851	9.42E-04	15.28	Up
	N-Acetylaspartate.12*	4.359–4.355	1.07E-02	–14.88	Down
	O-Phosphocholine.3, Threonine.1*	3.596–3.591	3.40E-03	–14.88	Down
	Histidine.10*	4.012–4.007	1.07E-04	14.87	Up
	Histidine.11*	3.338–3.315	1.18E-03	14.83	Up
	Isoleucine.7*	3.687–3.683	8.25E-05	14.66	Up
	Uridine.3*	3.845–3.839	7.42E-03	14.26	Up
	Tyrosine.2*	3.960–3.953	8.25E-05	–14.21	Down
	Alanine.2*	1.487–1.474	1.38E-04	14.02	Up
	Glutamate.15*	2.075–2.064	8.25E-05	–13.95	Down
	Glutaric Acid Monomethyl Ester.1	3.712–3.702	8.25E-05	13.89	Up
	β-Alanine.2*	3.171–3.165	1.78E-04	13.42	Up
	D-Threitol.1*	3.723–3.719	7.51E-04	–13.05	Down
	Histidine.12*	7.155–7.140	3.48E-02	13.04	Up
	Alanine.3*, Homoserine.11*	3.786–3.777	3.40E-03	13.01	Up
	Homoserine.12*	1.938–1.923	1.18E-03	12.98	Up
	Isoleucine.8*	1.013–1.004	1.18E-03	12.93	Up
	N-Acetylaspartate.13*	2.711–2.697	1.78E-04	–12.62	Down
	Alanine.4*	1.499–1.487	3.72E-04	12.62	Up
	4-Pyridoxate.1*	7.898–7.890	4.06E-02	–12.53	Down
	Serine.4*	4.039–4.031	1.38E-04	–12.53	Down
	Glutamate.16*	2.129–2.119	3.40E-03	–12.50	Down
	β-Alanine.3*	3.178–3.171	1.38E-04	12.42	Up
	Homoserine.13*	2.004–1.994	1.78E-04	12.25	Up

Left Cerebrum	O-Phosphocholine.4	4.136–4.125	1.78E-04	–12.22	Down
	Aspartate.4*	2.733–2.723	1.07E-04	12.22	Up
	Aspartate.5*	2.723–2.711	1.38E-04	12.21	Up
	Carnitine.4*, Levulinate.2*, Pyroglutamate.11*	2.391–2.385	8.25E-05	–12.13	Down
	Isoleucine.9*	1.423–1.414	3.72E-04	12.02	Up
	2-Aminoadipate.3*	3.757–3.750	1.38E-04	11.89	Up
	Glutamate.17*, Pyroglutamate.12*	2.056–2.045	1.82E-03	–11.65	Down
	Histidine.13*	3.217–3.195	8.94E-03	11.61	Up
	Choline.4*	3.511–3.492	2.98E-02	11.30	Up
	2-Aminoadipate.4*, 4-Aminobutyrate.1*, Glutaric Acid Monomethyl Ester.2	1.881–1.764	7.51E-04	11.28	Up
	Alanine.5*, Homoserine.14*	3.803–3.794	8.25E-05	11.11	Up
	Choline.5*	3.186–3.178	3.72E-04	10.94	Up
	Glutamate.18*	2.107–2.100	9.42E-04	–10.81	Down
	Threonine.2*	4.247–4.240	2.15E-02	–10.77	Down
	Choline.6*	3.532–3.524	1.28E-02	10.22	Up
	Aspartate.6*, Uridine.4*	3.905–3.900	2.29E-04	10.17	Up
	N-Acetylaspartate.14*	2.669–2.664	1.78E-04	–10.02	Down
	β-Alanine.4*	2.545–2.537	8.94E-03	9.94	Up
	Alanine.6*, Homoserine.15*	3.790–3.786	2.92E-04	9.92	Up
	Uridine.5*	3.919–3.912	5.97E-04	9.91	Up
	Choline.7*	3.538–3.532	5.06E-03	9.82	Up
	Lactate.3*	4.106–4.101	5.97E-04	–9.64	Down
	Lactate.4*, Threonine.3*	1.351–1.319	1.82E-03	–9.56	Down
	Adenosine.19*	8.278–8.268	5.06E-03	–9.41	Down
	Isoleucine.10*	3.683–3.677	3.72E-04	9.11	Up
	4-Pyridoxate.2*	7.887–7.878	3.48E-02	–9.02	Down
	Adenosine.20*	8.259–8.249	2.53E-02	–8.96	Down
	2-Aminoadipate.5*, 4-Aminobutyrate.2*	1.890–1.881	1.78E-04	8.64	Up

Left Cerebrum	Isoleucine.11*	1.432–1.423	9.42E-04	8.59	Up
	Nicotinurate.3*	3.971–3.963	4.15E-03	8.56	Up
	N-Acetylaspartate.15*	2.664–2.660	5.97E-04	–8.52	Down
	2-Aminoadipate.6*, 4-Aminobutyrate.3*	1.923–1.914	1.78E-04	8.37	Up
	Choline.8*	3.524–3.511	1.28E-02	8.20	Up
	Glycerol.3*	3.647–3.638	1.47E-03	–8.15	Down
	Uridine.6*	3.851–3.845	1.47E-03	8.01	Up
	Aspartate.7*, Homoserine.16*	3.878–3.870	1.47E-03	7.96	Up
	1,3-Dimethylurate.1*	3.241–3.232	4.15E-03	–7.94	Down
	Myo-Inositol.2*	4.093–4.055	1.82E-03	–7.81	Down
	2-Aminoadipate.7*, 4-Aminobutyrate.4*	1.902–1.890	2.29E-04	7.57	Up
	Ethanolamine.5*, Phenylalanine.16*	3.134–3.060	1.28E-02	7.51	Up
	D-Threitol.2*, Glycerol.4*, Myo-Inositol.3*	3.638–3.622	1.82E-03	–7.33	Down
	D-Threitol.3*	3.702–3.699	2.25E-03	–7.27	Down
	Lactate.5*	4.098–4.093	1.53E-02	–7.18	Down
	4-Aminobutyrate.5*	2.280–2.275	8.94E-03	7.16	Up
	2-Aminoadipate.8*, 4-Aminobutyrate.6*, Acetate*	1.914–1.902	4.72E-04	7.15	Up
	Choline.9*	3.195–3.186	3.40E-03	7.05	Up
	2-Aminoadipate.9*	2.275–2.270	6.14E-03	7.04	Up
	Tyrosine.3*	3.947–3.931	9.42E-04	–6.99	Down
	Agmatine.5*	3.027–3.016	5.97E-04	6.99	Up
	Choline.10*	4.044–4.039	4.72E-02	6.98	Up
	Homoserine.17*, Uridine.7*	3.811–3.806	4.15E-03	6.91	Up
	Glycerol.5*, Myo-Inositol.4*	3.550–3.538	2.77E-03	–6.83	Down
	N-Acetylaspartate.16*, Pyroglutamate.13*	2.498–2.485	1.53E-02	–6.77	Down
	Myo-Inositol.5*	3.428–3.417	1.53E-02	–6.77	Down

Left Cerebrum	Myo-Inositol.6*	3.289–3.278	8.94E-03	–6.61	Down
	O-Phosphocholine.5	4.148–4.136	3.72E-04	–6.57	Down
	2-Aminoadipate.10*	2.270–2.265	6.14E-03	6.54	Up
	Myo-Inositol.7*	3.441–3.428	1.28E-02	–6.52	Down
	β-Alanine.5*	2.561–2.556	8.94E-03	6.43	Up
	1,3-Dimethylurate.2*, Myo-Inositol.8*	3.304–3.289	5.06E-03	–6.14	Down
	Isoleucine.12*	3.670–3.662	4.72E-04	6.10	Up
	Aspartate.8*	2.697–2.687	5.06E-03	6.07	Up
	4-Aminobutyrate.7*	2.294–2.280	5.97E-04	6.04	Up
	2-Oxoglutarate.4*, 4-Aminobutyrate.8*	3.004–2.992	9.42E-04	5.87	Up
	Homoserine.18*	3.859–3.855	1.82E-02	5.71	Up
	2-Oxoglutarate.5*, 4-Aminobutyrate.9*	3.016–3.004	2.25E-03	5.70	Up
	D-Threitol.4*, Myo-Inositol.9*	3.622–3.611	2.77E-03	–5.69	Down
	Aspartate.9*, Uridine.8*	3.900–3.883	7.51E-04	5.55	Up
	β-Alanine.6*	2.571–2.565	7.42E-03	5.42	Up
	Isoleucine.13*	3.677–3.670	2.25E-03	5.25	Up
	4-Aminobutyrate.10*	2.306–2.294	6.14E-03	4.96	Up
	Glycerol.6*, Glycine	3.563–3.550	4.15E-03	–4.89	Down
	Creatinine.2*	3.049–3.027	5.06E-03	–4.77	Down
	Homoserine.19*	2.013–2.004	1.82E-02	4.51	Up
	Carnitine.5*, Levulinate.3*, Pyroglutamate.14*	2.385–2.379	2.98E-02	–3.74	Down
	D-Threitol.5*	3.719–3.712	2.53E-02	–2.25	Down
Right Cerebrum	Inosine.1	6.119–6.108	8.25E-05	–108.20	Down
	Inosine.2	6.108–6.097	8.25E-05	–106.69	Down
	Adenosine.1*, Inosine.3	8.378–8.354	8.25E-05	–102.02	Down
	Nicotinate.1	8.268–8.259	8.25E-05	–98.94	Down
	Methylmalonate.1	1.194–1.185	8.25E-05	–98.38	Down

Right Cerebrum	Uracil.1*	5.820–5.814	8.25E-05	91.81	Up
	Uracil.2*	5.809–5.803	8.25E-05	90.99	Up
	Inosine.4	6.097–6.088	8.25E-05	–87.98	Down
	Phenylalanine.1*	7.440–7.429	8.25E-05	86.76	Up
	Leucine.1*	0.980–0.948	8.25E-05	86.52	Up
	Phenylalanine.2*	7.352–7.337	8.25E-05	85.08	Up
	Phenylalanine.3*	7.429–7.418	8.25E-05	82.90	Up
	3-Phenylpropionate.1*, Phenylalanine.4*	7.337–7.324	8.25E-05	82.12	Up
	Tryptophan.1	7.166–7.155	8.25E-05	80.51	Up
	N-Acetylaspartate.1*	7.992–7.946	8.25E-05	–79.16	Down
	Guanosine.1	4.457–4.449	8.25E-05	–78.45	Down
	Tryptophan.2	7.210–7.199	8.25E-05	78.38	Up
	Adenosine.2*	6.088–6.074	1.07E-04	–76.58	Down
	Homocysteine.1	1.056–1.046	8.25E-05	76.53	Up
	Valine.1*	1.046–1.035	8.25E-05	76.26	Up
	N-Acetylaspartate.2*	2.681–2.677	8.25E-05	–76.09	Down
	Phenylalanine.5*	7.397–7.389	8.25E-05	74.69	Up
	Histidine.1*	7.199–7.185	8.25E-05	73.98	Up
	N-Acetylaspartate.3*	4.398–4.389	8.25E-05	–72.80	Down
	Glutamate.1*	2.358–2.348	8.25E-05	–72.21	Down
	Homocysteine.2	1.938–1.923	8.25E-05	71.96	Up
	Hypoxanthine*	8.224–8.211	8.25E-05	71.80	Up
	Valine.2*	0.995–0.985	8.25E-05	71.75	Up
	Glutamate.2*	2.348–2.336	8.25E-05	–71.45	Down
	Isoleucine.1*	0.948–0.938	8.25E-05	71.40	Up
	Phenylalanine.6*	7.450–7.440	8.25E-05	71.33	Up
	3-Phenylpropionate.2*, Phenylalanine.7*	7.389–7.377	8.25E-05	70.96	Up
	N-Acetylaspartate.4*	2.687–2.681	8.25E-05	–70.93	Down
	N-Acetylaspartate.5*	4.389–4.384	8.25E-05	–70.20	Down
	Niacinamide.1*	8.238–8.224	8.25E-05	69.94	Up

Right Cerebrum	N-Acetylaspartate.6*	4.384–4.379	8.25E-05	–68.17	Down
	Adenosine.3*	4.290–4.284	8.25E-05	–66.48	Down
	Tyramine.1	6.916–6.903	8.25E-05	65.19	Up
	Uracil.3*	7.576–7.567	8.25E-05	64.74	Up
	Glutamate.3*	2.336–2.328	8.25E-05	–64.66	Down
	Uracil.4*	7.567–7.556	8.25E-05	63.38	Up
	Histidine.2*	8.085–8.069	8.25E-05	62.90	Up
	Tyramine.2	6.929–6.916	8.25E-05	62.80	Up
	Glutamate.4*, N-Acetylaspartate.7*, Pyroglutamate.1*	2.035–2.013	8.25E-05	–62.80	Down
	Singlet 1.178 ppm	1.185–1.171	8.25E-05	–61.98	Down
	3-Phenylpropionate.3*, Phenylalanine.8*	7.377–7.368	8.25E-05	61.71	Up
	Inosine.5, N-Acetylaspartate.8*	4.379–4.373	8.25E-05	–61.45	Down
	Adenosine.4*	4.405–4.398	8.25E-05	–61.37	Down
	Isoleucine.2*	0.938–0.929	8.25E-05	61.25	Up
	Carnitine.1*	4.463–4.457	8.25E-05	–61.15	Down
	π-Methylhistidine	8.278–8.268	8.25E-05	–60.98	Down
	Homocysteine.3	1.023–1.013	8.25E-05	58.58	Up
	Agmatine.1*, Leucine.2*	1.764–1.621	8.25E-05	57.60	Up
	Glutamate.5*, Glycerol.1*	3.772–3.766	8.25E-05	–55.32	Down
	Glutamate.6*	2.129–2.119	8.25E-05	–55.27	Down
	Guanosine.2	4.449–4.439	8.25E-05	–55.16	Down
	Isoleucine.3*	1.004–0.995	8.25E-05	54.99	Up
	Glutamate.7*, Glycerol.2*	3.766–3.757	8.25E-05	–54.81	Down
	Glutamate.8*	2.372–2.362	8.25E-05	–54.43	Down
	Adenosine.5*	4.410–4.405	8.25E-05	–53.71	Down
	5,6-Dihydrouracil.1*	2.650–2.643	8.25E-05	53.50	Up
	Glutamate.9*	2.119–2.107	8.25E-05	–52.82	Down
	Adenosine.6*	4.284–4.274	8.25E-05	–52.46	Down
	Taurine.1*	3.360–3.353	8.25E-05	52.22	Up

Right Cerebrum	N-Acetylaspartate.9*	7.946–7.932	8.25E-05	–52.18	Down
	Alanine.1*, Isoleucine.4*	1.487–1.474	8.25E-05	51.39	Up
	Alanine.2*	1.499–1.487	8.25E-05	50.54	Up
	N-Acetylaspartate.10*, Pyroglutamate.2*	2.514–2.507	8.25E-05	–49.68	Down
	Guanosine.3, Histamine.1	8.020–8.014	8.25E-05	–49.34	Down
	Choline.1*	3.578–3.567	8.25E-05	49.32	Up
	Fumarate*	6.163–6.119	2.29E-04	–49.10	Down
	Methylmalonate.2	1.205–1.194	8.25E-05	–49.06	Down
	Nicotinate.2	8.288–8.278	8.25E-05	–48.44	Down
	1,3-Dimethylurate.1*	3.241–3.232	8.25E-05	–46.63	Down
	Glutamate.10*	2.085–2.075	8.25E-05	–46.57	Down
	Homocysteine.4, Isoleucine.5*	1.985–1.975	8.25E-05	46.37	Up
	Homocysteine.5, Isoleucine.6*	1.975–1.938	8.25E-05	46.04	Up
	Histidine.3*	4.007–4.003	8.25E-05	46.02	Up
	Homoserine.1*, Isoleucine.7*	1.994–1.985	8.25E-05	45.42	Up
	5,6-Dihydrouracil.2*	2.660–2.650	8.25E-05	45.37	Up
	Inosine.6	4.295–4.290	8.25E-05	–44.44	Down
	Aspartate.1*	2.798–2.789	8.25E-05	43.36	Up
	Histidine.4*	4.021–4.012	8.25E-05	42.94	Up
	Pyroglutamate.3*	2.533–2.521	8.25E-05	–42.82	Down
	Histidine.5*	3.344–3.338	8.25E-05	42.53	Up
	Aspartate.2*, Tyramine.3	2.811–2.798	8.25E-05	42.15	Up
	4-Aminobutyrate.1*, Acetate*	1.923–1.914	8.25E-05	42.04	Up
	Aspartate.3*	2.733–2.723	8.25E-05	41.31	Up
	Glutamate.11*, Glycerol.3*	3.777–3.772	8.25E-05	–41.23	Down
	Histidine.6*	4.012–4.007	8.25E-05	40.65	Up
	Isoleucine.8*	1.013–1.004	8.25E-05	40.31	Up

Right Cerebrum	Ethanolamine.1*	3.159–3.152	8.25E-05	40.24	Up
	Levulinate.1*, Pyroglutamate.4*	2.379–2.372	8.25E-05	–40.10	Down
	Tyramine.4	3.152–3.143	8.25E-05	39.93	Up
	Taurine.2*	3.353–3.344	8.25E-05	39.53	Up
	Agmatine.2*	3.249–3.241	8.25E-05	39.53	Up
	Aspartate.4*	2.723–2.711	8.25E-05	39.47	Up
	5,6-Dihydrouracil.3*	2.639–2.633	8.25E-05	39.39	Up
	4-Aminobutyrate.2*	1.914–1.902	8.25E-05	39.09	Up
	Adenosine.7*	6.009–5.938	9.42E-04	–38.78	Down
	Aspartate.5*, Tyramine.5	2.823–2.811	8.25E-05	38.18	Up
	Valine.3*	3.603–3.596	8.25E-05	38.14	Up
	Tyramine.6	2.836–2.823	8.25E-05	38.02	Up
	N-Acetylaspartate.11*, Pyroglutamate.5*	2.507–2.498	2.25E-03	–37.83	Down
	4-Aminobutyrate.3*	1.902–1.890	8.25E-05	37.80	Up
	N-Acetylaspartate.12*, Pyroglutamate.6*	2.498–2.485	5.97E-04	–37.61	Down
	4-Aminobutyrate.4*	2.280–2.275	8.25E-05	37.49	Up
	S-Adenosylhomocysteine.1	4.264–4.255	8.25E-05	37.18	Up
	D-Threitol.1*	3.695–3.691	8.25E-05	–37.12	Down
	4-Aminobutyrate.5*	2.294–2.280	8.25E-05	37.05	Up
	Choline.2*	4.025–4.021	8.25E-05	37.05	Up
	4-Aminobutyrate.6*	2.306–2.294	8.25E-05	36.36	Up
	Agmatine.3*	3.033–3.027	8.25E-05	36.06	Up
	Glutamate.12*	2.094–2.085	8.25E-05	–35.97	Down
	Homoserine.2*	3.971–3.963	8.25E-05	35.82	Up
	4-Aminobutyrate.7*, Agmatine.4*	3.016–3.004	8.25E-05	35.67	Up
	Histidine.7*	3.217–3.195	8.25E-05	35.64	Up
	N-Acetylornithine.1	4.155–4.148	8.25E-05	35.64	Up
	Tryptophan.3	7.812–7.806	1.38E-04	35.62	Up
	Isoleucine.9*	1.474–1.432	8.25E-05	35.45	Up

Right Cerebrum	Adenosine.8*, Creatine*, Tyrosine.1*	3.931–3.919	8.25E-05	–35.42	Down
	Homocysteine.6	1.414–1.351	8.25E-05	35.30	Up
	4-Aminobutyrate.8*	1.890–1.881	8.25E-05	35.25	Up
	Agmatine.5*	3.027–3.016	8.25E-05	35.05	Up
	D-Threitol.2*	3.691–3.687	8.25E-05	–34.98	Down
	Aspartate.6*, Uridine.1*	3.905–3.900	8.25E-05	34.79	Up
	2-Aminoadipate.1*	2.270–2.265	8.25E-05	34.78	Up
	Homoserine.3*, Isoleucine.10*	2.004–1.994	8.25E-05	34.54	Up
	Nicotinate.3	8.608–8.593	1.82E-03	–34.41	Down
	2-Aminoadipate.2*	2.275–2.270	8.25E-05	34.36	Up
	Niacinamide.2*	7.556–7.549	8.25E-05	33.81	Up
	2-Oxoglutarate.1*, 4-Aminobutyrate.9*	3.004–2.977	8.25E-05	33.69	Up
	2'-Deoxyadenosine	8.403–8.387	8.25E-05	33.53	Up
	5,6-Dihydrouracil.4*	3.492–3.480	1.38E-04	33.41	Up
	5,6-Dihydrouracil.5*	3.480–3.468	1.78E-04	32.46	Up
	Glutamate.13*	2.107–2.100	8.25E-05	–31.62	Down
	Glutamate.14*	2.321–2.317	8.25E-05	–31.16	Down
	Niacinamide.3*	8.712–8.699	2.29E-04	30.72	Up
	N-Acetylaspartate.13*	2.711–2.697	8.25E-05	–30.29	Down
	β-Alanine.1*	2.545–2.537	1.38E-04	30.25	Up
	D-Threitol.3*	3.699–3.695	8.25E-05	–30.17	Down
	Adenosine.9*	8.259–8.249	8.25E-05	–30.17	Down
	Ethanolamine.2*, Homoserine.4*	3.811–3.806	8.25E-05	29.91	Up
	Homocysteine.7	1.423–1.414	8.25E-05	29.59	Up
	Glutamate.15*	2.075–2.064	8.25E-05	–29.30	Down
	Valine.4*	3.611–3.603	8.25E-05	29.11	Up
	Formate*	8.475–8.453	8.25E-05	–28.94	Down
	Uridine.2*	3.855–3.851	8.25E-05	28.91	Up
	Uridine.3*	3.919–3.912	8.25E-05	28.48	Up

Right Cerebrum	β-Alanine.2*	3.171–3.165	8.25E-05	28.26	Up
	3-Phenylpropionate.4*, Phenylalanine.9*	7.304–7.295	2.29E-04	27.97	Up
	Alanine.3*, Homoserine.5*	3.803–3.794	8.25E-05	27.49	Up
	2-Aminoadipate.3*	3.746–3.737	8.25E-05	27.46	Up
	Glutamate.16*	2.064–2.056	8.25E-05	–27.23	Down
	Homocysteine.8	2.317–2.306	8.25E-05	27.09	Up
	Homoserine.6*	2.013–2.004	8.25E-05	26.84	Up
	Aspartate.7 *	2.768–2.755	8.25E-05	26.30	Up
	Taurine.3*	3.407–3.397	8.25E-05	26.17	Up
	2-Aminoadipate.4*, Leucine.3*	3.737–3.731	8.25E-05	26.07	Up
	D-Threitol.4*	3.702–3.699	8.25E-05	–25.88	Down
	Adenine.1	8.148–8.136	8.25E-05	–25.70	Down
	Choline.3*	3.532–3.524	1.38E-04	25.70	Up
	Isoleucine.11*	0.895–0.890	8.25E-05	25.51	Up
	Glutamate.17*	2.325–2.321	8.25E-05	–25.15	Down
	Ethanolamine.3*	3.143–3.134	8.25E-05	24.90	Up
	Nicotinurate.1*	3.953–3.947	8.25E-05	24.84	Up
	Carnitine.2*, Levulinate.2*, Pyroglutamate.7*	2.391–2.385	8.25E-05	–24.72	Down
	Histidine.8*	7.932–7.921	8.25E-05	24.56	Up
	Guanosine.4	3.996–3.989	8.25E-05	–24.40	Down
	Saccharopine.1	3.585–3.578	8.25E-05	24.15	Up
	Ethanolamine.4*, Homoserine.7*, Uridine.4*	3.818–3.811	8.25E-05	23.78	Up
	3-Phenylpropionate.5*	7.295–7.283	8.25E-05	23.71	Up
	S-Adenosylhomocysteine.2	4.255–4.247	1.38E-04	23.67	Up
	Leucine.4*	3.731–3.723	8.25E-05	23.22	Up
	Adenosine.10*, Inosine.7	4.300–4.295	8.25E-05	–23.14	Down
	S-Adenosylhomocysteine.3	4.439–4.430	7.51E-04	23.07	Up

Right Cerebrum	Homocysteine.9, Isoleucine.12*	1.432–1.423	8.25E-05	23.02	Up
	β-Alanine.3*	3.186–3.178	8.25E-05	22.99	Up
	β-Alanine.4*	3.178–3.171	8.25E-05	22.99	Up
	Myo-Inositol.1*	3.278–3.268	1.78E-04	–22.91	Down
	Adenosine.11*, Inosine.8	4.304–4.300	8.25E-05	–22.81	Down
	Choline.4*	3.567–3.563	8.25E-05	22.76	Up
	Histidine.9*	4.003–3.996	8.25E-05	22.56	Up
	Glutamate.18*	2.362–2.358	8.25E-05	–22.40	Down
	Creatine Phosphate	3.060–3.049	7.51E-04	–22.38	Down
	2-Aminoadipate.5*	2.265–2.255	8.25E-05	22.29	Up
	Lactate.1*	4.114–4.106	8.25E-05	–22.17	Down
	Aspartate.8*, Uridine.5*	3.900–3.883	8.25E-05	22.16	Up
	Aspartate.9*	2.697–2.687	8.25E-05	21.93	Up
	Saccharopine.2	3.596–3.591	8.25E-05	21.85	Up
	Tryptophan.4	7.752–7.729	6.14E-03	21.85	Up
	Homoserine.8*	3.980–3.971	8.25E-05	21.81	Up
	Adenosine Monophosphate	8.561–8.547	2.25E-03	21.66	Up
	Nicotinurate.2*	8.699–8.683	7.51E-04	21.50	Up
	Pyroglutamate.8*	4.125–4.114	8.25E-05	–21.40	Down
	Glutamate.19*, Glycerol.4*	3.786–3.777	2.25E-03	–21.26	Down
	Alanine.4*	3.806–3.803	8.25E-05	21.12	Up
	2-Aminoadipate.6*	3.757–3.750	8.25E-05	20.89	Up
	Myo-Inositol.2*	3.289–3.278	5.97E-04	–20.70	Down
	Lactate.2*	4.106–4.101	8.25E-05	–20.69	Down
	Taurine.4*	3.370–3.360	1.53E-02	20.64	Up
	3-Phenylpropionate.6*	7.283–7.273	1.07E-04	20.38	Up
	Carnitine.3*	3.428–3.417	3.72E-04	–20.29	Down
	Choline.5*	3.538–3.532	2.29E-04	20.08	Up
	1,3-Dimethylurate.2*	3.441–3.428	2.29E-04	–19.64	Down
	4-Aminobutyrate.10*	1.881–1.764	1.07E-04	19.50	Up
	Adenosine.12*, Tyrosine.2*	3.947–3.931	8.25E-05	–19.47	Down

Right Cerebrum	S-Adenosylhomocysteine.4	4.274–4.264	3.72E-04	19.31	Up
	Histamine.2	8.014–7.992	1.38E-04	–19.27	Down
	1,3-Dimethylurate.3*, Myo-Inositol.3*	3.304–3.289	1.47E-03	–18.98	Down
	N-Acetylaspartate.14*	2.669–2.664	8.25E-05	–18.95	Down
	Creatinine.1*	3.049–3.033	8.25E-05	–18.55	Down
	Choline.6 *	3.524–3.511	1.07E-04	18.23	Up
	Inosine.9, N-Acetylaspartate.15*	4.373–4.368	4.72E-04	–17.67	Down
	Guanosine.5	3.989–3.980	3.72E-04	–17.26	Down
	N-Acetylornithine.2	4.181–4.166	5.06E-03	17.26	Up
	Taurine.5*	3.397–3.391	8.25E-05	16.88	Up
	Uridine.6*	3.851–3.845	8.25E-05	16.87	Up
	Carnitine.4*	3.417–3.407	1.18E-03	–16.83	Down
	Caprate.1	0.804–0.793	7.42E-03	–16.32	Down
	Glutamate.20*	2.166–2.129	3.40E-03	–16.14	Down
	Homoserine.9*	3.831–3.824	1.78E-04	16.09	Up
	N-Acetylornithine.3	4.166–4.162	2.25E-03	16.02	Up
	Nicotinate.4	8.963–8.940	1.38E-04	–15.97	Down
	3-Hydroxybutyrate.1	1.113–1.106	3.72E-04	–15.84	Down
	Alanine.5*	3.790–3.786	8.25E-05	15.74	Up
	D-Threitol.5*	3.683–3.677	8.25E-05	–15.64	Down
	Lactate.3*, Threonine.1*	1.351–1.311	1.78E-04	–15.37	Down
	Ethanolamine.5*	3.165–3.159	2.29E-04	15.06	Up
	Pyroglutamate.9*	4.136–4.125	8.25E-05	–15.00	Down
	Guanosine.6	5.924–5.917	3.40E-03	–14.89	Down
	Agmatine.6*	3.232–3.217	1.07E-02	14.88	Up
	Isoleucine.13*	3.677–3.670	1.07E-04	14.86	Up
	Lactate.4*	4.098–4.093	1.38E-04	–14.81	Down
	N-Acetylaspartate.16*	2.664–2.660	2.29E-04	–14.79	Down
	Choline.7*	3.195–3.186	8.25E-05	14.02	Up

Right Cerebrum	Ethanolamine.6*, Homoserine.10*, Uridine.7*	3.824–3.818	8.25E-05	13.96	Up
	Serine.1*	4.031–4.025	8.25E-05	–13.90	Down
	Isoleucine.14*	1.214–1.205	2.29E-04	13.64	Up
	Threonine.2*	4.230–4.218	4.72E-02	–13.63	Down
	Caprate.2	0.793–0.780	4.15E-03	–13.62	Down
	Glycerol.5*, Myo-Inositol.4*	3.550–3.538	1.47E-03	–13.60	Down
	Agmatine.7*, Phenylalanine.10*	3.268–3.249	8.25E-05	13.59	Up
	Glycerol.6*	3.647–3.638	1.47E-03	–12.92	Down
	D-Threitol.6*, Glycerol.7*, Myo-Inositol.5*	3.638–3.622	1.47E-03	–12.90	Down
	3-Hydroxybutyrate.2	1.080–1.061	2.92E-04	–12.86	Down
	Choline.8*	4.044–4.039	7.51E-04	12.66	Up
	Threonine.3*	4.240–4.230	5.06E-03	–12.64	Down
	Pyroglutamate.10*	2.556–2.551	3.72E-04	–12.63	Down
	Indole-3-Acetate.1	7.611–7.605	9.42E-04	–12.52	Down
	Homoserine.11*	3.963–3.960	1.38E-04	12.37	Up
	N-Acetylornithine.4	4.162–4.159	8.94E-03	12.26	Up
	Homoserine.12*	2.045–2.035	2.25E-03	12.12	Up
	Homoserine.13*	3.960–3.953	1.07E-04	11.76	Up
	Xanthurenate.1	7.616–7.611	9.42E-04	–11.65	Down
	Alanine.6*, Homoserine.14*	3.794–3.790	1.53E-02	11.57	Up
	Nicotinate.5	8.735–8.723	2.92E-04	–11.44	Down
	2-Oxoglutarate.2*	2.429–2.415	4.72E-02	11.24	Up
	Carnitine.5*	3.315–3.304	1.47E-03	–10.76	Down
	D-Threitol.7*	3.719–3.712	1.38E-04	–10.64	Down
	N-Acetylornithine.5	4.159–4.155	4.06E-02	10.63	Up
	Serine.2*	4.039–4.031	1.78E-04	–10.48	Down
	Guanosine.7	5.913–5.906	2.15E-02	–10.16	Down
	Saccharopine.3	3.591–3.585	3.72E-04	9.94	Up
	Nicotinate.6	8.723–8.712	3.72E-04	–9.93	Down

Right Cerebrum	Inosine.10, N-Acetylaspartate.17*	4.368–4.359	1.82E-02	–9.92	Down
	Adenosine.13*, Serine.3*	3.845–3.839	9.42E-04	–9.83	Down
	Homoserine.15*	3.839–3.831	8.94E-03	9.73	Up
	Doublet 3.881 ppm	3.883–3.878	1.38E-04	–9.55	Down
	β-Alanine.5*	2.571–2.565	8.25E-05	9.53	Up
	D-Threitol.8*, Myo-Inositol.6*	3.622–3.611	1.47E-03	–9.53	Down
	Homocysteine.10, Isoleucine.15*	1.242–1.233	2.92E-04	9.33	Up
	Indole-3-Acetate.2	7.623–7.616	1.47E-03	–9.25	Down
	Xanthurenate.2	7.605–7.598	5.97E-04	–9.12	Down
	Carnitine.6*	3.391–3.370	9.42E-04	–9.07	Down
	D-Threitol.9*	3.687–3.683	2.25E-03	–8.98	Down
	Isoleucine.16*	3.653–3.647	5.97E-04	8.88	Up
	5,6-Dihydrouracil.6*	3.468–3.464	7.51E-04	8.79	Up
	Caprate.3	2.187–2.176	3.40E-03	–8.63	Down
	4-Pyridoxate*	7.898–7.890	1.07E-02	–8.56	Down
	Glycerol.8*	3.563–3.550	1.47E-03	–8.21	Down
	Caprate.4	0.831–0.804	3.40E-03	–8.09	Down
	Levulinate.3*	2.868–2.862	8.94E-03	–8.012	Down
	Isoleucine.17*	1.251–1.242	1.28E-02	8.00	Up
	Aspartate.10*, Homocysteine.11	2.677–2.672	1.18E-03	7.35	Up
	Histidine.10*	3.338–3.315	1.28E-02	7.28	Up
	Homocysteine.12, Homoserine.16*	3.878–3.870	1.07E-02	7.15	Up
	Adenine.2, Inosine.11	8.211–8.206	2.98E-02	–6.96	Down
	Phenylalanine.11*	3.134–3.060	7.42E-03	6.14	Up
	Levulinate.4*	2.943–2.931	1.82E-03	–6.11	Down
	Carnitine.7*, Levulinate.5*, Pyroglutamate.11*	2.385–2.379	1.28E-02	–5.98	Down

Right Cerebrum	Methylamine	2.607–2.603	1.82E-02	–5.68	Down
	Creatinine.2*	4.051–4.044	4.72E-02	–5.61	Down
	Homocysteine.13, Valine.5*	2.255–2.243	2.77E-03	5.59	Up
	β-Alanine.6*	2.561–2.556	2.25E-03	5.19	Up
	Levulinate.6*	2.243–2.234	2.25E-03	–5.17	Down
	Lactate.5*	4.101–4.098	4.06E-02	–5.12	Down
	Homocysteine.14	2.223–2.216	2.25E-03	4.56	Up
	Myo-Inositol.7*	4.093–4.055	2.98E-02	–4.45	Down
	Glycerol.9*	3.670–3.662	1.82E-02	–4.43	Down
	Doublet 3.865 ppm	3.870–3.859	7.42E-03	–4.37	Down
	Levulinate.7*	2.918–2.868	2.15E-02	–3.63	Down
	Aspartate.11*	2.755–2.733	4.06E-02	2.98	Up
	N-Acetylornithine.6	4.148–4.136	2.98E-02	2.62	Up
	Uridine.8*	3.912–3.905	3.48E-02	2.02	Up

Table A3. *Left and right cerebrum metabolites found to be significantly altered by stress in a Mann- Whitney U test. Metabolite regulation is shown as a function of relative concentration in high early postnatal stress individuals. Metabolites for which more than one NMR resonance peak was identified as significant are represented as metabolite.1, metabolite.2, … metabolite.n.* *Indicates metabolites that were significantly altered by stress in both left and right cerebra.*

Region	Metabolite	*r*	*p*	Correlation
Left Cerebrum	Aspartate.1†	–0.78	0.000012	Negative
	Aspartate.3†	–0.76	0.000028	Negative
	Agmatine.1†, Phenylalanine.1†, Taurine.1†	–0.76	0.000029	Negative
	Myo-Inositol.1†	0.75	0.000033	Positive
	Glutamate.12†	0.75	0.000043	Positive
	Glutamate.10†	0.74	0.000058	Positive
	Glutamate.7†	0.73	0.000067	Positive
	Agmatine.4†	–0.73	0.000070	Negative
	Aspartate.2†	–0.73	0.000074	Negative
	Tyrosine.2†	0.73	0.000077	Positive
	2-Aminobutyrate.2, Leucine.2†	–0.72	0.000097	Negative
	Isoleucine.1†	–0.72	0.000106	Negative
	2-Aminoadipate.1†	–0.71	0.000128	Negative
	Aspartate.5†	–0.71	0.000140	Negative
	Glutamate.14†	0.71	0.000158	Positive
	Agmatine.2†	–0.71	0.000161	Negative
	Ethanolamine.1†, Homoserine.1†, Uridine.1†	–0.71	0.000164	Negative
	Glutamate.15†	0.71	0.000168	Positive
	Glutamate.8†	0.70	0.000179	Positive
	Adenosine.4†	0.70	0.000182	Positive
	Adenosine.1†	0.70	0.000203	Positive
	Pyroglutamate.6†	0.70	0.000215	Positive
	Adenosine.9†	0.70	0.000226	Positive
	Aspartate.4†	–0.70	0.000232	Negative
	Aspartate.6†, Uridine.4†	–0.69	0.000253	Negative
	Adenosine.13†	0.69	0.000256	Positive
	Glutamate.5†	0.69	0.000256	Positive

Left Cerebrum	Hypoxanthine†	–0.69	0.000272	Negative
	Glutamate.3†	0.69	0.000285	Positive
	Glutamate.2†	0.69	0.000285	Positive
	Glutamate.1†	0.69	0.000286	Positive
	Niacinamide.2†	–0.69	0.000293	Negative
	Glutaric Acid Monomethyl Ester.1	–0.69	0.000309	Negative
	Isoleucine.3†	–0.68	0.000346	Negative
	Glutamate.13†	0.68	0.000360	Positive
	N-Acetylaspartate.15†	0.68	0.000387	Positive
	Histidine.10†	–0.67	0.000411	Negative
	Histidine.7†	–0.67	0.000455	Negative
	Glutamate.9†, Glycerol.2†	0.67	0.000467	Positive
	Glutamate.6†, Glycerol.1†	0.67	0.000469	Positive
	Adenosine.2†	0.67	0.000473	Positive
	Creatine†, Tyrosine.1†	0.67	0.000476	Positive
	Fumarate†	0.67	0.000479	Positive
	5,6-Dihydrouracil.2†	–0.67	0.000516	Negative
	Adenosine.5†	0.67	0.000524	Positive
	Adenosine.3†	0.66	0.000581	Positive
	Uridine.5†	–0.66	0.000689	Negative
	Aspartate.8†	–0.65	0.000699	Negative
	Histidine.11†	–0.65	0.000707	Negative
	Histidine.8†	–0.65	0.000763	Negative
	Taurine.2†	–0.65	0.000775	Negative
	5,6-Dihydrouracil.1†	–0.65	0.000793	Negative
	Histidine.4†	–0.65	0.000819	Negative
	N-Acetylaspartate.14†	0.64	0.000927	Positive
	Adenosine.6†	0.64	0.000955	Positive
	Tyrosine.3†	0.64	0.001029	Positive
	β-Alanine.3†	–0.64	0.001050	Negative

Left Cerebrum	Formate†	0.63	0.001137	Positive
	Uracil.6†	–0.63	0.001148	Negative
	5,6-Dihydrouracil.3†	–0.63	0.001150	Negative
	Lactate.1†	0.63	0.001271	Positive
	Valine.1†	–0.63	0.001301	Negative
	Histidine.6†	–0.63	0.001305	Negative
	Histidine.5†	–0.62	0.001648	Negative
	Valine.4†	–0.62	0.001675	Negative
	Adenosine.14†	0.61	0.001812	Positive
	Isoleucine.2†, Valine.2†	–0.61	0.002013	Negative
	Phenylalanine.7†	–0.61	0.002112	Negative
	Uracil.7†	–0.61	0.002189	Negative
	Alanine.1†, Homoserine.3†	–0.60	0.002271	Negative
	Nicotinurate.1†	–0.60	0.002277	Negative
	Taurine.3†	–0.60	0.002422	Negative
	Adenosine.16†	0.60	0.002423	Positive
	Choline.5†	–0.59	0.002747	Negative
	Lactate.2†	0.59	0.002808	Positive
	Creatinine.2†	0.59	0.002814	Positive
	Carnitine.1†	0.59	0.002898	Positive
	Choline.10†	–0.59	0.002902	Negative
	Valine.3†	–0.59	0.002913	Negative
	Phenylalanine.8†	–0.59	0.003008	Negative
	O-Phosphocholine.5	0.59	0.003024	Positive
	2-Oxoglutarate.1†	–0.59	0.003244	Negative
	N-Acetylaspartate.7†	0.59	0.003275	Positive
	Adenosine.15†	0.59	0.003330	Positive
	2-Aminoadipate.2†	–0.59	0.003333	Negative
	O-Phosphocholine.4	0.58	0.003444	Positive
	Adenosine.19†	0.58	0.003533	Positive

Left Cerebrum	Homoserine.17†, Uridine.7†	–0.58	0.003576	Negative
	2-Oxoglutarate.2†	–0.58	0.003611	Negative
	Pyridoxine	–0.58	0.003686	Negative
	2-Oxoglutarate.3†	–0.58	0.003901	Negative
	2-Aminobutyrate.5, Leucine.6†	–0.58	0.003928	Negative
	N-Acetylaspartate.3†	0.57	0.004124	Positive
	Adenosine.7†	0.57	0.004610	Positive
	Histidine.1†	–0.57	0.004646	Negative
	β-Alanine.2†	–0.57	0.004684	Negative
	N-Acetylaspartate.5†	0.57	0.004824	Positive
	Adenosine.18†	0.56	0.005228	Positive
	N-Acetylaspartate.1†	0.56	0.005342	Positive
	Adenosine.8†	0.56	0.005578	Positive
	Adenosine.12†	0.56	0.005748	Positive
	Adenosine.10†	0.56	0.005801	Positive
	Carnitine.4†, Levulinate.2†, Pyroglutamate.11†	0.56	0.005842	Positive
	Aspartate.9†, Uridine.8†	–0.56	0.005907	Negative
	2-Aminoadipate.3†	–0.56	0.005935	Negative
	Alanine.6†, Homoserine.15†	–0.55	0.006075	Negative
	Homoserine.2†	–0.55	0.006559	Negative
	Phenylalanine.4†	–0.55	0.006869	Negative
	Adenosine.17†	0.55	0.006974	Positive
	Choline.3†	–0.54	0.007268	Negative
	Phenylalanine.5†	–0.54	0.007283	Negative
	Homoserine.5†	–0.54	0.007480	Negative
	β-Alanine.1†	–0.54	0.007668	Negative
	Glycerol.3†	0.54	0.008285	Positive
	Uracil.5†	–0.53	0.009576	Negative
	Adenosine.11†	0.53	0.009670	Positive

Left Cerebrum	N-Acetylaspartate.2†	0.53	0.009674	Positive
	Phenylalanine.3†	–0.53	0.009701	Negative
	Phenylalanine.6†	–0.53	0.009892	Negative
	Glutamate.4†, N-Acetylaspartate.4†, Pyroglutamate.1†	0.52	0.010548	Positive
	Histidine.2†	–0.52	0.011065	Negative
	Ethanolamine.4†	–0.51	0.012025	Negative
	Choline.1†	–0.51	0.012210	Negative
	Myo-Inositol.2†	0.51	0.012210	Positive
	Uracil.4†	–0.51	0.012632	Negative
	Alanine.5†, Homoserine.14†	–0.51	0.012669	Negative
	Phenylalanine.9†	–0.51	0.013432	Negative
	D-Threitol.2†, Glycerol.4†, Myo-Inositol.3†	0.51	0.013441	Positive
	β-Alanine.4†	–0.51	0.013762	Negative
	D-Threitol.1†	0.51	0.013800	Positive
	Choline.2†	–0.51	0.013855	Negative
	Glutamate.18†	0.50	0.014369	Positive
	2-Aminobutyrate.1, Leucine.1†	–0.50	0.014723	Negative
	3-Phenylpropionate.1†	–0.50	0.014819	Negative
	Lactate.3†	0.50	0.015064	Positive
	Serine.3†	0.50	0.015336	Positive
	Histidine.9†	–0.50	0.015464	Negative
	Serine.1†	0.50	0.015567	Positive
	Glutamate.11†	0.50	0.015813	Positive
	β-Alanine.5†	–0.49	0.016366	Negative
	Lactate.4†, Threonine.3†	0.49	0.016643	Positive
	Homoserine.7†	–0.48	0.019590	Negative
	Histidine.3†	–0.48	0.019955	Negative
	Choline.9†	–0.48	0.020157	Negative
	Glycerol.5†, Myo-Inositol.4†	0.48	0.020250	Positive

Left Cerebrum	Alanine.3†, Homoserine.11†	–0.48	0.021168	Negative
	β-Alanine.6†	–0.48	0.021180	Negative
	Carnitine.5†, Levulinate.3†, Pyroglutamate.14†	0.48	0.021803	Positive
	Isoleucine.10†	–0.48	0.021963	Negative
	Homoserine.9†	–0.46	0.025610	Negative
	D-Threitol.4†, Myo-Inositol.9†	0.46	0.025697	Positive
	N-Acetylaspartate.8†	0.46	0.025986	Positive
	Choline.4†	–0.46	0.026183	Negative
	Phenylalanine.12†	–0.46	0.027698	Negative
	N-Acetylaspartate.9†	0.46	0.027884	Positive
	Agmatine.3†, Leucine.3†	–0.46	0.028332	Negative
	Phenylalanine.11†	–0.45	0.032205	Negative
	Isoleucine.7†	–0.45	0.033228	Negative
	Ethanolamine.3†, Homoserine.6†	–0.44	0.033761	Negative
	4-Pyridoxate.1†	0.44	0.033803	Positive
	Homoserine.8†	–0.44	0.036145	Negative
	Serine.2†	0.44	0.037181	Positive
	N-Acetylaspartate.11†	0.43	0.039226	Positive
	Glutamate.17†, Pyroglutamate.12†	0.43	0.040708	Positive
	Glycerol.6†, Glycine	0.43	0.041132	Positive
	Serine.4†	0.43	0.041629	Positive
	2-Aminoadipate.4†, 4-Aminobutyrate.1, Glutaric Acid Monomethyl Ester.2	–0.43	0.042619	Negative
	Nicotinurate.3†	–0.42	0.044673	Negative
	Ethanolamine.5†, Phenylalanine.16†	–0.42	0.045083	Negative
	Phenylalanine.13†	–0.42	0.047338	Negative
	Adenosine.20†	0.42	0.047400	Positive
	Lactate.5†	0.42	0.047989	Positive

Right Cerebrum	Aspartate.9†	–0.80	0.000005	Negative
	Aspartate.5†, Tyramine.5	–0.80	0.000006	Negative
	Aspartate.4†	–0.79	0.000006	Negative
	Uridine.3†	–0.79	0.000007	Negative
	Aspartate.1†	–0.79	0.000007	Negative
	Aspartate.6†, Uridine.1†	–0.79	0.000007	Negative
	Aspartate.3†	–0.79	0.000007	Negative
	Aspartate.7†	–0.79	0.000008	Negative
	Aspartate.2†, Tyramine.3	–0.78	0.000010	Negative
	Tyramine.6	–0.77	0.000015	Negative
	Methylmalonate.2	0.77	0.000018	Positive
	N-Acetylaspartate.14†	0.77	0.000020	Positive
	β-Alanine.1†	–0.76	0.000027	Negative
	Aspartate.8†, Uridine.5†	–0.76	0.000028	Negative
	Homoserine.13†	–0.76	0.000029	Negative
	Histidine.6†	–0.75	0.000033	Negative
	Nicotinate.2	0.75	0.000038	Positive
	Creatinine.1†	0.75	0.000038	Positive
	Histidine.8†	–0.75	0.000039	Negative
	Adenosine.12†, Tyrosine.2†	0.75	0.000039	Positive
	D-Threitol.5†	0.75	0.000039	Positive
	Inosine.4	0.75	0.000044	Positive
	π-Methylhistidine	0.74	0.000057	Positive
	Adenine.1	0.74	0.000062	Positive
	Singlet 1.178 ppm	0.73	0.000067	Positive
	Histidine.4†	–0.73	0.000068	Negative
	Hypoxanthine†	–0.73	0.000069	Negative
	Niacinamide.1†	–0.73	0.000071	Negative
	Methylmalonate.1	0.73	0.000072	Positive
	Inosine.2	0.73	0.000081	Positive

Right Cerebrum	Adenosine.1†, Inosine.3	0.73	0.000082	Positive
	N-Acetylaspartate.16†	0.73	0.000082	Positive
	Doublet 3.881 ppm	0.73	0.000086	Positive
	N-Acetylaspartate.1†	0.72	0.000094	Positive
	Choline.1†	–0.72	0.000097	Negative
	N-Acetylaspartate.4†	0.72	0.000097	Positive
	Taurine.1†	–0.72	0.000102	Negative
	D-Threitol.3†	0.72	0.000110	Positive
	Inosine.1	0.72	0.000113	Positive
	Alanine.4†	–0.72	0.000115	Negative
	Homocysteine.2	–0.72	0.000116	Negative
	Adenosine.2†	0.72	0.000116	Positive
	Nicotinate.1	0.72	0.000119	Positive
	N-Acetylaspartate.2†	0.72	0.000121	Positive
	Taurine.2†	–0.72	0.000122	Negative
	Leucine.4†	–0.72	0.000124	Negative
	Ethanolamine.1†	–0.71	0.000128	Negative
	N-Acetylaspartate.9†	0.71	0.000129	Positive
	N-Acetylaspartate.3†	0.71	0.000133	Positive
	N-Acetylaspartate.6†	0.71	0.000141	Positive
	Ethanolamine.2†, Homoserine.4†	–0.71	0.000147	Negative
	Choline.2†	–0.71	0.000150	Negative
	Glutamate.12†	0.71	0.000153	Positive
	Adenosine.8†, Creatine†, Tyrosine.1†	0.71	0.000153	Positive
	D-Threitol.2†	0.71	0.000155	Positive
	Adenosine.9†	0.71	0.000157	Positive
	Guanosine.1	0.71	0.000160	Positive
	Adenosine.3†	0.71	0.000161	Positive
	N-Acetylaspartate.5†	0.71	0.000166	Positive
	Nicotinurate.1†	–0.71	0.000166	Negative

Right Cerebrum	Histidine.5†	–0.71	0.000167	Negative
	β-Alanine.3†	–0.71	0.000170	Negative
	Adenosine.6†	0.70	0.000174	Positive
	1,3-Dimethylurate.1	0.70	0.000174	Positive
	Phenylalanine.6†	–0.70	0.000175	Negative
	Formate†	0.70	0.000177	Positive
	Phenylalanine.1†	–0.70	0.000181	Negative
	Tyramine.4	–0.70	0.000184	Negative
	Homoserine.2†	–0.70	0.000185	Negative
	3-Hydroxybutyrate.1	0.70	0.000191	Positive
	Adenosine.4†	0.70	0.000191	Positive
	N-Acetylornithine.1	–0.70	0.000193	Negative
	Histidine.3†	–0.70	0.000204	Negative
	5,6-Dihydrouracil.4†	–0.70	0.000215	Negative
	Inosine.6	0.70	0.000217	Positive
	Inosine.5, N-Acetylaspartate.8†	0.70	0.000219	Positive
	Uracil.4†	–0.70	0.000221	Negative
	Caprate.2	0.70	0.000221	Positive
	2-Aminoadipate.4†, Leucine.3†	–0.70	0.000222	Negative
	Caprate.1	0.70	0.000230	Positive
	Phenylalanine.5†	–0.69	0.000236	Negative
	5,6-Dihydrouracil.5†	–0.69	0.000239	Negative
	Guanosine.3, Histamine.1	0.69	0.000240	Positive
	Glutamate.4†, N-Acetylaspartate.7†, Pyroglutamate.1†	0.69	0.000243	Positive
	Histidine.1†	–0.69	0.000248	Negative
	Homocysteine.1	–0.69	0.000250	Negative
	4-Aminobutyrate.1, Acetate.1	–0.69	0.000253	Negative
	Homocysteine.8	–0.69	0.000261	Negative
	2-Aminoadipate.6†	–0.69	0.000267	Negative

Right Cerebrum	3-Phenylpropionate.2†, Phenylalanine.7†	–0.69	0.000268	Negative
	Valine.1†	–0.69	0.000269	Negative
	Phenylalanine.3†	–0.69	0.000272	Negative
	4-Aminobutyrate.2	–0.69	0.000277	Negative
	Valine.3†	–0.69	0.000278	Negative
	Histidine.2†	–0.69	0.000281	Negative
	Ethanolamine.3†	–0.69	0.000283	Negative
	β-Alanine.2†	–0.69	0.000288	Negative
	Adenosine.5†	0.69	0.000289	Positive
	4-Aminobutyrate.6	–0.69	0.000293	Negative
	Guanosine.2	0.69	0.000298	Positive
	Agmatine.2†	–0.69	0.000299	Negative
	Caprate.4	0.69	0.000301	Positive
	β-Alanine.4†	–0.69	0.000301	Negative
	2-Aminoadipate.3†	–0.69	0.000305	Negative
	4-Aminobutyrate.7, Agmatine.4†	–0.69	0.000306	Negative
	Taurine.3†	–0.69	0.000310	Negative
	Phenylalanine.2†	–0.68	0.000312	Negative
	Glutamate.18†	0.68	0.000316	Positive
	4-Aminobutyrate.3	–0.68	0.000321	Negative
	5,6-Dihydrouracil.6†	–0.68	0.000325	Negative
	4-Aminobutyrate.5	–0.68	0.000328	Negative
	Levulinate.1†, Pyroglutamate.4†	0.68	0.000330	Positive
	Tryptophan.2	–0.68	0.000335	Negative
	D-Threitol.1†	0.68	0.000337	Positive
	Choline.8†	–0.68	0.000338	Negative
	Alanine.2†	–0.68	0.000344	Negative
	Valine.2†	–0.68	0.000349	Negative
	Alanine.1†, Isoleucine.4†	–0.68	0.000355	Negative
	Uracil.1†	–0.68	0.000371	Negative

Right Cerebrum	5,6-Dihydrouracil.2†	–0.68	0.000372	Negative
	Glutamate.10†	0.68	0.000375	Positive
	Agmatine.5†	–0.68	0.000379	Negative
	Leucine.1†	–0.68	0.000384	Negative
	Valine.4†	–0.68	0.000394	Negative
	Ethanolamine.6†, Homoserine.10†, Uridine.7†	–0.68	0.000398	Negative
	Fumarate†	0.68	0.000399	Positive
	Histamine.2	0.68	0.000400	Positive
	Tyramine.1	–0.68	0.000410	Negative
	Carnitine.1†	0.67	0.000430	Positive
	3-Phenylpropionate.3†, Phenylalanine.8†	–0.67	0.000438	Negative
	Glutamate.7†, Glycerol.2†	0.67	0.000442	Positive
	3-Phenylpropionate.1†, Phenylalanine.4†	–0.67	0.000448	Negative
	Myo-Inositol.1†	0.67	0.000452	Positive
	Glutamate.1†	0.67	0.000487	Positive
	Tryptophan.1	–0.67	0.000494	Negative
	2-Oxoglutarate.1†, 4-Aminobutyrate.9	–0.67	0.000502	Negative
	Glutamate.2†	0.67	0.000502	Positive
	Tyramine.2	–0.67	0.000506	Negative
	Glutamate.8†	0.67	0.000508	Positive
	Glutamate.3†	0.67	0.000510	Positive
	Glutamate.5†, Glycerol.1†	0.67	0.000523	Positive
	Levulinate.6†	0.67	0.000524	Positive
	Alanine.3†, Homoserine.5†	–0.67	0.000524	Negative
	β-Alanine.5†	–0.67	0.000528	Negative
	Glutamate.13†	0.66	0.000551	Positive
	Taurine.5†	–0.66	0.000559	Negative
	Histidine.9†	–0.66	0.000560	Negative
	Saccharopine.1	–0.66	0.000561	Negative

Right Cerebrum	D-Threitol.4†	0.66	0.000561	Positive
	N-Acetylaspartate.13†	0.66	0.000562	Positive
	4-Aminobutyrate.8	–0.66	0.000571	Negative
	Lactate.1†	0.66	0.000589	Positive
	Uracil.2†	–0.66	0.000598	Negative
	Glutamate.17†	0.66	0.000616	Positive
	Glutamate.9†	0.66	0.000624	Positive
	Nicotinate.3	0.66	0.000629	Positive
	Adenosine.11†, Inosine.8	0.66	0.000635	Positive
	Adenosine.10†, Inosine.7	0.66	0.000638	Positive
	Homocysteine.3	–0.66	0.000650	Negative
	Homoserine.6†	–0.65	0.000698	Negative
	Glutamate.15†	0.65	0.000723	Positive
	Agmatine.1†, Leucine.2†	–0.65	0.000730	Negative
	Homoserine.8†	–0.65	0.000745	Negative
	Homocysteine.5, Isoleucine.6†	–0.65	0.000759	Negative
	Uridine.6†	–0.65	0.000784	Negative
	Isoleucine.1†	–0.65	0.000789	Negative
	Uracil.3†	–0.65	0.000806	Negative
	5,6-Dihydrouracil.1†	–0.65	0.000822	Negative
	S-Adenosylhomocysteine.1	–0.65	0.000828	Negative
	Myo-Inositol.2†	0.65	0.000855	Positive
	Guanosine.4	0.65	0.000884	Positive
	2'-Deoxyadenosine	–0.64	0.000929	Negative
	Homocysteine.4, Isoleucine.5†	–0.64	0.000932	Negative
	Saccharopine.3	–0.64	0.000940	Negative
	1,3-Dimethylurate.2	0.64	0.000979	Positive
	Lactate.2†	0.64	0.000987	Positive
	Homoserine.1†, Isoleucine.7†	–0.64	0.000990	Negative
	Isoleucine.3†	–0.64	0.001003	Negative

Right Cerebrum	Histidine.7†	–0.64	0.001016	Negative
	2-Aminoadipate.1†	–0.64	0.001019	Negative
	Carnitine.3†	0.64	0.001053	Positive
	Glutamate.6†	0.64	0.001093	Positive
	Isoleucine.2†	–0.64	0.001112	Negative
	Glutamate.14†	0.63	0.001137	Positive
	3-Hydroxybutyrate.2	0.63	0.001208	Positive
	Choline.4†	–0.63	0.001214	Negative
	Agmatine.3†	–0.63	0.001229	Negative
	1,3-Dimethylurate.3, Myo-Inositol.3†	0.63	0.001262	Positive
	4-Aminobutyrate.4	–0.63	0.001271	Negative
	Pyroglutamate.8†	0.63	0.001277	Positive
	Adenosine.7†	0.63	0.001280	Positive
	Saccharopine.2	–0.63	0.001306	Negative
	5,6-Dihydrouracil.3†	–0.63	0.001315	Negative
	Homocysteine.6	–0.63	0.001327	Negative
	Serine.1†	0.63	0.001327	Positive
	Choline.6†	–0.63	0.001384	Negative
	Choline.7†	–0.63	0.001428	Negative
	Uridine.2†	–0.62	0.001458	Negative
	Carnitine.2†, Levulinate.2†, Pyroglutamate.7†	0.62	0.001468	Positive
	2-Aminoadipate.2†	–0.62	0.001569	Negative
	Choline.3†	–0.62	0.001698	Negative
	Nicotinate.4	0.62	0.001781	Positive
	Homoserine.9†	–0.61	0.001969	Negative
	Carnitine.4†	0.61	0.002019	Positive
	Isoleucine.9†	–0.61	0.002037	Negative
	Homoserine.3†, Isoleucine.10†	–0.61	0.002061	Negative
	D-Threitol.9†	0.61	0.002142	Positive

Right Cerebrum	Isoleucine.13†	–0.61	0.002148	Negative
	Nicotinate.5	0.60	0.002233	Positive
	S-Adenosylhomocysteine.2	–0.60	0.002283	Negative
	Agmatine.7†, Phenylalanine.10†	–0.60	0.002488	Negative
	Alanine.5†	–0.60	0.002700	Negative
	Guanosine.5	0.60	0.002739	Positive
	Xanthurenate.1	0.59	0.002807	Positive
	Homoserine.11†	–0.59	0.002871	Negative
	Levulinate.4†	0.59	0.002983	Positive
	Ethanolamine.5†	–0.59	0.003036	Negative
	Glutamate.11†, Glycerol.3†	0.59	0.003092	Positive
	Tryptophan.3	–0.59	0.003244	Negative
	Niacinamide.2†	–0.59	0.003252	Negative
	D-Threitol.7†	0.58	0.003615	Positive
	2-Aminoadipate.5†	–0.58	0.003631	Negative
	Glutamate.16†	0.58	0.003716	Positive
	Nicotinate.6	0.58	0.003754	Positive
	Pyroglutamate.9†	0.58	0.004102	Positive
	Homocysteine.7	–0.57	0.004142	Negative
	N-Acetylornithine.2	–0.57	0.004177	Negative
	Isoleucine.8†	–0.57	0.004275	Negative
	Choline.5†	–0.57	0.004485	Negative
	S-Adenosylhomocysteine.3	–0.57	0.004599	Negative
	D-Threitol.6†, Glycerol.7†, Myo-Inositol.5†	0.56	0.005477	Positive
	Lactate.3†, Threonine.1†	0.56	0.005710	Positive
	Ethanolamine.4†, Homoserine.7†, Uridine.4†	–0.55	0.006217	Negative
	Uridine.8†	–0.55	0.006270	Negative
	Indole-3-Acetate.2	0.55	0.006276	Positive
	Glycerol.6†	0.55	0.006319	Positive

Right Cerebrum	S-Adenosylhomocysteine.4	–0.55	0.006840	Negative
	Isoleucine.11†	–0.55	0.006877	Negative
	4-Aminobutyrate.10	–0.54	0.007208	Negative
	Lactate.4†	0.54	0.007864	Positive
	Glycerol.5†, Myo-Inositol.4†	0.54	0.007948	Positive
	N-Acetylaspartate.10†, Pyroglutamate.2†	0.54	0.008146	Positive
	N-Acetylornithine.3	–0.54	0.008170	Negative
	Doublet 3.865 ppm	0.53	0.008806	Positive
	Xanthurenate.2	0.53	0.008860	Positive
	3-Phenylpropionate.5†	–0.52	0.011520	Negative
	Homocysteine.9, Isoleucine.12†	–0.51	0.012005	Negative
	Pyroglutamate.3†	0.51	0.012120	Positive
	Guanosine.6	0.51	0.012729	Positive
	Carnitine.7†, Levulinate.5†, Pyroglutamate.11†	0.50	0.014242	Positive
	Carnitine.5†	0.50	0.014458	Positive
	Inosine.9, N-Acetylaspartate.15†	0.50	0.016323	Positive
	Indole-3-Acetate.1	0.49	0.016517	Positive
	3-Phenylpropionate.6†	–0.49	0.016788	Negative
	D-Threitol.8†, Myo-Inositol.6†	0.49	0.016804	Positive
	Taurine.4†	–0.49	0.018520	Negative
	Isoleucine.16†	–0.48	0.019431	Negative
	β-Alanine.6†	–0.48	0.019568	Negative
	N-Acetylornithine.4	–0.48	0.019621	Negative
	Tryptophan.4	–0.47	0.022120	Negative
	Homoserine.15†	–0.47	0.022777	Negative
	Pyroglutamate.10†	0.46	0.025517	Positive
	Niacinamide.3†	–0.46	0.026227	Negative
	Agmatine.6†	–0.46	0.027441	Negative
	N-Acetylaspartate.12†, Pyroglutamate.6†	0.46	0.027594	Positive

Right Cerebrum	Homoserine.12†	–0.46	0.028687	Negative
	4-Pyridoxate†	0.45	0.032337	Positive
	Aspartate.10†, Homocysteine.11	–0.45	0.033013	Negative
	N-Acetylornithine.5	–0.45	0.033099	Negative
	Glycerol.9†	0.44	0.034055	Positive
	Isoleucine.14†	–0.44	0.035009	Negative
	Glycerol.8†	0.44	0.037385	Positive
	Serine.2†	0.43	0.038908	Positive
	3-Phenylpropionate.4†, Phenylalanine.9†	–0.43	0.039236	Negative
	Adenosine.13†, Serine.3†	0.43	0.042223	Positive
	Aspartate.11†	–0.42	0.044139	Negative
	Histidine.10†	–0.42	0.044478	Negative
	N-Acetylaspartate.11†, Pyroglutamate.5†	0.42	0.048339	Positive
	Adenine.2, Inosine.11	0.41	0.049318	Positive

Table A4. *Left and right cerebrum metabolites found to be significantly correlated to precocious visual behaviour. Pearson correlations were used to assess the relationship between behaviours indicative of precocious visual behaviour (i.e., less time spent in the deep region of the visual cliff apparatus) and relative concentrations of metabolites found to be significantly altered by stress in a Mann-Whitney U test. Positive correlations indicate that precocious development of depth perception was linked to lower metabolite concentrations, while negative correlations indicate that precocious development of depth perception was linked to higher metabolite concentrations. Metabolites for which more than one NMR resonance peak was identified are represented as metabolite.1, metabolite.2, … metabolite.n. †Indicates metabolites that were significantly correlated to precocious visual behaviour in both left and right cerebra.*